NUMERICAL SIMULATION OF LOCAL DESTRATIFICATION OF LAKES

By

AHMED ALI BUSNAINA

Bachelor of Science

University of Al-Fateh

Tripoli, Libya

1976

Submitted to the Faculty of the Graduate College
of the Oklahoma State University
in partial fulfillment of the requirements
for the Degree of
MASTER OF SCIENCE
December, 1979

NUMERICAL SIMULATION OF LOCAL DESTRATIFICATION

OF LAKES

Thesis Approved:

Robert M. Morelli

Thesis Adviser

D K McLaughlin

David G. Lilley

Norman N Durham

Dean of the Graduate College

ACKNOWLEDGMENTS

I would like to express my gratitude to my adviser, Dr. P. M. Moretti, and to Dr. D. G. Lilley, for their valuable suggestions and advice throughout the progress of this research. Further advice and criticism of my committee member, Dr. D. K. McLaughlin, is gratefully appreciated. The most appreciation goes to my wife for her patience and sacrifices during my research. I deeply appreciate the encouragement and financial support given by my parents, Mr. and Mrs. Ali Busnaina.

This project was funded by a grant from the Waterways Experiment Station in Vicksburg, Mississippi.

TABLE OF CONTENTS

Chapter		Page
I.	INTRODUCTION	1
	Background	2
	Hydraulic Modeling	3
	Previous Theoretical and Numerical Analysis	4
	Outline of the Thesis	5
II.	THEORETICAL MODEL	6
	The Governing Equations	6
	The Flow Domain and Grid System	8
	Boundary Conditions	10
III.	SOLUTION PROCEDURE	12
	The Finite Difference Equations	12
	Iterative Procedure	14
	Imposition of Boundary Conditions	15
	Convergence and Stability	17
	Accuracy	19
IV.	RESULTS AND DISCUSSION	22
	Dilution Factor as a Function of Time	22
	Dilution Factor as a Function of Fr_d	23
	Dilution Factor as a Function of Q^*	26
	Dilution Factor as a Function of D^*	27
	Dilution Factor as a Function of Z_T^*	28
	Penetration Depth Prediction	29
V.	CONCLUSIONS	32
	Summary	32
	Conclusions	32
	Recommendations for Further Study	34
A SELECTED BIBLIOGRAPHY		35
APPENDIX A - FIGURES		37
APPENDIX B - FINITE DIFFERENCE FORMULATION		68

Chapter Page

APPENDIX C - PENETRATION DEPTH ANALYSIS 71

APPENDIX D - HYDROSTATIC PRESSURE 77

APPENDIX E - THE DIMENSIONLESS GOVERNING EQUATIONS 81

APPENDIX F - COMPUTER PROGRAM LISTING 86

LIST OF FIGURES

Figure		Page
1.	Physical Flow Domain	38
2.	Arrangement of Variables in a Typical Cell	38
3.	Velocity Vector Plot	39
4.	General Mesh Arrangement Showing New Input and Output Boundary Conditions	40
5.	Effect of Donor Cell Coefficient on Calculated Mass Fraction m_1 at Three Locations	41
6.	Dilution Factor, DF, As a Function of Nondimensional Time, t*	42
7.	Dilution Factor, DF, As a Function of Densimetric Froude Number, Fr_d, at D* = 0.211, for Q* = 0.44	43
8.	Dilution Factor, DF, As a Function of Densimetric Froude Number, Fr_d, at D* = 0.211, for Q* = 2.50	44
9.	Dilution Factor, DF, As a Function of Densimetric Froude Number, Fr_d, at D* = 0.211, for Q* = 0.17	45
10.	Dilution Factor, DF, As a Function of Densimetric Froude Number, Fr_d, at D* = 0.183, for Q* = 0.75	46
11.	Dilution Factor, DF, As a Function of Densimetric Froude Number, Fr_d, at D* = 0.183, for Q* = 0.20	47
12.	Dilution Factor, DF, As a Function of Densimetric Froude Number, Fr_d, at D* = 0.183, for Q* = 0.3	48
13.	Dilution Factor, DF, As a Function of Densimetric Froude Number, Fr_d, at D* = 0.183, for Q* = 2.50	49
14.	Dilution Factor, DF, As a Function of Densimetric Froude Number, Fr_d, at D* = 0.131, for Q* = 0.44	50
15.	Dilution Factor, DF, As a Function of Densimetric Froude Number, Fr_d, at D* = 0.131, for Q* = 0.18	51

Figure Page

16. Dilution Factor, DF, As a Function of Densimetric Froude Number, Fr_d, at D* = 0.131, for Q* = 2.6 52

17. Dilution Factor, DF, As a Function of Densimetric Froude Number, Fr_d, at D* = 0.117, for Q* = 0.43 53

18. Dilution Factor, DF, As a Function of Densimetric Froude Number, Fr_d, at D* = 0.117, for Q* = 0.17 54

19. Dilution Factor, DF, As a Function of Flow Rate Ratio, Q*, and Densimetric Froude Number, Fr_d, at D* = 0.211 55

20. Dilution Factor, DF, As a Function of Flow Rate Ratio, Q*, and Densimetric Froude Number, Fr_d, at D* = 0.183 56

21. Dilution Factor, DF, As a Function of Flow Rate Ratio, Q*, and Densimetric Froude Number, Fr_d, at D* = 0.131 57

22. Dilution Factor, DF, As a Function of Flow Rate Ratio, Q*, and Densimetric Froude Number, Fr_d, at D* = 0.171 58

23. Dilution Factor, DF, As a Function of Nondimensional Propeller Diameter, D*, and Densimetric Froude Number, Fr_d, at Q* = 0.44 59

24. Dilution Factor, DF, As a Function of Nondimensional Propeller Diameter, D*, and Densimetric Froude Number, Fr_d, at Q* = 2.50 60

25. Location of the Interface With Nondimensional Time t* Increment for Fr_d = 0.30 61

26. Location of the Interface With Nondimensional Time t* Increment for Fr_d = 1.05 62

27. Nondimensional Penetration Depth, Z_p^*, As a Function of Densimetric Froude Number, Fr_d, at D* = 0.211 63

28. Nondimensional Penetration Depth, Z_p^*, As a Function of Densimetric Froude Number, Fr_d, at D* = 0.175 64

29. Dilution Factor, DF, As a Function of Initial Height of Metalimnion, Z_T^*, at D* = 0.211 65

30. Hydrostatic Pressure Profile 66

31. Jet at Stagnation Point 67

32. Density Profile 67

NOMENCLATURE

A_i	central area at cell i-1
C	constant
D	jet diameter
D_P	propeller diameter
D*	nondimensional propeller diameter, $D^* = D_P/H$
DF	dilution factor, $DF = (\rho_{rel} - \rho_h/\rho_e - \rho_h = \rho_{rel} - \rho_2/\rho_1 - \rho_2)$
Fr_d	densimetric Froude number, $Fr_d = V/[g(\Delta\rho/\rho_o)H]^{1/2}$
g	gravitational acceleration
g_x	body force in direction x
g_y	body force in direction y
h	depth or height
h_s	stagnation point depth or jet penetration depth
$\overline{h_t}$	mean thermocline depth
H	total depth of model
I	number of cells in x-direction
IBAR	number of cells of radius of flow field in x-direction
IREL-1	number of cells of release gate in x-direction
J	number of cells in y-direction
JBAR	number of cells of total depth of flow field in y-direction
ℓ_m	mixing length
m_1	mass fraction of fluid of density ρ_1 (epilimnion)
m_2	mass fraction of fluid of density ρ_2 (hypolimnion)
M_{li}	mass fraction of epilimnion at cell i

M_{2i}	mass fraction of hypolimnion at cell i
P	deviation from hydrostatic pressure
$\bar{P}$	total pressure
P_o	reference pressure at propeller
P_s	pressure at stagnation point
Q_e	epilimnion water input flow rate
Q_h	hypolimnion water input flow rate
Q_p	propeller flow rate
Q_{rel}	release flow rate
Q^*	nondimensional flow rate, $Q^* = Q_p/Q_{rel}$
r	propeller radius
R	release gate radius
S	mass fraction (symbol used in program) for epilimnion
S_2	mass fraction (symbol used in program) for hypolimnion
t	time
t_c	characteristic time, t_c = volume under the propeller/Q_p
t^*	nondimensional time, $t^* = t/t_c$
U	velocity in radial direction
U_{TB}	input velocity for hypolimnion
U_{Te}	input velocity for epilimnion
V	velocity in axial direction y
V_p	propeller velocity
V_{rel}	release water velocity
V_o	initial jet velocity
V_y	velocity at any location along axis y
V_s	velocity at stagnation point ($V_s = 0$)
x	radial axis

y	axial direction
Z_p	penetration depth measured from the surface
Z_p^*	nondimensional penetration depth, $Z_p^* = Z_p/H$
Z_T	metalimnion location measured from the bottom
Z_T^*	nondimensional metalimnion location, $Z_t^* = Z_T/H$

Greek Letters

Δx	cell width
Δy	cell height
ΔP	pressure change
Δt	time increment
ν	kinematic viscosity
μ	laminar viscosity
μ_t	turbulent viscosity
ρ	density
ρ_1, ρ_e, ρ_o	epilimnion or top density
ρ_2, ρ_h	hypolimnion density
ρ_{rel}	release water density
ρ_b	mean metalimnion density
δ	jet half width
σ_{sc}	Schmidt number
α	donor cell coefficient

Subscripts

c	characteristic
d	densimetric
e, 1	epilimnion

h, 2	hypolimnion
i	axial at cell i
m	mixing
o	jet location
p	propeller
rel	release
s	stagnation point
T, t	thermocline
Te	epilimnion input
TB	hypolimnion input
x	radial
y	axial

CHAPTER I

INTRODUCTION

During the hot months of summer, thermal stratification may occur in water reservoirs. This presents a serious problem for quality of water released from reservoirs with low-level release structures. The reservoir stratifies into three main regions of different densities. The epilimnion, the top layer, contains warm-low density water (usually rich in oxygen and thus considered as a high-quality water). The hypolimnion, the bottom layer, consists of cold high-density water (poor in oxygen and thus considered as a low-quality water). The region of rapid temperature change (between the other two layers) is called the thermocline or metalimnion. Many of the old reservoirs have the release structure located near the bottom, and in this case the quality of water downstream of the impoundment is poor.

In spring the reservoir temperature is approximately uniform where there is no significant density gradient in the vertical direction. As the season progresses, the upper layer in the lake warms faster than the lower layer, creating a positive density gradient in the downward direction. The bottom layer will be at lower temperature due to low thermal conductivity of water and when the density gradient has a significant value across the top and bottom layers, the lake is said to be stratified.

The epilimnion water is rich in oxygen because of the atmosphere reaeration and photosynthesis. The lack of oxygen in the hypolimnion is referred to the lack of mixing with the epilimnion as a result of the density gradient. The low oxygen content is a characteristic of poor water quality.

Background

Artificial destratification, localized mixing, and modifications of the release structures of the dam can be used to improve the released water quality. Artificial destratification can be either mechanical pumping (with assorted piping) or diffused air pumping. These mixing devices (1), however, require a substantial amount of energy to destratify a large body of water. Localized mixing is proven to be effective and economical to enhance the quality of water released from low-level release gates. Structural modification of the dam involves elevating of the release gate position in order to allow a release water made of the epilimnion. This method is effective for quality improvement; however, it is extremely costly. There has been a continued interest in local (mechanical) destratification of reservoirs to improve water quality. Garton (2) (3) has used a low-energy axial flow propeller pump to locally mix reservoirs near the release structure of the dam. The Garton pump has been used in Lake Okatibbee, Mississippi (3) (4), and at Pine Creek Reservoir, Oklahoma (2).

Local mixing improves the release water quality by inducing a jet of epilimnion water down to the release structure to dilute the hypolimnion water being released. The propeller used in References (2) and (3) was a 72-inch Acme Windmaster fan. This propeller pump is capable

of producing 1.8 m^3/sec at 19.1 rpm. Dortch and Wilhelms (4) performed a local destratification test at Lake Okattibbee (using the same propeller) and concluded that it caused a significant change in the quality of low-flow releases.

Hydraulic Modeling

Hydraulic modeling of the mechanical destratification by a propeller pump has been the main interest of hydraulic researchers at Oklahoma State University. Moretti and McLaughlin (5) have modeled the fluid dynamics of destratification using the Garton pump in a vertically distorted model of Ham's Lake constructed by Gibson (6). Using the model, Gibson (6) and Sharabianlou (7) concluded that prototype simulation by hydraulic modeling was successful when the Richardson number (or the related densimetric Froude number) and a nondimensional time scale are used as the modeling parameters. Givens (8) performed a hydraulic model study of local destratification using a propeller pump (Garton type). He developed dimensionless parameters to indicate that the released water quality as well as the penetration depth using normalized initial conditions for the propeller diameter, the relative magnitude of the propeller, the released flowrates, and the metalimnion location. Moon (9) performed a hydraulic model study of the near flowfield induced by an axial-flow propeller pump used to enhance the quality of water being released from the hypolimnion by diluting the released water with higher quality epilimnion water. He concluded that the dilution factor, DF, and penetration depth are functions of the densimetric Froude number, the nondimensional propeller diameter, the nondimensional propeller depth, the flow rate ratio of propeller flow rate and release flow rate, and the nondimensional metalimnion location. He successfully performed hydraulic

modeling of local destratification at Okattibee, Mississippi, using a scale model of the release structure in a laboratory. Buoyancy forces in reserviors are due to density gradients caused by temperature difference. Modeling thermal stratification is very difficult because of heat transfer and temperature controls required on the boundaries. The thermal stratification can be modeled by dissolved salt provided that the two fluids (of the model and prototype) have similar thermal and molecular diffusivity (10) or eddy-diffusivity.

Previous Theoretical and Numerical Analysis

There has been a continued interest in the theoretical analysis of a jet issuing into a density stratified environment. Baines (11) (12) studied the rate of entrainment through the end of a plume or jet which impinges on a density interface. He concluded that the entrainment flux into the plane must be a function of the local width, velocity, and buoyancy difference. He combined them into a single parameter, the Froude number (densimetric), Fr_d. Ditmars (13) studied the use of a pumping system to mix density-stratified impoundment by means of a buoyant jet. He developed a one-dimensional simulation technique to predict the changes in the density structure of an impoundment caused by mixing using a pumping system. Abraham and Eysink (14) investigated the case of a jet issuing vertically upwards into fluid with a density gradient. They introduced a theoretical approach to determine the ceiling level of a jet under the above mentioned conditions. Huber, Harleman, and Ryan (15) developed a mathematical model to predict the vertical temperature distribution in stratified reservoirs. Their model includes the effect of distribution of heat within the reservoirs by advection and

diffusion, heat source and sinks at boundaries, and internal absorption of solar radiation. Boulot and Daubert (16) developed a mathematical model of intrusion of salinity in stratified layers (salt wedge). The model deals with unsteady flows of two fluids with a small density difference. The model has been used to calculate the salt wedge in the grand Rhône, France. Comparisons of the results with measurements show the position of the salt wedge and its movement under the effect of tide. Difficulties of calibration and impossibility of getting data for a stationary salt wedge were reported.

Outline of the Thesis

This thesis presents work in the primitive-variable finite difference solution procedure for two-dimensional axisymmetric transient flows, with a primary interest in the steady state solution. Based on the Los Alamos SOLA (17) technique, the present work extends this to include the computation of mass diffusion and buoyancy forces. Complexities can be added as needed such as a non-uniform grid, turbulence, swirl, or a semi-implicit method for each time step (18). Predictions of the near flow field of a jet induced by an axial-flow propeller pump into a stratified environment are given in Chapter IV showing good agreement with the experimental data. This shows that a useful and valuable tool is now available to show the influence of design parameters on flowfield mixing.

CHAPTER II

THEORETICAL MODEL

The modeling and prediction technique presented in this work is the development of a primitive-variable finite difference procedure for two-dimensional axisymmetric flow to represent flows of stratified fluids. The technique is based on the Marker and Cell (MAC) method in the form of the SOLA algorithm (17). The computational code using an Eulerian finite difference formulation solves directly for the primitive pressure and velocity variables. In addition, the velocity components are positioned between nodes where pressure and other variables are stored. At each time step the time advanced values of U,V are substituted in the continuity equation and then the pressure and velocity are corrected through an iterative process until the continuity equation is satisfied.

The Governing Equations

For incompressible stratified fluid flow the partial differential equations in cylindrical (axisymmetric) coordinates of conservation of mass (continuity equation), momentum, and mass diffusion may be taken in conservative form as (18)

$$\frac{\partial U}{\partial x} + \frac{\partial V}{\partial y} + \frac{U}{x} = 0$$

$$\frac{\partial U}{\partial t} + \frac{\partial}{\partial x}(U^2) + \frac{\partial}{\partial y}(UV) + \frac{U^2}{x} = \frac{-1}{\rho_1}\frac{\partial P}{\partial x} + \frac{\mu}{\rho_1}\left(\frac{\partial^2 U}{\partial x^2} + \frac{\partial^2 U}{\partial y^2}\right.$$

$$+ \frac{1}{x} \frac{\partial U}{\partial x} - \frac{U}{x^2}) + g_x$$

$$\frac{\partial V}{\partial t} + \frac{\partial}{\partial x}(VU) + \frac{\partial}{\partial y}(V^2) + \frac{UV}{x} = \frac{-1}{\rho_1}\frac{\partial P}{\partial y} + g_y\left(\frac{\rho - \rho_1}{\rho_1}\right)$$

$$+ \frac{\mu}{\rho_1}\left(\frac{\partial^2 V}{\partial x^2} + \frac{\partial^2 V}{\partial y^2} + \frac{1}{x}\frac{\partial V}{\partial x}\right)$$

$$\frac{\partial m_1}{\partial t} + \frac{\partial}{\partial x}(m_1 U) + \frac{\partial}{\partial y}(m_1 V) + \frac{m_1 U}{x} = \frac{\mu}{\rho_1 \sigma_{sc}}\left[\frac{\partial^2 m_1}{\partial x^2} + \frac{\partial^2 m_1}{\partial y^2} + \frac{1}{x}\frac{\partial m_1}{\partial x}\right]$$

$$m_1 + m_2 = 1$$

$$\rho = m_1 \rho_1 + m_2 \rho_2 \qquad (1)$$

where

x = radial coordinates;

y = axial coordinates;

U,V = velocity components in x (= r) and y direction (ft/sec);

m_1, m_2 = mass fractions of two different density fluids, of densities ρ_1 and ρ_2 ($\rho_1 < \rho_2$);

μ = absolute viscosity (lbm-sec/ft^2);

σ_{sc} = Schmidt number;

ρ, ρ_1 = weighted average density and the reference density (slugs/ft^3);

g = gravitational acceleration = $(g_x, g_y) = (0, -32.2)$ (ft/sec^2); and

P = deviation from hydrostatic pressure.

Notice that the actual pressure $\bar{P}$ which is a function of depth and fluid motion has been replaced by two separate terms:

$$\bar{P} = P - g_y \rho h$$

$$-g_y \rho_1 h = \text{hydrostatic pressure}$$

where h is the depth below the surface and P is the deviation from the hydrostatic pressure. This simplifies the righthand side of the y-equation when both the pressure and buoyancy are small and this, among other things, reduces numerical error (see Appendix D).

The diffusion equation is used to calculate the mass fraction m_1 and m_2 and using this one can calculate the weighted average density and the release water quality (dilution factor).

The Flow Domain and Grid System

The flow domain shown in Figure 1 represents the physical problem and it has a vertical axis of symmetry provided with a downward flowing jet of fluid from the rotor disk (propeller). A vector velocity plot, in Figure 3, shows the flow field velocity in a typical computation cycle at t = 0.56 second to further illustrate the problem. Initially, two fluids occupy positions above and below the interface as shown, so that their mass fractions are $m_1 = 1$ and $m_2 = 0$ (for $h > h_1$, the height of the interface) and vice versa. The release gate of the dam is represented in Figure 4 by a circular opening in the bottom of the flowfield under the propeller. This may not represent exactly the release gate in the dam because of some structural details where the position of the release gate is on one side of the propeller and this cannot be represented in an axisymmetric flowfield. However, this representation will be fairly acceptable to represent the amount of release water, the position of the gate (roughly), and to calculate the release water quality

(dilution factor). The available volume of the flow domain is very limited and so as to allow the outlet of release water without dramatically decreasing the fluid level, there is an equal amount of input fluid shared between the top and bottom layers in amounts equal to the epilimnion and hypolimnion water released. The feeding is at two different locations in such a way that the epilimnion water is feeding through a circumferential opening into the upper layer and does not disturb the density profile. Also, the large circumferential opening allows the feeding to be at low velocity in order to cause no disturbance to the flow field. As with the epilimnion, hypolimnion water is fed into the bottom layer, as shown in Figure 4 which represents the mesh arrangement.

This feeding allows the fluid to maintain its level, thus simulating an infinite width or volume of water (as in the case of big lakes). The general mesh arrangement is shown in Figure 4 where the cylindrical region is divided into equal sized rectangular cell divisions with a width of Δx and height Δy. The mesh region containing fluid consists of IBAR cells in the x-direction which has the index i, and JBAR cells in the y-direction with the index j. The flow domain is surrounded by a single layer of fictitious cells on all sides to allow simulation of the required boundary conditions. These fictitious cells increase the total number of cells so that IMAX = IBAR + 2 and JMAX = JBAR + 2. A single cell is shown in Figure 2; the pressure and mass fractions m_1, m_2 are located at the cell center, and the radial and axial velocities on the right and top boundaries, respectively. Thus (see Figure 4), the normal velocities lie on the physical boundaries of the flow domain while the pressure and mass fractions are displaced half a cell interval inside the flow field boundary.

Boundary Conditions

The finite difference form of the governing equation (to be presented in Chapter III) are solved by a time-march procedure applied to the flow domain cells. Boundary conditions are imposed on the fictitious cells surrounding the mesh by setting appropriate velocity values in these cells.

The right boundary is a no-slip rigid wall with U = V = 0 on the boundary. Because of the locations of these variables, this is imposed via:

$$U_{IM1,J} = 0$$

$$V_{IMAX,J} = -V_{IM1,J} \qquad \text{(for all J)}$$

where IM1 = IMAX-1 and JM1 = JMAX-1.

The lefthand boundary is the axis of symmetry with free slip conditions and in this case the normal (radial) velocity U will be zero and tangential velocity V will have a zero normal gradient with $\frac{\partial V}{\partial x} = 0$. Thus

$$U_{1,J} = 0$$

$$V_{1,J} = V_{2,J} \qquad \text{(for all J)}$$

Free-slip conditions are taken also at the top boundary (along the free surface) with V = 0 and $\frac{\partial U}{\partial y} = 0$; no-slip conditions are taken at the bottom boundary where both U and V will be zero. The mass fraction boundary condition will have a zero normal gradient at all the boundaries. The boundary conditions are imposed on the velocities after each time step and after each sweep of the mesh during the pressure iteration (see Chapter IV). This includes the specification of known inlet and outlet

normal velocities. The propeller or the rotor disk has specified downward velocity values imposed at its location. The outlet flow (through the release gate) velocity is specified from the nondimensional flow rate ratio $Q^* = \frac{\text{Propeller flow rate}}{\text{Release flow rate}}$, since the propeller flow rate is specified. The inlet flow into the domain of interest is meant to allow re-entry of the released water in order to maintain the fluid level constant. Inlet flow velocities are specified so that the total mass of water inside the flow domain is constant. The inlet mass flow rate of epilimnion water is equal to its fraction of the release water multiplied by the release water mass flow rate. It is similar for the re-entry of hypolimnion water. The calculation is shown in detail in Chapter IV and the resulting velocities are imposed as boundary conditions for the next time-step.

CHAPTER III

SOLUTION PROCEDURE

The steps for one calculation cycle can be summarized in three steps:

1. Computing the velocity guesses for all the cells.

2. Adjusting the velocities and pressure iteratively to satisfy the continuity equation by making appropriate changes in the cell pressure until velocity divergence becomes zero.

3. When the convergence is achieved, the pressure and velocity values will be at the advanced time level and can be used to start calculation for the next time step.

The Finite Difference Equations

The finite difference technique used for the governing equation is based on the Marker and Cell (MAC) method (17), using the estimates of one-sided first derivatives, centered first derivatives, and centered second derivatives in representing the governing equations in the finite difference form. Subscripts n and (blank) are used to indicate t and $t + \Delta t$ time level, respectively. Most MAC reports use a fraction index for velocities located at the cell edges like $U_{i+1/2}$ to represent the radial velocity at the righthand face of the cell (I,J). In FORTRAN language fractional indexes are not allowed; therefore, the index of the cell will be used for all the variables located in edges or center of

the cell. In the equation the time derivatives are approximated by a one-sided derivative. Spatial derivatives are approximated by central differences using t-time level values. In representing the convection terms, the upstream differencing is required. The equation is now set for one forward time-step starting with initial values and boundary conditions through the mesh. A time-march process is then used to advance the computation to a steady-state final solution.

$$U_{i,j} = U^n_{i,j} + \Delta t \{\frac{1}{\Delta x} (P^n_{i,j} - P^n_{i+i,j}) + g_x - FUX - FUY - FUC + VISX\}$$

$$V_{i,j} = V^n_{i,j} + \Delta t \{\frac{1}{\Delta y} (P^n_{i,j} - P^n_{i,j+1}) + g_y - FVX - FVY - FVC + VISY\}$$

$$S_{i,j} = S^n_{i,j} + \Delta t \{- FMX - FMY - FMC + VIMX\} \qquad (2)$$

where $S_{i,j}$ is the symbol used for mass fraction m_1 in the computer program. The four terms on the righthand side of each equation, FUX, FUY, etc., are shown in Appendix B. The coefficient α in these terms (see Appendix B) is a constant that gives the desired amount of upstream (donor cell) differencing in the convective terms. It takes a value between 0.0 and 1.0, a value of zero changes the difference equations to the original MAC formulation (centered in space), but in this case instability problems arise. When α equals unity, this gives the full upstream or donor cell form which is stable (although introducing truncation or discretization errors) provided that the fluid is not allowed to cross more than one cell in one time step.

The new calculated velocities using conservation of momentum (Navier-Stokes equations) will not, in general, satisfy the continuity

equation. Expressed in the finite difference form, the continuty equation is:

$$\frac{1}{\Delta x}\,(U_{i,j} - U_{i-1,j}) + \frac{1}{\Delta y}\,(V_{i,j} - V_{i,j-1}) + \frac{1}{2\Delta x\,(i - 1.5)}\,(U_{i,j} - U_{i-1,j}) = 0 \qquad (3)$$

Iterative Procedure

The incompressibility condition is imposed by iteratively adjusting the cell pressure. If the divergence D of a cell (the lefthand side of the continuity equation) is positive, this corresponds to a net mass outflow from the cell, so the pressure is decreased to draw it back. If the divergence is negative, then there is a net flow of mass into the cell, so the cell pressure is increased to eliminate the flow. In this way the divergence of each cell can be driven to zero by adjusting the pressure iteratively, and this is done by sweeping the mesh rows from left to right starting with the bottom row. Terms in the equation are evaluated at a time-level $t + \Delta t$. The pressure change Δp used to drive the divergence D to zero is:

$$\Delta p = -D/[2\ \Delta t\ (1/\Delta x^2 + 1/\Delta y^2)] \qquad (4)$$

The new cell pressure $p + \Delta p$ is obtained by adjusting the velocity component on the four faces of the cell; this adjustment given by a linear analysis is:

$$\begin{aligned} U_{i,j} &= U_{i,j} + \Delta t\ \Delta p/\Delta x \\ U_{i-1,j} &= U_{i-1,j} - \Delta t\ \Delta p/\Delta x \\ V_{i,j} &= V_{i,j} + \Delta t\ \Delta p/\Delta y \end{aligned} \qquad (5)$$

$$V_{i,j-1} = V_{i,j-1} - \Delta t \, \Delta p/\Delta y$$

Substitution of Equation (5) in the divergence Equation (3) and solving for Δp gives Equation (4). The convergence of the iterations is achieved when the D value of each cell is less than ε; a prescribed small positive quantity in the order of 10^{-3} times the inlet mass flow rate can be adjusted to obtain higher accuracy. Convergence can be speeded up by multiplying Equation (4) by an over-relaxation factor ω where $1 \leq \omega \leq 2$. A value of 1.8 is often optimum in typical 15 x 15 grid sizes.

Imposition of Boundary Conditions

Boundary conditions are imposed on the velocities and mass fractions after each time step and after each pass through the mesh during pressure iterations. Calculations of the inlet velocities, weighted average density, and dilution factors are done each time step starting with calculation of the propeller flow rate.

$$Q_p = V_p \, \pi \, r^2 = V_p \, \pi \, (\Delta x)^2$$

where $r = \Delta x$ from Figure 4. The nondimensional flow rate, Q^*, is the ratio between propeller flow rate and release flow rate, Q_{rel}:

$$Q_{rel} = Q_p/Q^*$$

and the release water velocity will be

$$V_{rel} = Q_{rel}/\pi R^2 = Q_{rel}/\pi (2\Delta x)^2$$

where

$$R = 2\Delta x \text{ (from Figure 4)}$$

$$= (IREL - 1)\Delta x$$

Then the epilimnion and hypolimnion inlet flow rates will be calculated using release water velocity and mass fractions. The released epilimnion water flow rate will be

$$Q_e = \sum_{i=1}^{i} M_{1i} \, (\pi R_i^2 - A_i) \, V_{rel}$$

where

$$A_i = \pi R_{i-1}^2$$

and the released hypolimnion flow rate is

$$Q_h = \sum_{i=1}^{i} M_{2i} \, (\pi R_i^2 - A_i) \, V_{rel}$$

where M_{1i} is the mass fraction of the epilimnion water and M_{2i} is the mass fraction of the hypolimnion water. Then the input velocity for epilimnion (feeding in the top layer) is:

$$U_{Te} = Q_e / 2\pi (IBAR) \Delta x \; (h) \Delta y$$

and for hypolimnion (feeding in the bottom layer) is:

$$U_{TB} = Q_h / 2\pi (IBAR) \Delta x \; (h) \Delta y$$

where $(IBAR)\Delta x$ is the radius of the flow field and $(h)\Delta y$ is the inlet flow circumferential opening height; it is the same for the top and bottom inlet openings.

Then the release water density is calculated using Q_e and Q_h:

$$\rho_{rel} = \frac{Q_e \, \rho_e + Q_h \, \rho_h}{\pi R^2 \, V_{rel}}$$

Then the dilution factor can be easily calculated as follows:

$$DF = \frac{\rho_{rel} - \rho_h}{\rho_e - \rho_h} = \frac{\rho_{rel} - \rho_2}{\rho_1 - \rho_2}$$

The dilution factor represents the percentage of epilimnion water in the release water; in other words, it represents the release water quality. The dilution factor, DF, has a maximum value of 1.0 when the release water consists of epilimnion, i.e., $\rho_{rel} = \rho_e$. The minimum value for DF is zero, and this means the release water is made up of hypolimnion water, i.e., $\rho_{rel} = \rho_h$.

Convergence and Stability

Convergence of the finite difference equations to the steady-state solution is established by taking many forward time steps. It has been found that the solution comes to a steady state condition after about 300 time steps which are equal to a nondimensional time $t^* = t/t_c$ of 6.6, where $t_c = \frac{\text{volume under the propeller}}{\text{propeller flow rate}}$. The choice of time increment must be restricted (for stability) in two ways. First, fluid should not pass through more than one cell in one time step. So Δt must be less than (usually 0.25 to 0.33 times) the minimum cell transit time taken over all cells.

$$\Delta t < \min\left\{\frac{\Delta x}{|U|}, \frac{\Delta y}{|V|}\right\}$$

When a nonzero value of kinematic viscosity is used, the momentum should not diffuse more than one cell in one time step; a linear stability analysis shows

$$V\Delta t < \frac{1}{2}\frac{\Delta x^2 \Delta y^2}{\Delta x^2 + \Delta y^2}$$

When the time increment Δt satisfies the above two conditions, then the upstream (donor cell) differencing can be achieved by choosing α larger than (1.2 to 1.5 times) the righthand side of the inequality:

$$1 \geq \alpha > \max \left(\left| \frac{U\Delta t}{\Delta x} \right|, \left| \frac{V\Delta t}{\Delta y} \right| \right)$$

The maximum value of α is 1.0. This will provide stability at the expense of introducing diffusion-like truncation errors. Figure 5 shows the effect of variation of α on calculated mass fraction m_1 at some locations in the flow field. A value of $\alpha = 0.6$ is being used in this program. Initial velocity and field velocity do not satisfy the continuity equation during the first time step. If these velocity values are used immediately in the diffusion equation, gross errors will occur in the computed m_1, mass fractions values, and hence concentration values. These obvious errors may be reduced by shortening the time step and/or not allowing computation of m_1, until the first short time step has been accomplished and new velocities (which do satisfy the continuity requirement) have been found. The latter approach was found to be more accurate and it has been used.

During computations the axisymmetric cylindrical finite difference form of the mass diffusion equation exhibited an unstable behavior, and the calculated values of the mass fraction m_1 far exceeded the value of 1.0 (which is the maximum possible value for the mass fraction m_1 or m_2); furthermore, this m_1 computation diverged.

In spite of the axisymmetric cylindrical finite difference form of the mass diffusion equation, the two-dimensional version was stable and the m_1 computation did converge. This indicated that the source of errors was additional terms occurring in the axisymmetric cylindrical

polar form of the equations. Thus the new terms of the equation (in conservative form) were examined. It was noticed that errors occurred when Using an upwind (donor cell) (19) difference form for the cylindrical term Um_1/x. Normally this aids stability at the expense of a slight inaccuracy. However, stability was no problem in this case and so the centered difference form was used for this particular term. The computation was stable and converged.

Accuracy

Accuracy is established by using small space and time intervals. Choice of the interval size will depend on the expense of computer time. However, the mesh increments must be chosen small enough to resolve the expected spatial variations in all dependent variables taking into consideration, of course, computing time and memory requirement limitation.

The main dynamic effect of the flow field is simulated; however, the effect of turbulence should be inspected for any significant changes it may have on the flow field. In order to do that, an algebraic turbulent viscosity model is considered to calculate the order of magnitude of the eddy (turbulent) viscosity; the Prandtl's mixing-length model

$$\mu_t = \rho \, \ell_m^2 \left| \frac{\partial U}{\partial y} \right|$$

where ℓ_m is the mixing length. The mixing length, ℓ_m, for a round jet in a stagnant surrounding (20) is

$$\ell_m = 0.075 \, \delta$$

where δ is the jet half width.

So the turbulent viscosity for the hydraulic model using its data and dimensions (which is the same for the computer model) at a point under the propeller which is chosen to give the maximum eddy viscosity value will be:

$$\mu_t = \frac{62.4}{32.2} (0.1875 \times 0.075)^2 \left|\frac{0.7}{0.1875}\right| = 1.43 \times 10^{-3}$$

The laminar dynamic viscosity used was $\mu = 2.73 \times 10^{-5}$ and so the ratio between μ_t and μ will be

$$\frac{\mu_t}{\mu} = 52$$

which is very small to cause a significant difference in the solution. This value for eddy viscosity was tested by using it throughout the entire flow field instead of the laminar viscosity, and a difference of (5 percent less than experimental and predicted results) was noticed. The case tested was for $Fr_d = 1.86$, $Q^* = 0.44$, and $D^* = 0.211$. The ratio was increased to 100 and the difference was about 7.5 percent less. Compared to an experimental data uncertainty of 15 percent, the turbulence model effect looks so small that we can use the present model (which models the dynamic effect and not the turbulence effect) effectively to predict the flow field. Another important thing is that the present process is different from the lake mixing, where the goal is to mix the whole lake with no release water. In this case the turbulence effect is more effective than the case for local destratification with release water outflow where released water will reduce the mixing effect.

The propeller used in the hydraulic model is an axial-flow propeller. The jet is considered axial and circular although it may have some

nonuniform swirl. The computer model considering an axial circular jet in the computations gave good predictions compared to the experimental results. This is an indication to the weak effect of swirl.

CHAPTER IV

RESULTS AND DISCUSSION

The results presented and discussed in this chapter refer to computer predictions made for low speed laminar nonswirling stratified flows in an axisymmetric simulation. Predictions were made for the effect of time, densimetric Froude number Fr_d, flow rate ratio Q*, normalized diameter D*, and the metalimnion location Z_T^*, on the dilution factor, DF. Also, the effect of densimetric Froude number on penetration depth Z_p^* is presented. All experimental data used for comparison purposes are from a previous study (9), except for Figure 28 which was performed during this study.

Dilution Factor as a Function of Time

The time required for the density of the release water to change (from the hypoliminion density value) is in the order of nondimensional time t* = 1. This means that the jet penetrated as far as the release gate during this time period. Also in this period of time the dilution factor increases from zero to a maximum value and then levels off to a steady state constant value, as shown in Figure 6. The t* value required for the jet to penetrate to the bottom is a storing function of Fr_d. It can be seen from the figure that the time required for the dilution factor to reach steady state is t* = 4.88 (for a densimetric Froude number of 1.58). This is different for other values of Froude number.

Dilution Factor as a Function of Fr_d

The dilution factor is an indicator of the release water quality; it represents the percentage of epilimnion in the release water. The dilution factor is a function of several parameters, namely, the densimetric Froude number Fr_d, the normalized propeller diameter D*, the flow rate ratio Q*, the nondimensional metalimnion depth Z_t^*, and penetration depth Z_p^*. Figures 7 through 18 show the dilution factor as a function of densimetric Froude number for different values of Q* and D*, and show the prediction along with the experimental data of the hydraulic model of the flow field. Figures 7 through 9 show the dilution factor for D* = 0.211 and different values of Q*. In Figure 7, where Q* = 0.44, the prediction shows a good agreement with the experimental data, where the dilution factor drops to zero at Fr_d = 0.75 for both models. However, the maximum value of the dilution factor predicted is lower than the experimental data (6 percent lower).

Figure 8, for Q* = 2.50, shows a good agreement with experimental data, where the maximum value of the dilution factor predicted is equal to the experimental value. Dilution factor drops to zero at Fr_d = 0.925 for both computer and hydraulic models. However, at Fr_d = 1.12, the predicted value of DF shows a higher value than the experimental data. This can be explained by the different position of the release gate in the computer model (see Chapter II). Figure 9, for Q* = 0.17 (high release flow rates), shows a very close low value of DF for all values of Froude number. Prediction shows almost the same values as the experimental data, except they are increasing with Froude number while experimental values are decreasing. This is perfectly acceptable where we

expect the dilution factor to increase with Fr_d. Figures 10 through 13 show the dilution factor for D* = 0.183 and different values of Q*. In Figure 10, for Q* = 0.75, predictions agree with experimental data very well above Fr_d = 1.25; meanwhile below this value, a slight difference of about 4 to 12 percent higher than experimental values was noticed. The value of Fr_d, where DF drops to zero, is lower than experimental values (5 percent lower). The same general good agreement is displayed by Figure 11 for Q* = 0.20, although at Fr_d = 1.40 the experimental value of DF is slightly higher than predictions.

The predictions in Figure 12, for Q* = 0.30, are lower than the experimental data of the hydraulic model at Fr_d = 1.40 and 2.10. This can be explained by the position of the release gate which is right under the jet, and because of the high release water flow rate compared to the propeller flow rate. This extracts much of the hypolimnion (bottom water) through the annular opening (annular opening is used for D* = 0.183 and 0.131, in order to model the release gate area because of the limitation of the axisymmetric model) which is different in the hydraulic model, where the release gate on the side of the jet can extract more of the epilimnion water than the annular lower opening.

When we have a low release water flow rate Q* = 2.50, this means that more mixing is taking place at the release gate which means a high value of dilution factor, and indeed we have a higher value of DF in Figure 13. In this case the prediction is higher because the low release flow rate allows the jet to flow away radially in all directions. This will enable the annular opening to have more epilimnion water than the release gate of the hydraulic model, which is on one side only.

Figures 14 through 16 represent the dilution factor as a function of Fr_d for D* = 0.131 and different values of Q*. Predictions in Figure 14, for Q* = 0.44, show a somewhat similar behavior to Figure 10 in which the Fr_d value, where DF drops to zero, is lower than the experimental value; this can be referred to the position of the release gate as mentioned before. This effect of the position (at high release water,flow rate) gives an earlier start for the dilution at a lower Froude number than experimental data, but as Fr_d increases and reaches a constant value, the experiment gives a high dilution factor value (this was discussed previously in Figure 12).

Figure 15, for Q* = 0.18, is very similar to Figure 12, and the discrepancy with the experimental data can be explained in the same way. As for Figure 16, for Q* = 2.60, it is somewhat similar to Figure 13, although discrepancies with experiments are greater at low Froude number. The diameter effect on the Fr_d value, when mixing starts and thus DF, can be observed from the formally discussed figures, where for D* = 0.211 DF starts at a Fr_d value of 0.80, for D* = 0.183 DF starts at a Fr_d value of 1.10, and for D* = 0.131 DF starts at Fr_d value of 1.50. Meanwhile, the prediction starting value of the dilution factor is at Fr_d between 0.80 and 1.00 for all diameters. This is because in the hydraulic model (with the release gate on one side) as the jet diameter decreases the distance between the jet boundary and the release gate increases, which delays the starting value of the dilution factor where in the computer model the gate is under the propeller. Thus, the propeller's normalized diameter D* has no effect on the starting value of Fr_d when mixing takes place in the release water.

Figures 17 and 18 are for D* = 0.117, where Figure 18, for Q* = 0.17, is very similar in behavior to Figures 11 and 12 and can be explained very much the same way as the two mentioned figures.

Figure 17, for Q* = 0.43, has a great discrepancy with experimental data for all values of Froude number except at Fr_d = 2.10, where the two graphs coincide. The thing that prediction graph is similar in behavior to all other graphs predicted and experimental where it has a concave curvature (downward), while the experimental graph in Figure 17 is concave upward and then downward after the inflection point at Fr_d = 2.10. This favors the prediction graph from this point of view; however, experiments give a higher value for DF (at Fr_d = 2.10 and higher). This can be explained the same way as in Figure 18.

Dilution Factor as a Function of Q*

The relationship between the dilution factor and the flow rate ratio Q* are represented in Figures 19 through 21. Figure 19 shows the dilution factor as a function of Q* for D* = 0.211 and Fr_d = 1.00 and 2.00. The dilution factor is strongly dependent upon Q* for Q* < 0.6 where as Q* increases the release flow rate decreases. This means more mixing will be allowed to take place near the release gate (bottom). Thus higher dilution factor predictions show good agreement with experiments for Fr_d = 2.0, but for Fr_d = 1.0 the two graphs agree for Q* < 0.9. Then the experimental graph starts dropping (this is explained in the discussion of Figures 8 and 13).

Figure 20, for D* = 0.183, shows a greater discrepancy between prediction and experiments, especially at Fr_d = 1.0 for Q* > 0.3; this is because of the diameter effect where mixing starts at higher Froude

number as D* decreases. This effect is not valid for the computer model, as discussed before in Figures 14 and 15. Figure 21, for D* = 0.131, is very similar in behavior to Figure 20, where the diameter effect (at higher values of Q*) is shown in this graph also at Fr_d = 1.50 (higher than Fr_d for D* = 0.183) and this can be shown very clearly in Figure 16. Predicted values of the dilution factor are higher than experimental values for high Q*; this is explained in the discussion of Figure 13. Figure 21, for D* = 0.117, shows predictions for the dilution factor, and the behavior is somewhat similar to Figure 19.

Dilution Factor as a Function of D*

The normalized diameter D* effect on the dilution factor is shown in Figures 22 and 23 for Q* = 0.44 and 2.50, respectively. Figure 22, for Q* = 0.44, shows an agreement in behavior between predictions and experiments for Fr_d = 1.5 and 2.0. The low value of dilution factor at D* = 0.117 is referred to the diameter effect on Froude number value to begin mixing at the release gate which was discussed before. The figure further shows that for this value of Q* (0.44), a normalized diameter D* value of 0.131 gives the best results for experimental data and predictions for a Froude number value of 2.0.

The same value of D* of 0.131 still gives the best results (maximum dilution factor) for Q* = 2.50 in Figure 23 for predictions, but for the experimental data it is entirely different. First, at Fr_d = 1.50 the diameter effect on the starting value of Fr_d is very clear at D* = 0.131 for the experimental graph, while the predictions are not affected by such an effect, as explained previously. Second, at Fr_d = 2.0 the experimental graph gives maximum dilution factor at D* = 0.211, where as

the diameter D* increases the momentum flux increases (for high propeller flow rate or high Q*). The reason the prediction gives high values at D* = 0.131 and D* = 0.183 at this value of Q* is explained in the discussion of Figure 13. In addition, for D* = 0.117 and D* = 0.211 the release gate was not annular because the hydraulic release structure was different from the structure for D* = 0.183 and 0.131, where the Cave Run release structure was used for D* = 0.211 and 0.117; the Okattibbee release structure was used for D* = 0.183 and 0.131.

Dilution Factor as a Function of Z_T^*

The relation between the dilution factor and the normalized metalimnion location is presented in Figure 29. The location of the metalimnion has a strong effect on the penetration depth and thus the dilution factor. As the metalimnion (interface) height (above the base) increases, buoyancy forces increase and this will hinder the jet penetration and thus the dilution factor (which is a function of the penetration depth Z_p^*).

The effect of the metalimnion location can be shown in the expression for the penetration depth prediction

$$V_y^2 = V_o^2 \left(\frac{CD}{y}\right)^2 - 2g \int_{ht}^{y} \frac{\rho_b - \rho_o}{\rho_o} dh \qquad y \geq CD;\ y > ht$$

where $(H - \overline{h_t})$ is the metalimnion location height above the base. The equation shows that the second term which represents the buoyancy force is a function of $\overline{h_t}$ and y the penetration depth.

Penetration Depth Prediction

The penetration process of the jet is shown in Figures 24 and 25 with a nondimensional time t* increment, where $t^* = t/t_c$ and t_c, the characteristic time, is equal to

$$t_c = \frac{\text{Volume under the propeller}}{\text{Propeller flow rate}}$$

The two figures show the location of the interface (metalimnion) in the flow field for $Fr_d = 0.35$ in Figure 24 and $Fr_d = 1.05$ in Figure 25 during a t* value of 1.37. The figures show very clearly that at the low value of Froude number the jet stopped penetrating at a certain depth and did not penetrate further as the time increases. At $Fr_d = 1.05$ the jet did penetrate to the bottom of the flow field at $t^* = 1.37$. The characteristic time for the two cases was $t_c = 1.46$ seconds.

Penetration depth as a function of densimetric Froude number is shown in Figures 26 and 27. In Figure 26, for $D^* = 0.211$, it is evident that the prediction and the experimental data of the hydraulic model match exactly. The reason we did not have such an excellent agreement in the other cases was because they involve the release gate structure difference between the computer and hydraulic model, where this has no effect (in this case) because the release flow rate is zero, $Q^* = \infty$. The figures show also some predictions calculated using an empirical expression for the penetration depth (Appendix C):

$$V_y^2 = V_o^2 \left(\frac{CD}{y}\right)^2 - 2g \int_o^y \frac{\rho - \rho_o}{\rho_o} dy \qquad \text{for } y \geq CD$$

The penetration can be calculated using this equation by setting $V_y = 0$

(stagnation point) and solving for y. The penetration depth predictions made using this equation showed a difference (up to 5 percent) from the experimental data, as shown in Figures 26 and 27.

Figure 27 presents some experimental data of the hydraulic model for $D^* = 0.175$ and $Z_T^* = 0.40$ (where Z_T^* used for all former cases was 0.6) along with predictions made using the preceding equation. The predictions shows good agreement for $Fr_d > 0.75$; below that a difference of 4 to 12 percent was noticed where predictions were slightly higher than experiments.

Modeling of the flow field in the computer model was performed by matching the densimetric Froude number, but the physical dimensions used in the hydraulic model were actually matched (and not the nondimensional parameters such as D^*, Q^*, and Z_T^*). The velocity used was chosen as 0.7 ft/sec, an average of the velocities used in the hydraulic model experiments. The velocity was kept constant and different stratification ($\Delta\rho/\rho$) values were used to match the densimetric Froude number (see Appendix E).

Most of the predictions in this study were run for a value of $L^*/D^* = 1.0$, where L^* is the nondimensional propeller depth except for $D^* = 0.211$, where a value of $L^* = 0.183$ was used in this case.

The release gate area used in the computations was increased in order to slow down the velocities on the bottom near the gate, but the release water flow rate, Q_{rel}, was not changed. This change in area was used to eliminate some of the differences between the release structure in the hydraulic model and the axisymmetric model, where the velocities (on the bottom under the jet) are higher in the latter model because the release gate is under the jet.

Predictions for large D* values (D* = 0.211 and 0.183) were more accurate than the other small D* values. This is due to the difficulty in modeling the release area for small values of D* (where the grid size is taken as a function of D*). This can be solved by using a very fine grid; however, this may be very costly.

CHAPTER V

CONCLUSIONS

Summary

Computer simulation of the near flow field of a jet induced by an axial-flow propeller pump (used to mix the epilimnion high quality water with the released hypolimnion water) is accomplished by solving the governing equations of the flow field. The two-dimensional Los Alamos SOLA prediction technique (with a finite difference scheme based on the Marker and Cell method) has been modified to include the computation of mass diffusion and buoyancy forces in an axisymmetric stratified flow. The finite difference equations are in terms of the primitive pressure-velocity variables. Prediction and interpretation of the experimental data show that simulation of the flow field is adequate for design purposes; futhermore, the simplified code represents a useful (low cost) basic tool to show the influence of the different design parameters on the flow field.

Conclusions

The conclusions derived from this study may be stated as follows:

1. A prediction procedure for an axisymmetric stratified flow has been developed to predict the dilution factor (released water quality) and the jet penetration depth.

2. The main dynamic effect was modeled using continuity, Navier-Stokes, and mass diffusion equations. The turbulence effort on the flow field was shown to be small for the velocities used in the computations; therefore, the use of a turbulence model was not needed at this time.

3. The computer simulation on the basis of a circular jet without swirl gives adequate results for penetration depth and dilution factor within the limits of accuracy of currently available data.

4. Predictions were made of the effect of densimetric Froude number Fr_d, flow rate ratio Q*, normalized propeller diameter D*, and metalimnion location Z_T^*, on the dilution factor DF, for a low speed laminar nonswirling flow in an axisymmetric stratified flow field simulation, and the effect of some of the above parameters on the penetration depth are as follows:

a. The densimetric Froude number $Fr_d = V/[g(\Delta\rho/\rho)H]^{1/2}$ was the major modeling parameter, and it was adequate for comparing the computer model and the hydraulic model. The dilution factor is a strong function of Fr_d when Fr_d is less than 1.5 for large D* values (0.211 and 0.183), and Fr_d is less than 1.8 for small D* values (0.131). For values of Fr_d larger than 1.5 for (D* = 0.211 and 0.183), and 1.8 (D = 0.131) the dilution factor is a very weak function of Fr_d.

b. The dilution factor is a strong function of Q* for Q* values less than 0.6, and when Q* is greater than 0.6 the dilution factor is a weak function of Q*.

c. A small normalized propeller diameter D* value (0.131) gives a maximum dilution factor at low Q*, and large D* gives a maximum value for high values of Q*.

d. The effect of D* on the value of Fr_d where mixing starts (DF begins to exceed zero) in the hydraulic model was not adequately simulated by the axisymmetric computer model.

e. The dilution factor DF tends to decrease as the metalimnion (interface or thermocline) height above the base increases.

f. Computer predictions of the penetration depth as a function of Fr_d was accurate (as compared with the very limited available experimental data) in the absence of release flow. Penetration depth Z_p^* is a strong function of densimetric Froude number.

5. An empirical expression for prediction of the penetration depth has been introduced; it exhibits good prediction compared with experimental data.

Recommendations for Further Study

Recommendations for further study of the flow field may be stated as follows:

1. To model an off-center release outlet by means of a three-dimensional model in order to represent the release structure correctly.

2. To study the effect of trubulence on the flow field for high propeller velocities.

3. To study the possible effect of swirl for high propeller velocities by solving for the swirl velocity along with axial and radial velocities using the Navier-Stokes equations.

A SELECTED BIBLIOGRAPHY

(1) Symons, J. M., W. H. Irwin, E. L. Robinson, and G. G. Robeck. "Impoundment Destratification for Raw Water Quality Control Using Either Mechanical or Diffused-Air-Pumping." Journal of the American Water Works Association, Vol. 59, No. 10 (October, 1967), pp. 1268-1291.

(2) Garton, J. E., and R. C. Peralta. "Water Quality Enhancement by Point Destratification, Gillham Lake, Arkansas." A special report of the OWRII, February, 1978.

(3) Garton, J. E., and H. R. Jarrell. "Demonstration of Water Quality Enhancement Through Use of the Garton Pump." Supplement to the Technical Completion Report, OWRII C-5228-A, March, 1976.

(4) Dortch, M. S., and S. C. Wilhelms. "Enhancement of Releases From a Stratified Impoundment by Localized Mixing, Okattibbe Lake, Mississippi." Misc. Paper H-78-1. Hydraulics Laboratory, U.S. Army Engineers, Waterways Experiment Station, Vicksburg, Mississippi, January, 1978.

(5) Moretti, P. M., and D. K. McLaughlin. "Hydraulics Modeling of Mixing in Stratified Lakes." Journal of the Hydraulics Division, ASCE, Vol. 103, No. HY4, Paper 12868 (April, 1977), pp. 367-380.

(6) Gibson, T. A. "Investigation of Artificial Lake Destratification --A Hydraulic Model Study." (Unpublished M.S. thesis, Oklahoma State University, 1974.)

(7) Sharabianlou, N. "Hydraulic Modeling of Mechanical Destratification of Lakes." (Unpublished M.S. thesis, Oklahoma State University, 1975.)

(8) Givens, M. R. "Hydraulic Modeling of Local Destratification of Lakes Using Propeller Pumps." (Unpublished M.S. thesis, Oklahoma State University, 1978.)

(9) Moon, J. J. "Enhancement of Release Water Quality by Localized Mixing--A Hydraulic Model Study." (Unpublished M.S. thesis, Oklahoma State University, 1978.)

(10) Turner, J. S. "The Influence of Molecular Diffusivity on Turbulent Entrainment Across a Density Interface." Journal of Fluid Mechanics, Vol. 33 (April, 1968), pp. 639-656.

(11) Baines, W. D. "Entrainment by a Plume or Jet at a Density Interface." Journal of Fluid Mechanics, Vol. 68 (April, 1974), pp. 309-320.

(12) Baines, W. D. "Turbulent Buoyant Plumes." Heat Transfer and Buoyant Convection. Vol. 1. Washington, D.C.: Hemisphere Publishing Corporation, 1977, pp. 235-250.

(13) Ditmars, J. D. "Mixing of Density Stratified Impoundments With Buoyant Jets." Report No. KH-R-22. W. M. Keck Laboratory of Hydraulics and Water Resources, California Institute of Technology, Pasàdena, California, September, 1970.

(14) Abraham, G., and W. D. Eysink. "Jets Issuing Into Fluid With a Density Gradient." Journal of Hydraulic Research, Vol. 7 No. 2 (April, 1969), pp. 145-175.

(15) Huber, W. C., D. R. F. Harleman, and P. J. Ryan. "Temperature Prediction in Stratified Reservoirs." Journal of the Hydraulics Division, ASCE, Vol. 98, No. HY4 (April, 1972), pp. 645-665.

(16) Boult, F., and A. Daubert. "Mathematical Model of the Recovery of Salinity Stratification in the Unsteady Flow Regime." International Association for Hydraulic Research Cong. Proc. 13 (1969), pp. 353-362.

(17) Hirt, C. W., B. D. Nichols, and N. C. Romero, SOLA. "A Numerical Solution Algorithm for Transient Fluid Flows." Report LA-5882. Los Alamos Scientific Laboratory, Los Alamos, New Mexico, 1975.

(18) Croft, D. R., and D. G. Lilley. Heat Transfer Calculations Using Finite Difference Equations. London: Applied Science Publishers, 1977.

(19) Hirt, C. W. "Heuristic Stability Theory for Finite-Difference Equations." Journal of Computational Physics, Vol. 2, No. 4 (June, 1968), pp. 339-355.

(20) Forestall, W., and A. H. Shapiro. "Momentum and Mass Transfer in Coaxial Gas Jets." Journal of Applied Mechanics, Vol. 17 (1950), p. 399.

(21) Schlichting, H. Boundary Layer Theory. 6th ed. New York: McGraw-Hill, 1968.

(22) Moretti, P. M. "Investigation of Alternative Mixing Devices for Lakes by Model Studies." Technical Completion Report, OWRRIA -050-Oklahoma. (Part 1) Technical completion Report ER 76-ME-2, School of Mechanical and Aerospace Engineering, Oklahoma State University, Stillwater, July, 1979.

APPENDIX A

FIGURES

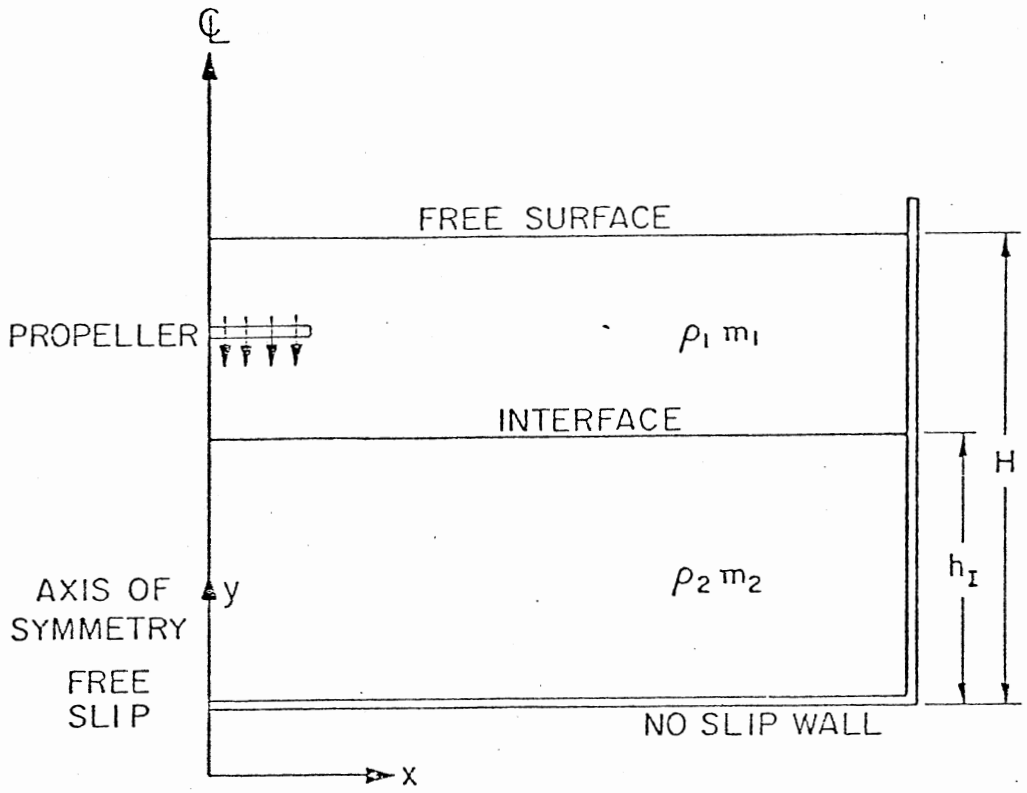

Figure 1. Physical Flow Domain

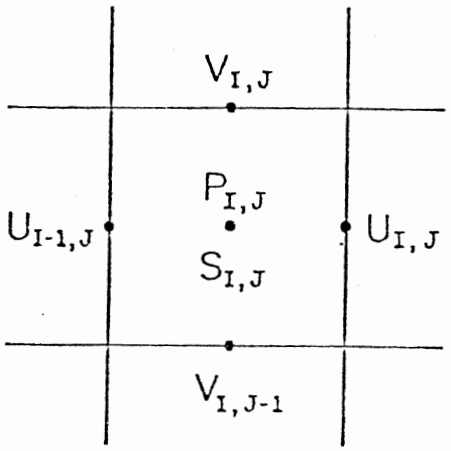

Figure 2. Arrangement of Variables in a Typical Cell

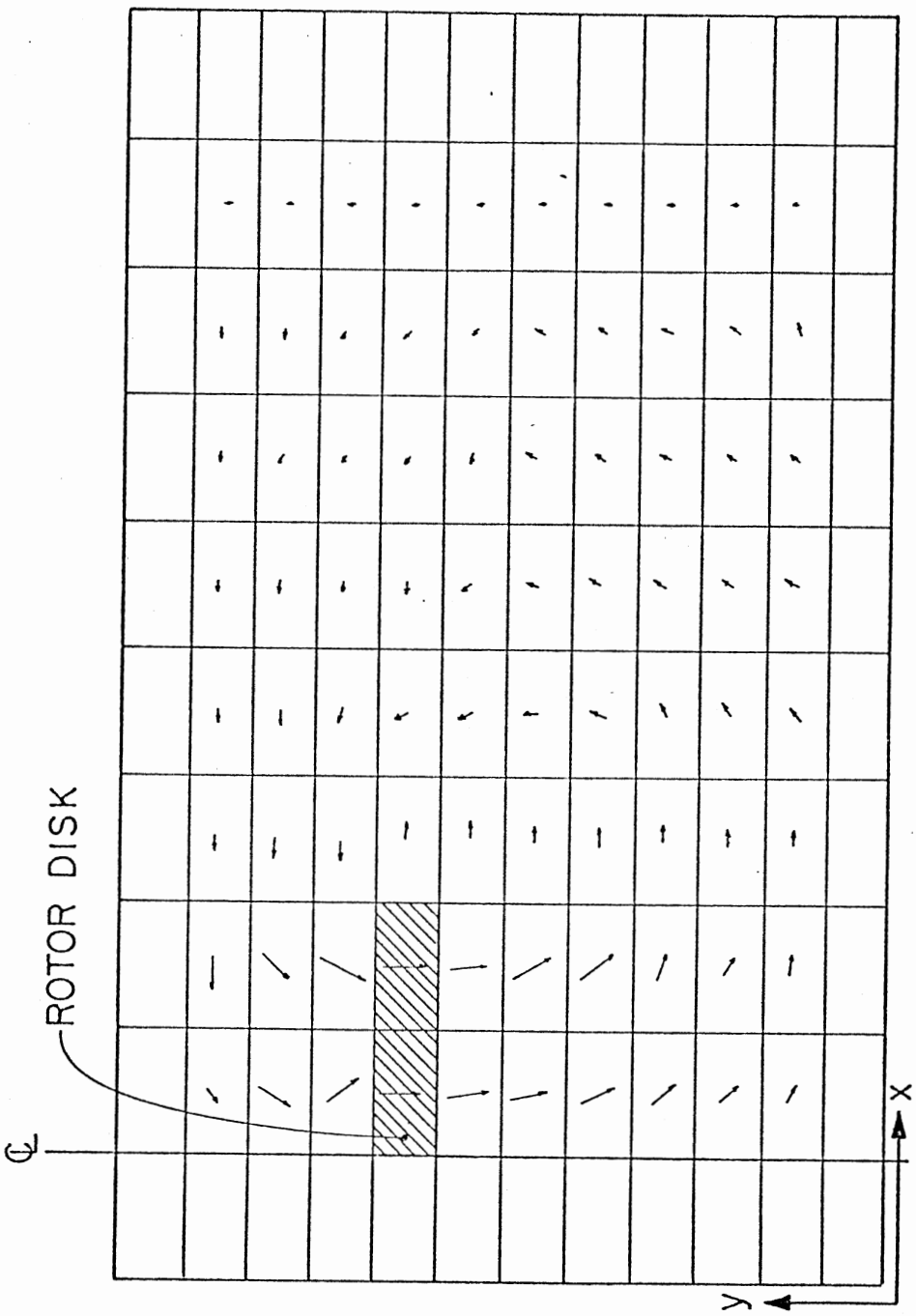

Figure 3. Velocity Vector Plot

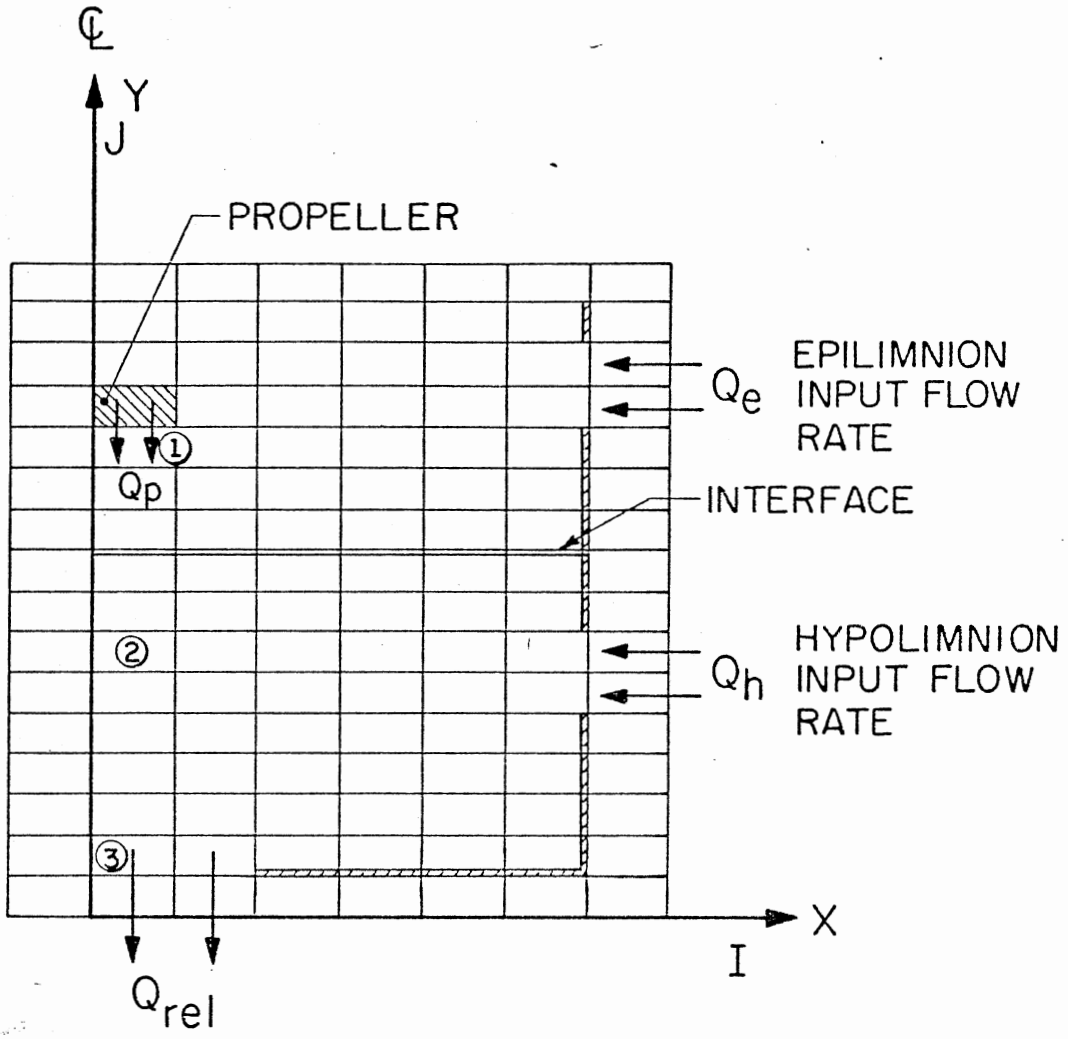

Figure 4. General Mesh Arrangement Showing New Input and Output Boundary Conditions

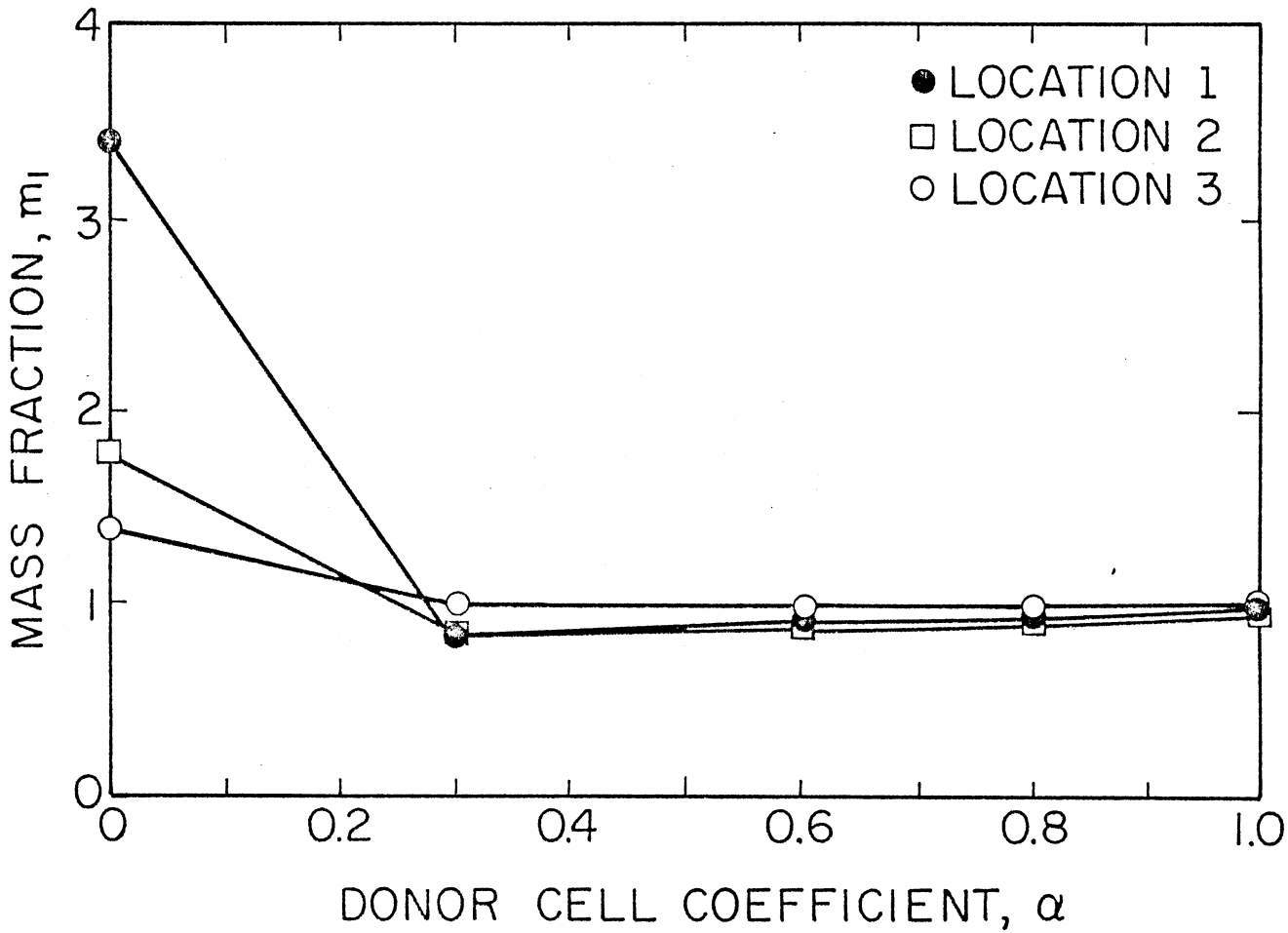

Figure 5. Effect of Donor Cell Coefficient on Calculated Mass Fraction m_1 at Three Locations

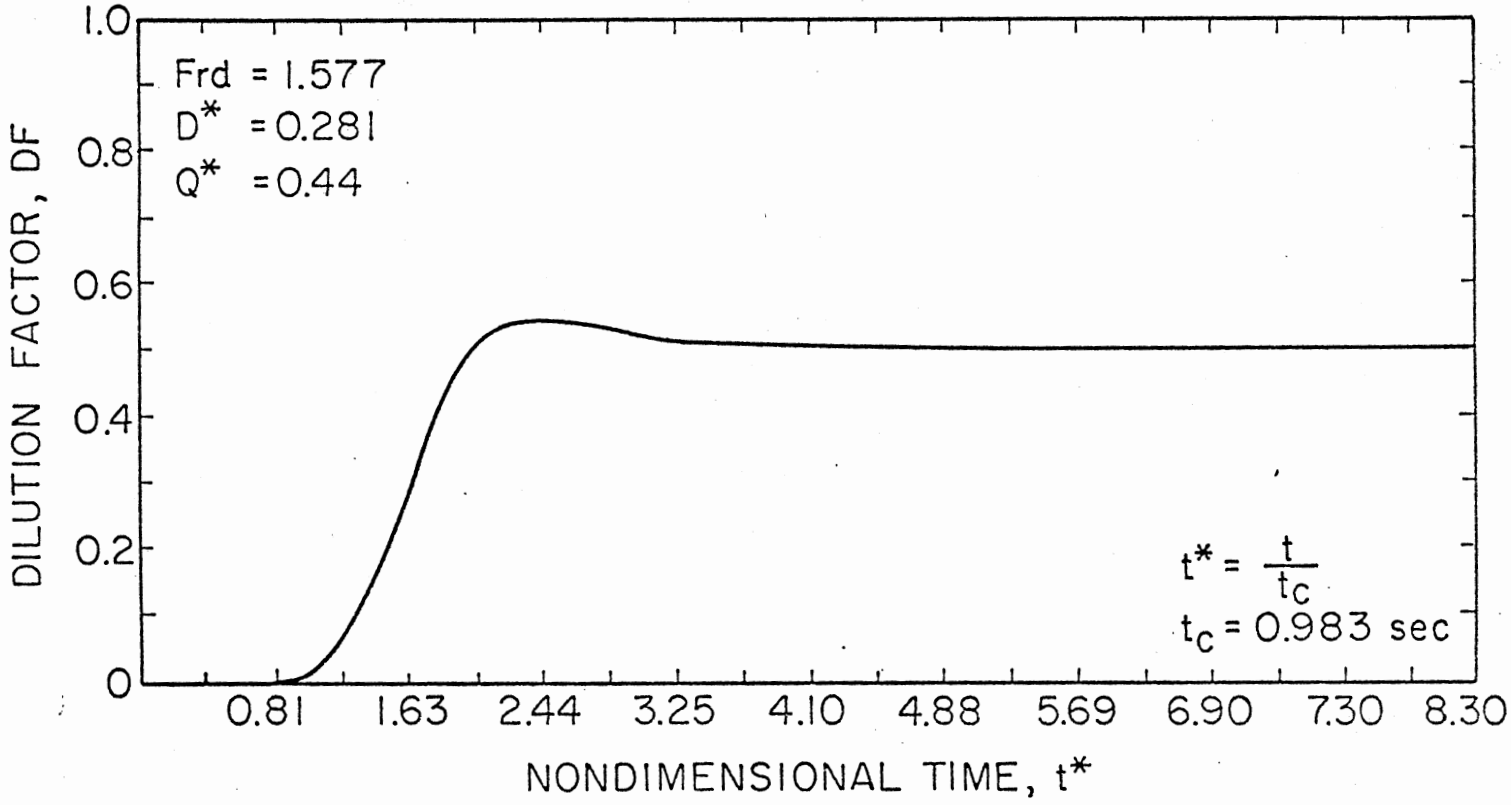

Figure 6. Dilution Factor, DF, As a Function of Nondimensional Time, t*

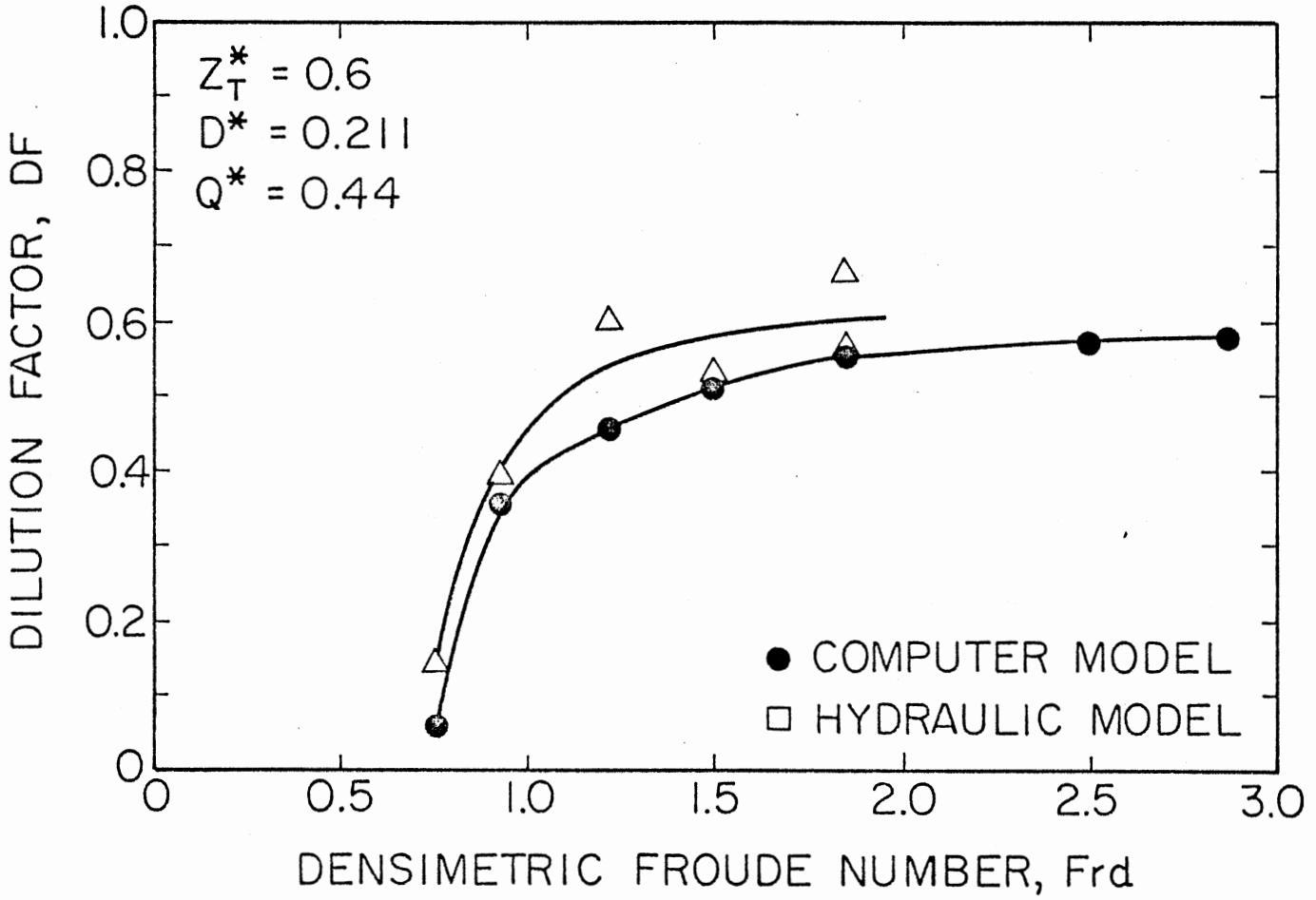

Figure 7. Dilution Factor, DF, As a Function of Densimetric Froude Number, Fr_d, at D* = 0.2111, for Q* = 0.44

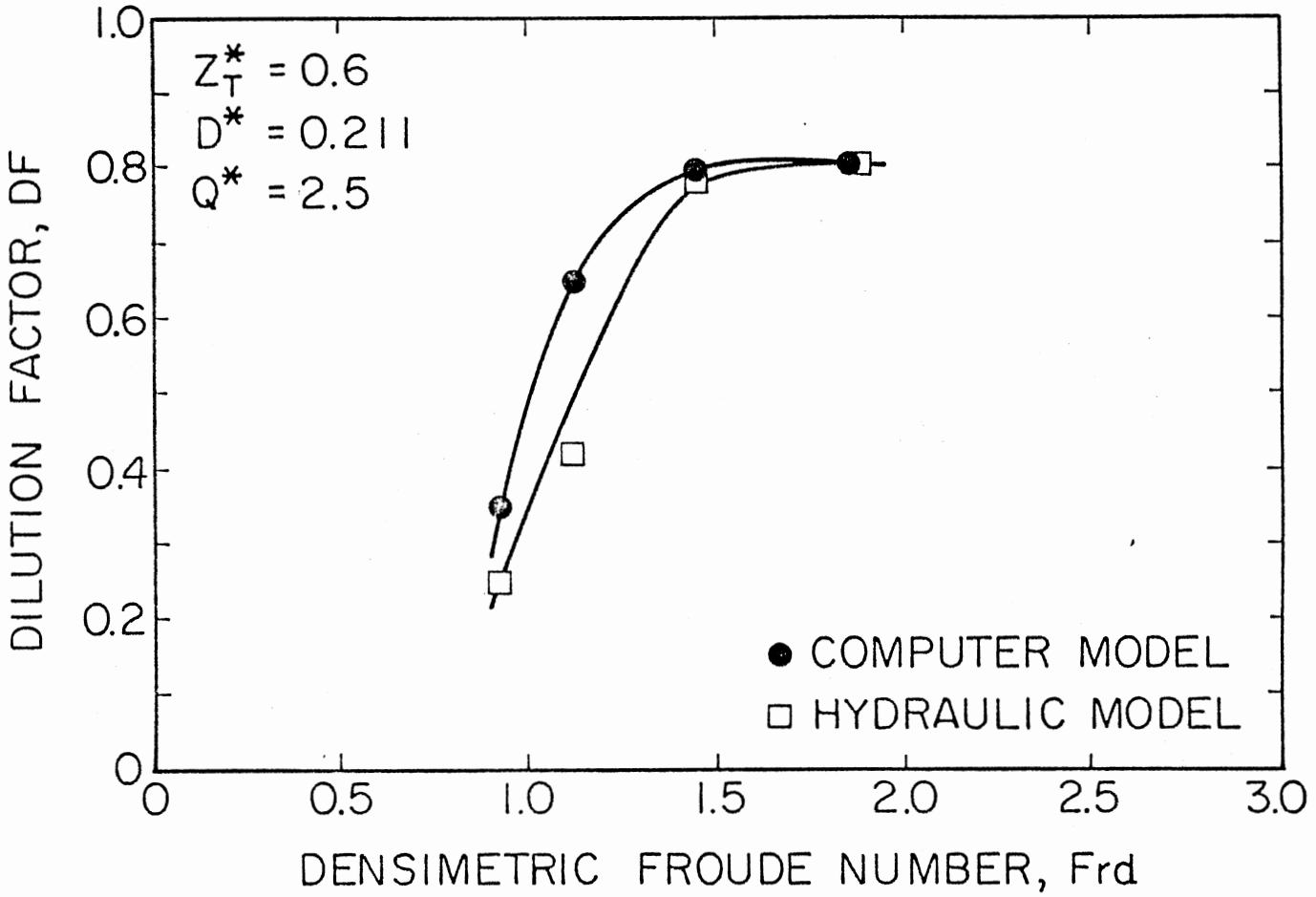

Figure 8. Dilution Factor, DF, As a Function of Densimetric Froude Number, Fr_d, at D* = 0.211, for Q* = 2.50

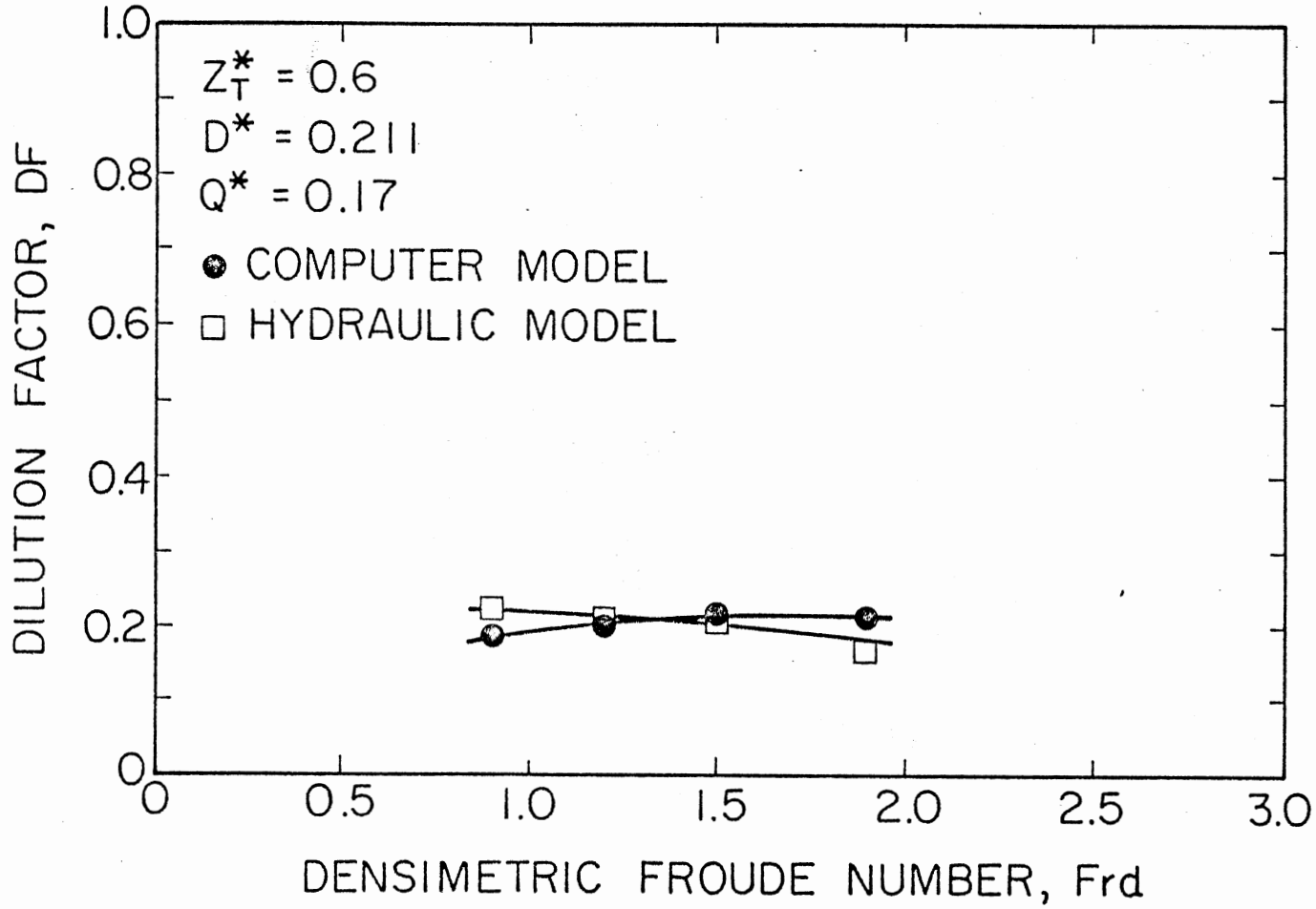

Figure 9. Dilution Factor, DF, As a Function of Densimetric Froude Number, Fr_d, at D* = 0.211, for Q* = 0.17

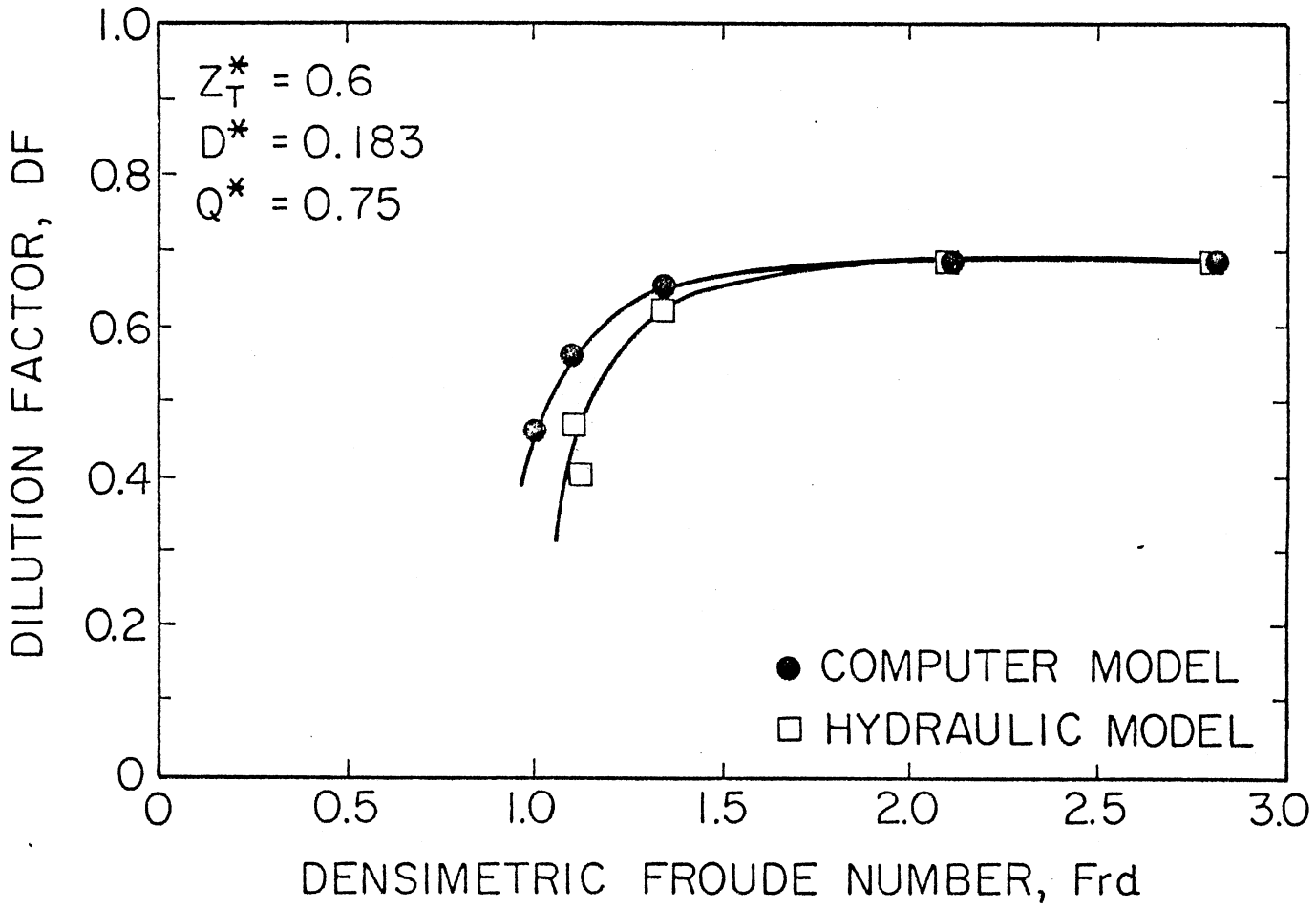

Figure 10. Dilution Factor, DF, As a Function of Densimetric Froude Number, Fr_d, at D* = 0.183, for Q* = 0.75

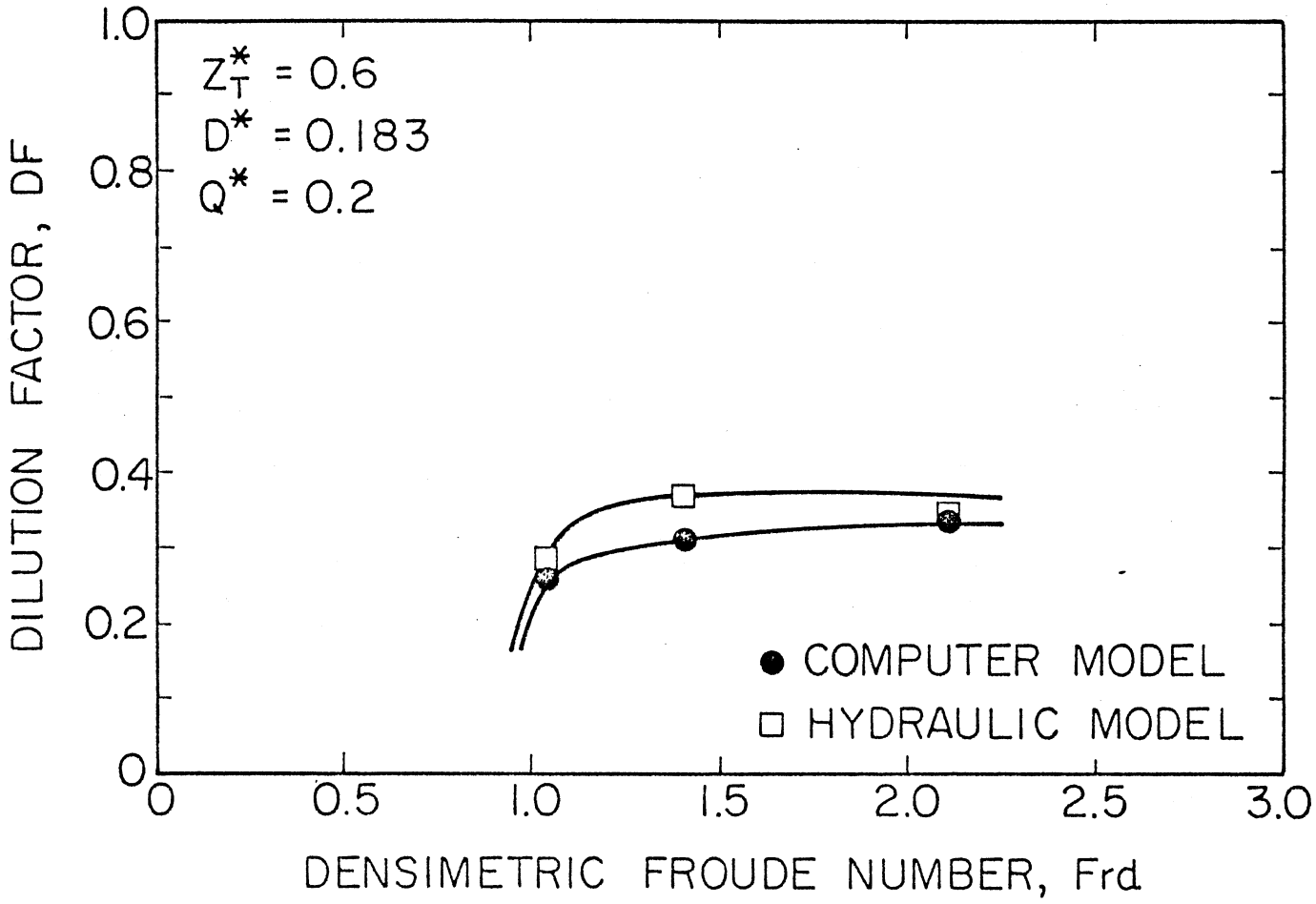

Figure 11. Dilution Factor, DF, As a Function of Densimetric Froude Number, Fr_d, at D* = 0.183, for Q* = 0.20

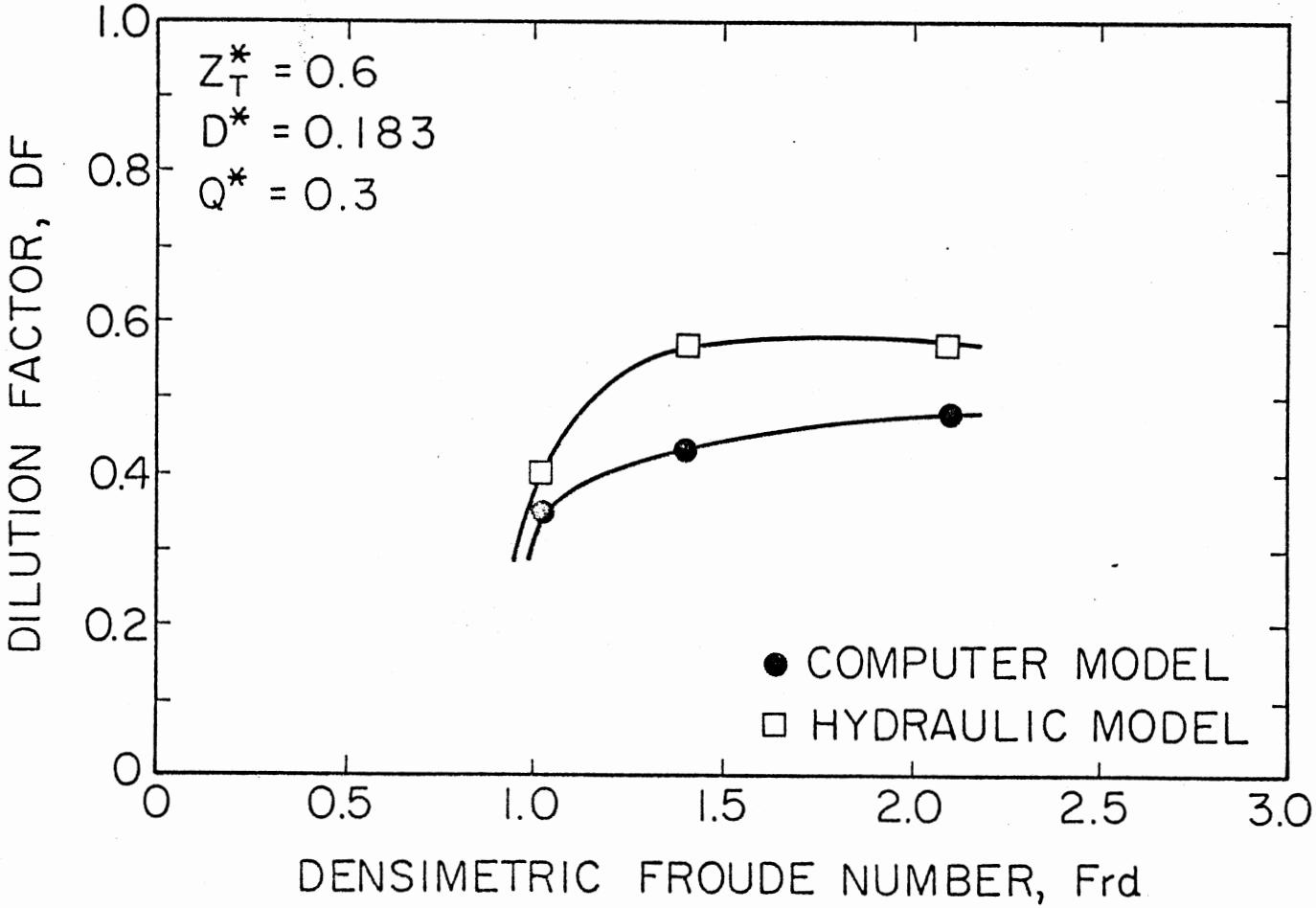

Figure 12. Dilution Factor, DF, As a Function of Densimetric Froude Number, Fr_d, at D* = 0.183, for Q* = 0.3

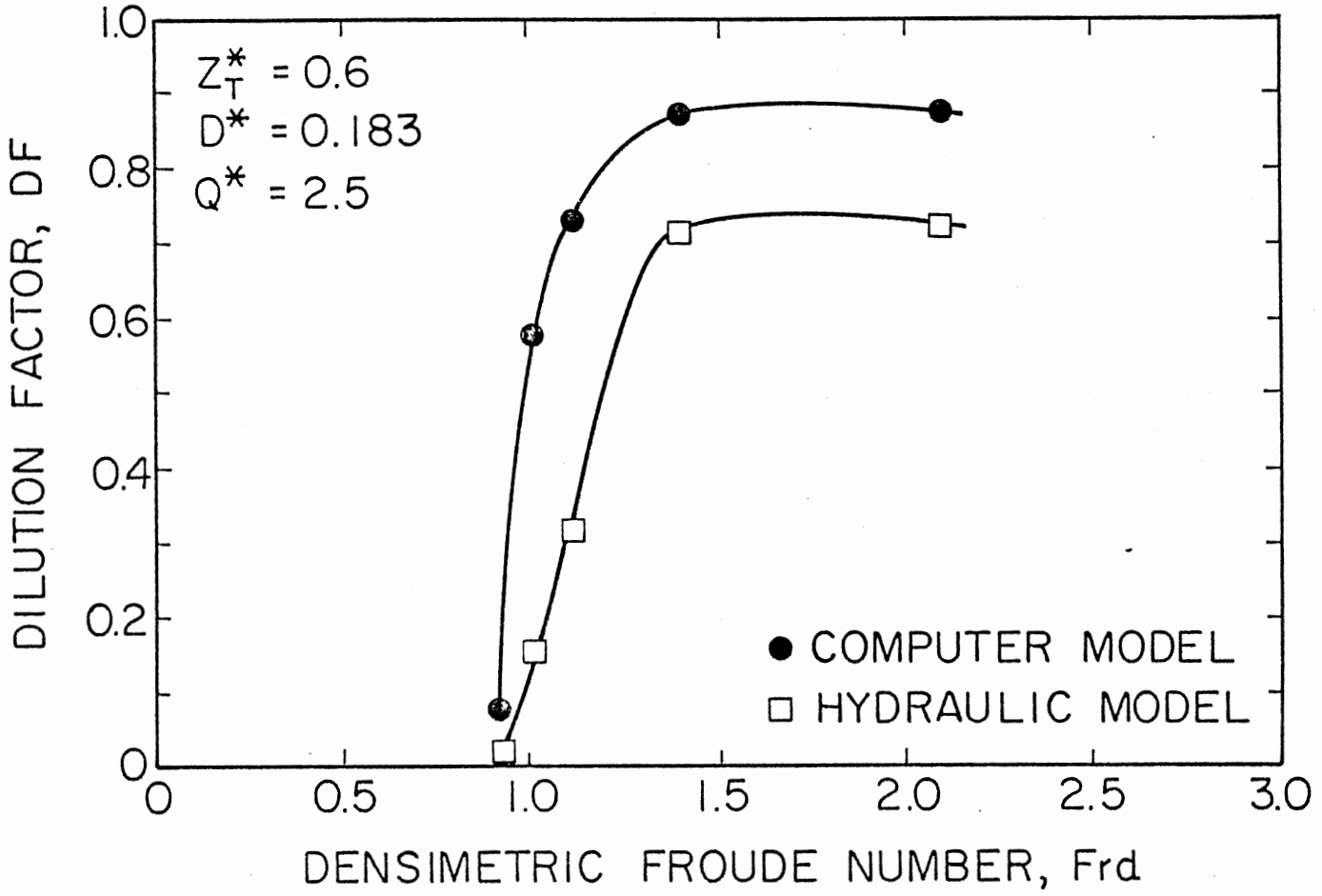

Figure 13. Dilution Factor, DF, As a Function of Densimetric Froude Number, Fr_d, at D* = 0.183, for Q* = 2.50

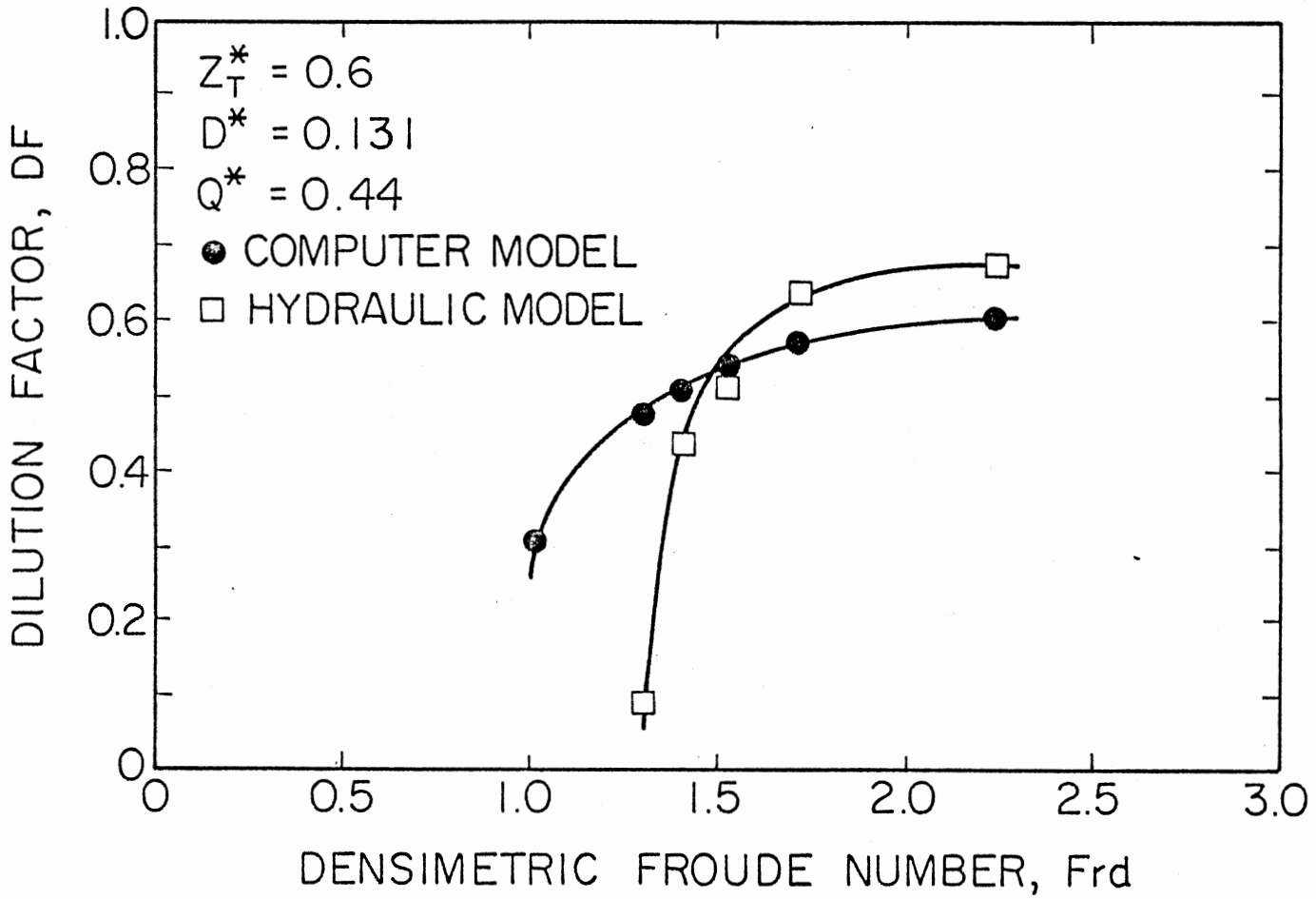

Figure 14. Dilution Factor, DF, As a Function of Densimetric Froude Number, Fr_d, at D* = 0.131, for Q* = 0.44

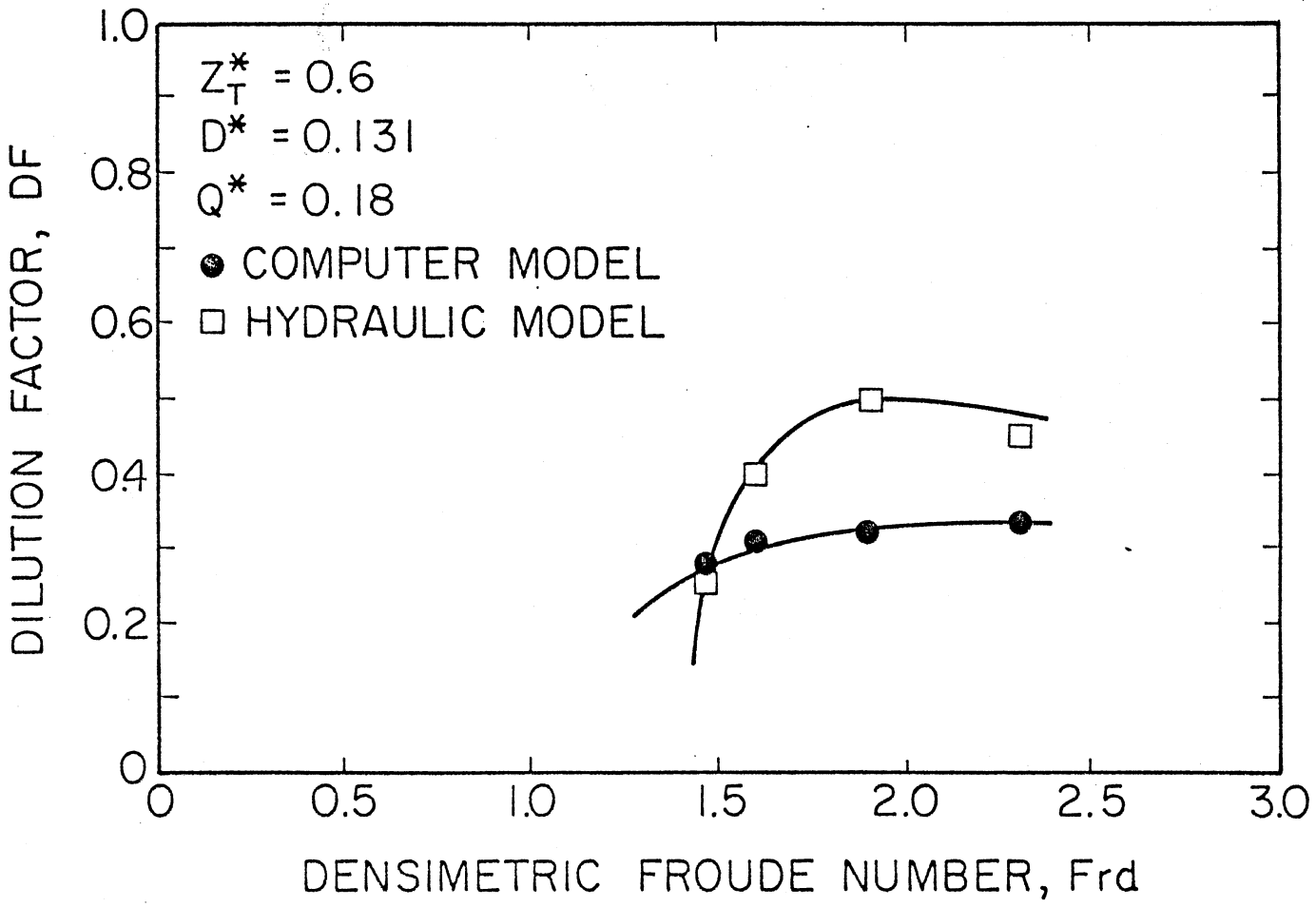

Figure 15. Dilution Factor, DF, As a Function of Densimetric Froude Number, Fr_d, at D* = 0.31, for Q* = 0.18

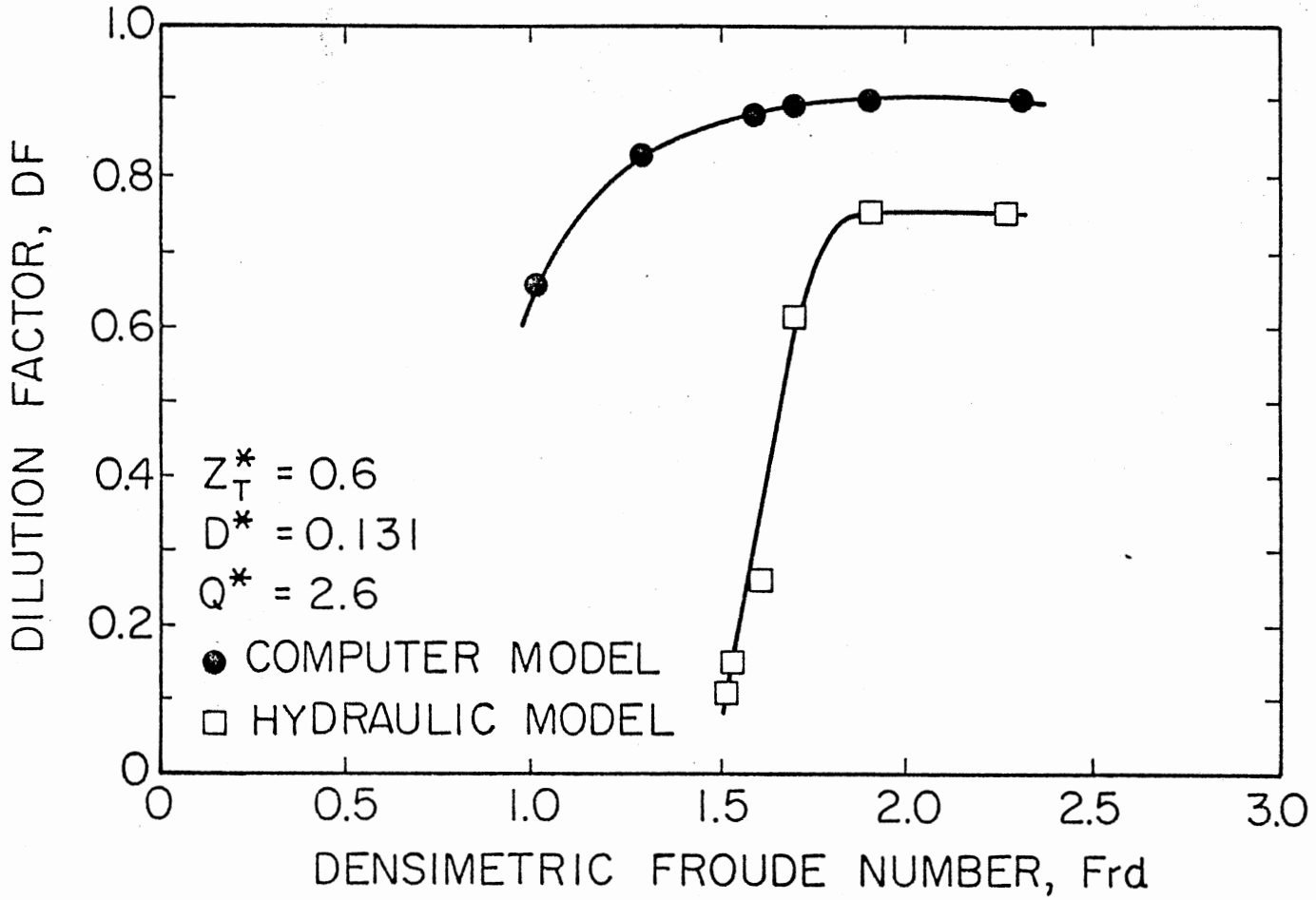

Figure 16. Dilution Factor, DF, As a Function of Densimetric Froude Number, Fr_d, at D* = 0.131, for Q* = 2.6

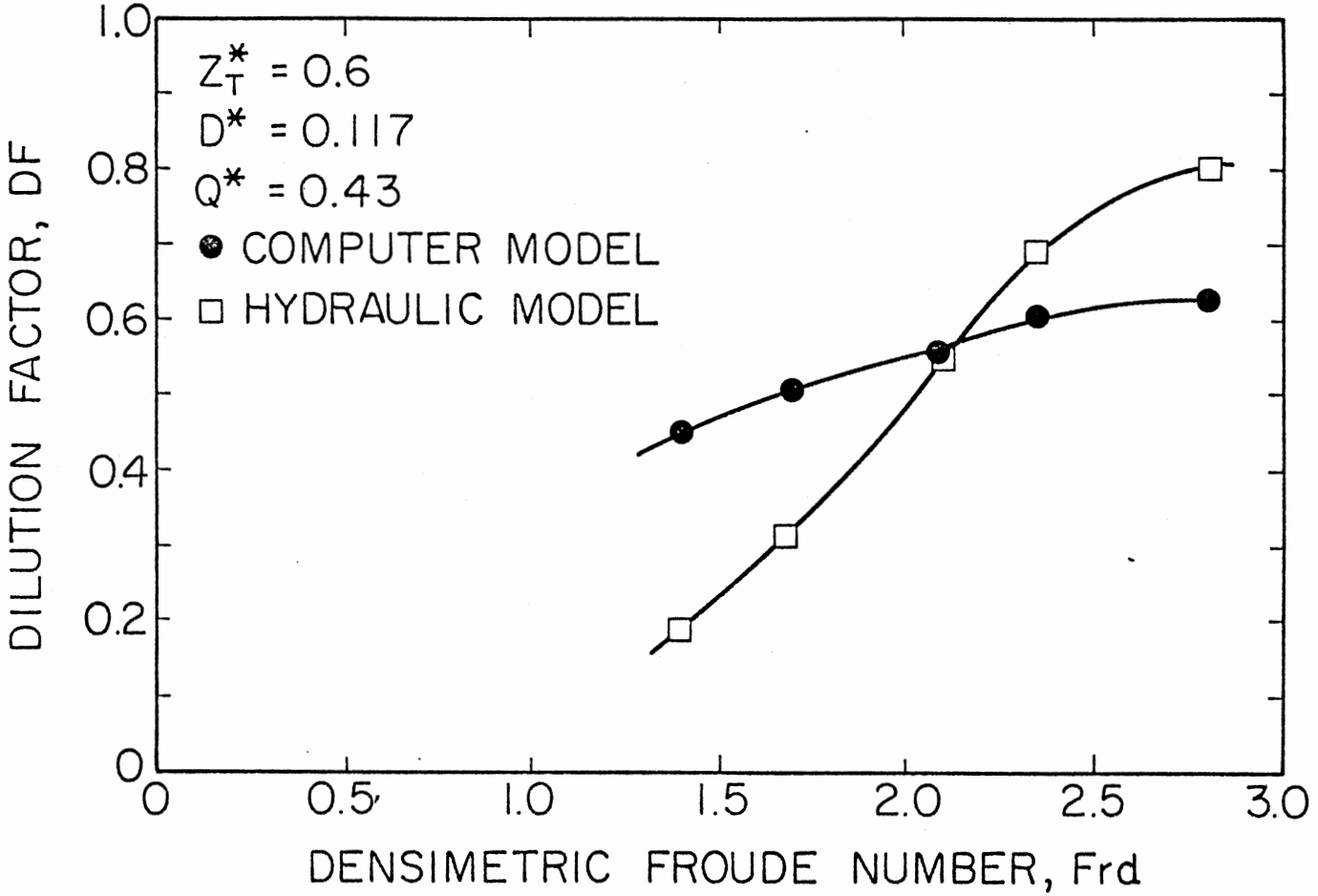

Figure 17. Dilution Factor, DF, As a Function of Densimetric Froude Number, Fr_d, D* = 0.117, for Q* = 0.43

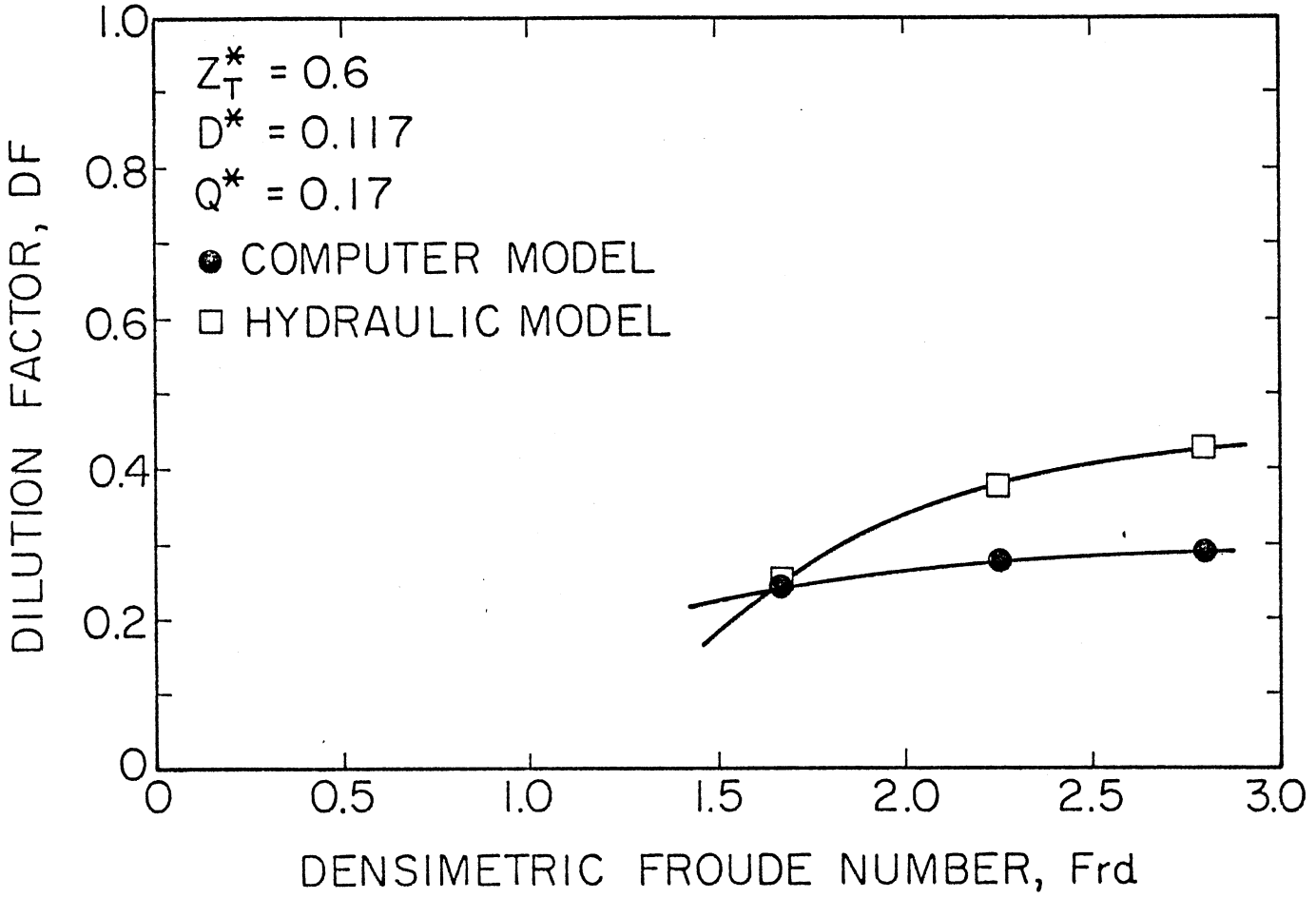

Figure 18. Dilution Factor, DF, As a Function of Densimetric Froude Number, Fr_d, at D* = 0.117, for Q* = 0.17

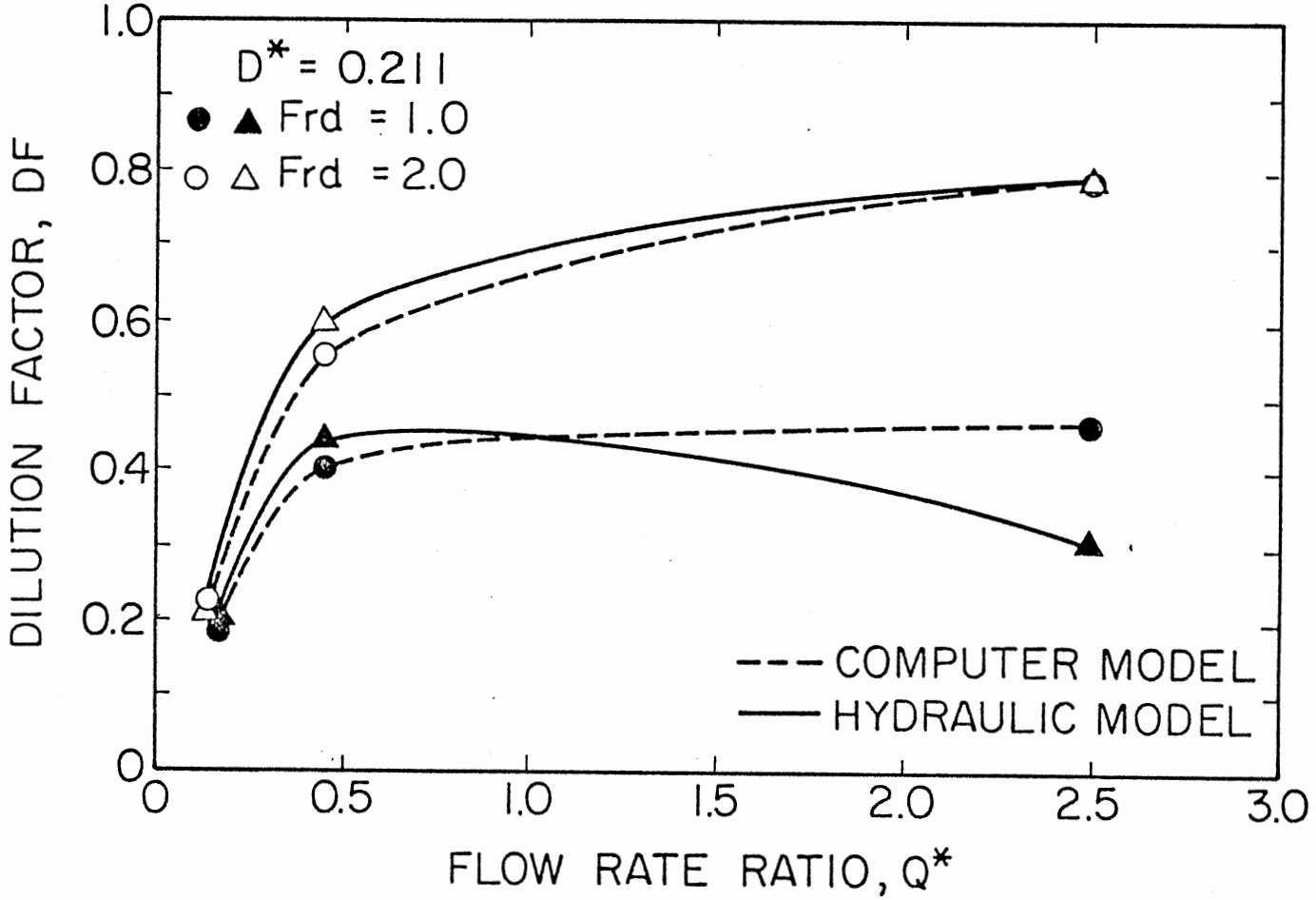

Figure 19. Dilution Factor, DF, As a Function of Flow Rate Ratio, Q*, and Densimetric Froude Number, Fr_d, at D* = 0.211

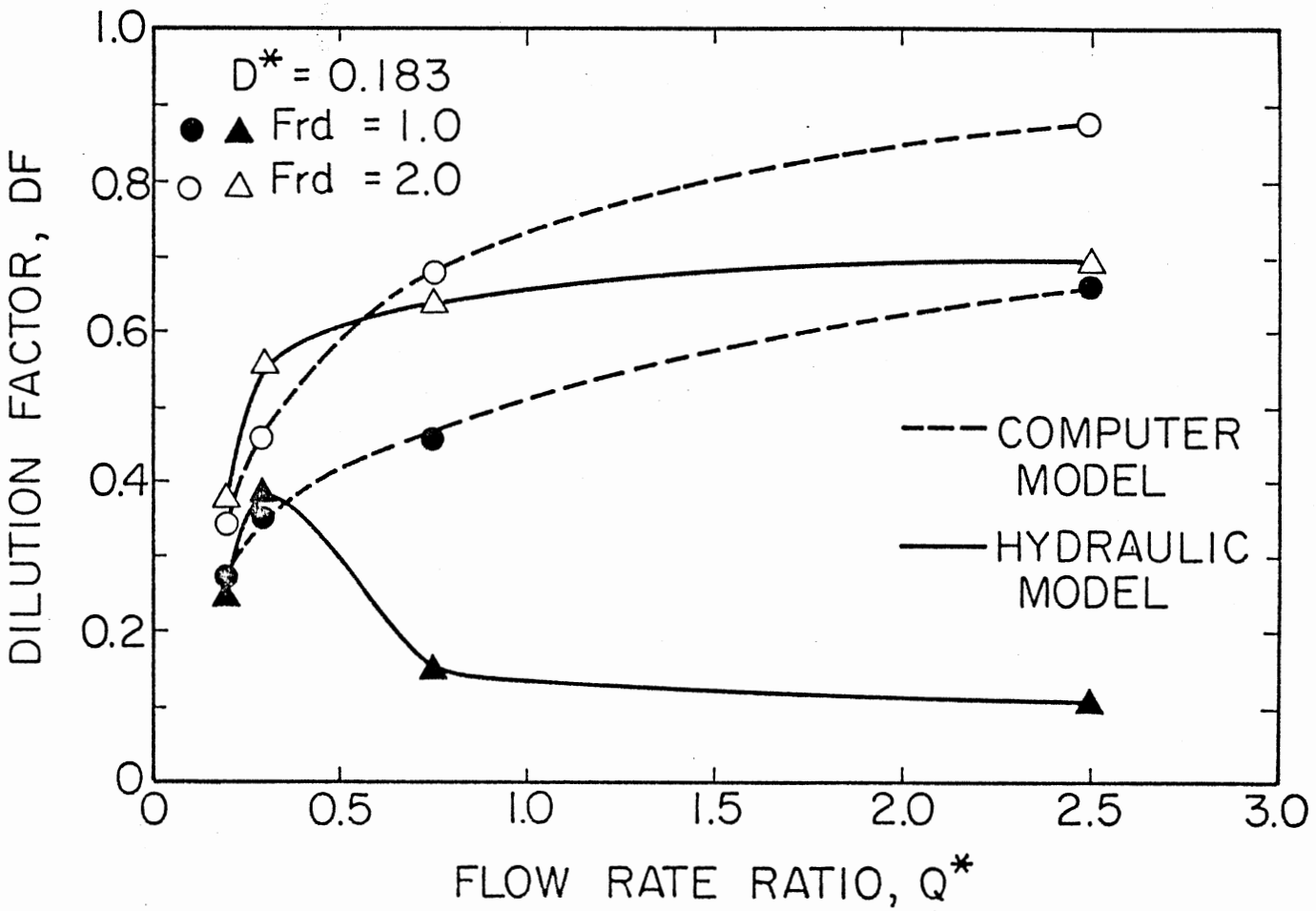

Figure 20. Dilution Factor, DF, As a Function of Flow Rate Ratio, Q*, and Densimetric Froude Number, Fr_d, at D* = 0.183

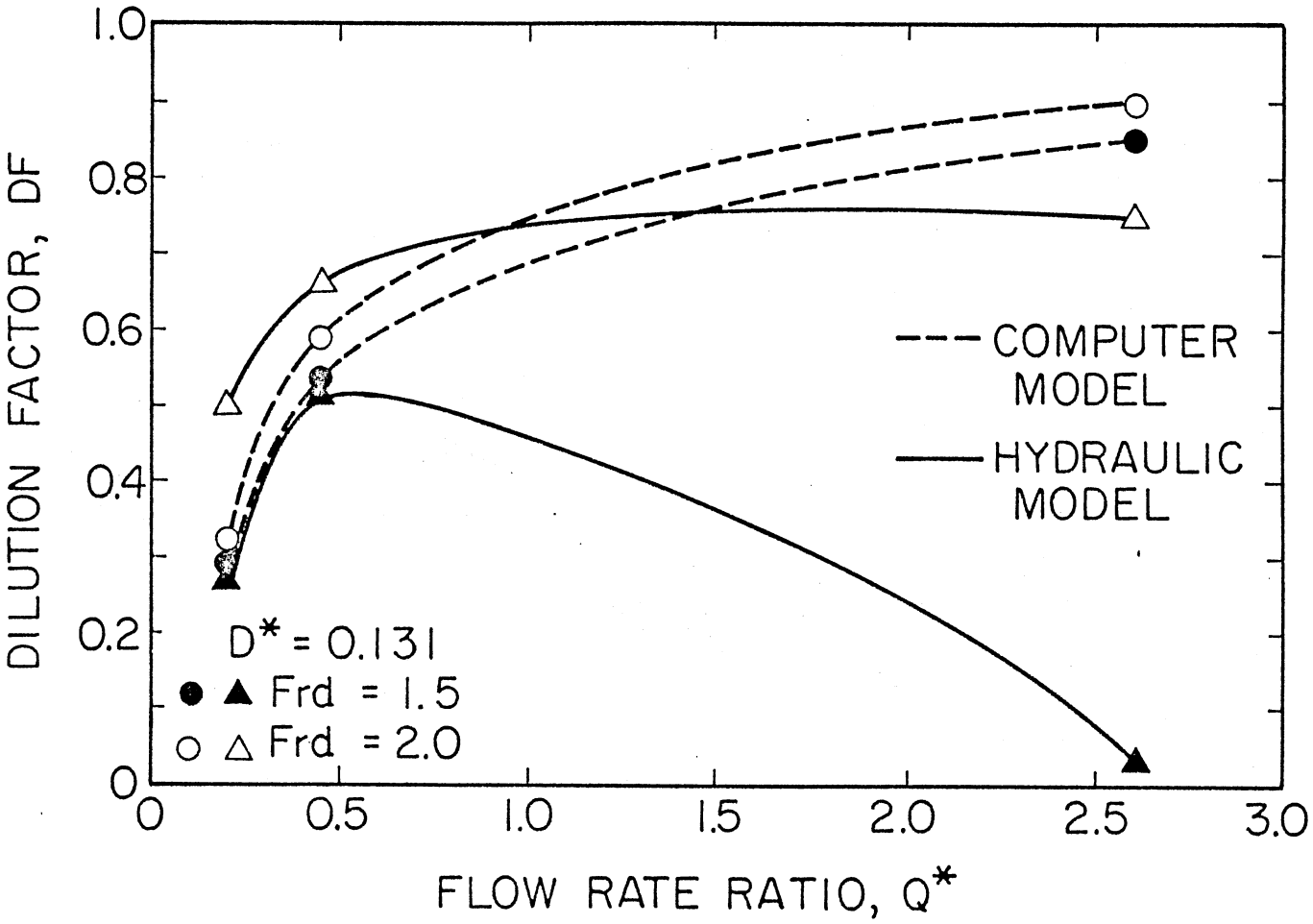

Figure 21. Dilution Factor, DF, As a Function of Flow Rate Ratio, Q*, and Densimetric Froude Number, Fr_d, at D* = 0.131

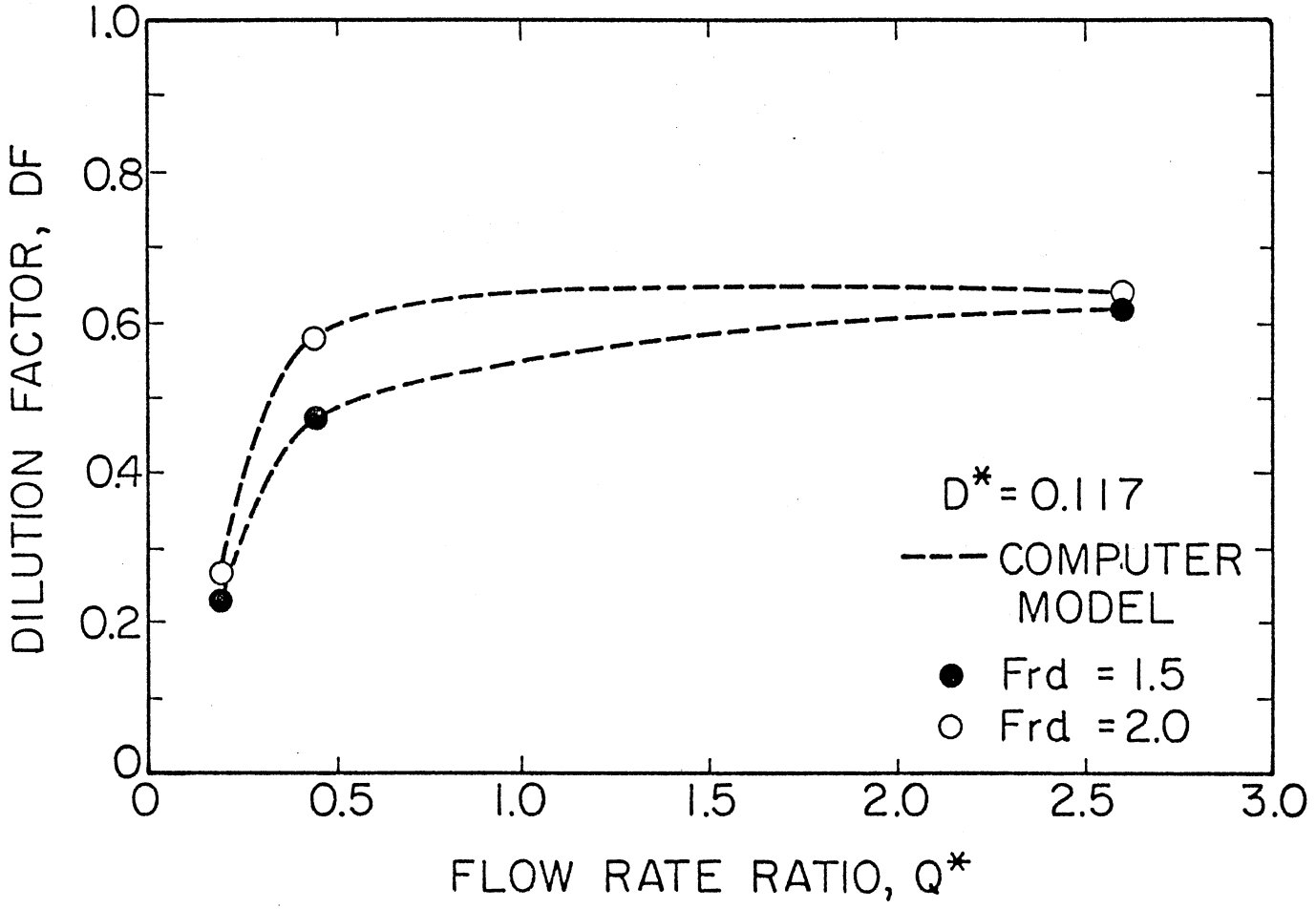

Figure 22. Dilution Factor, DF, As a Function of Flow Rate Ratio, Q*, and Densimetric Froude Number, Fr_d, at D* = 0.171

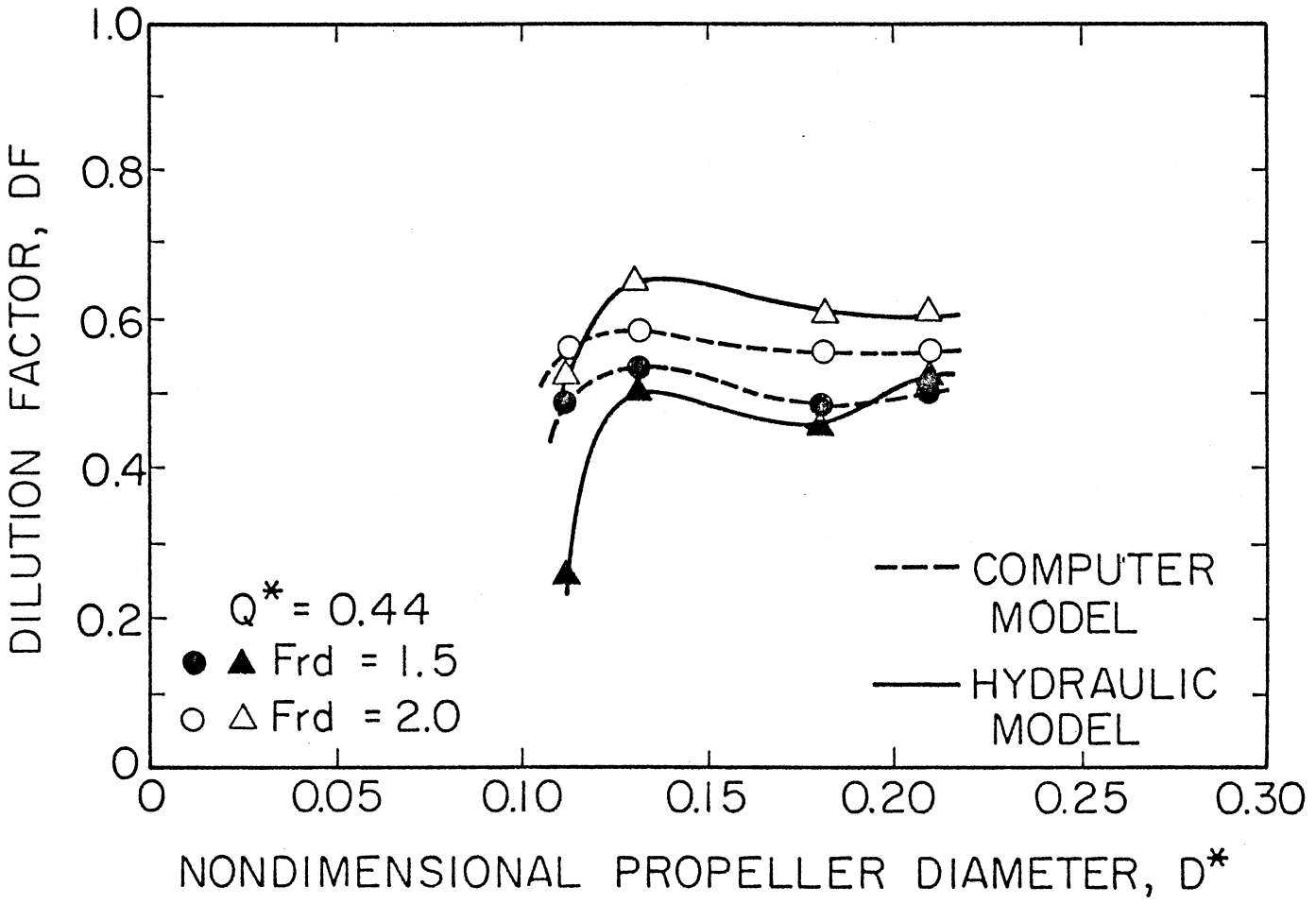

Figure 23. Dilution Factor, DF, As a Function of Nondimensional Propeller Diameter, D*, and Densimetric Froude Number, Fr_d, at Q* = 0.44

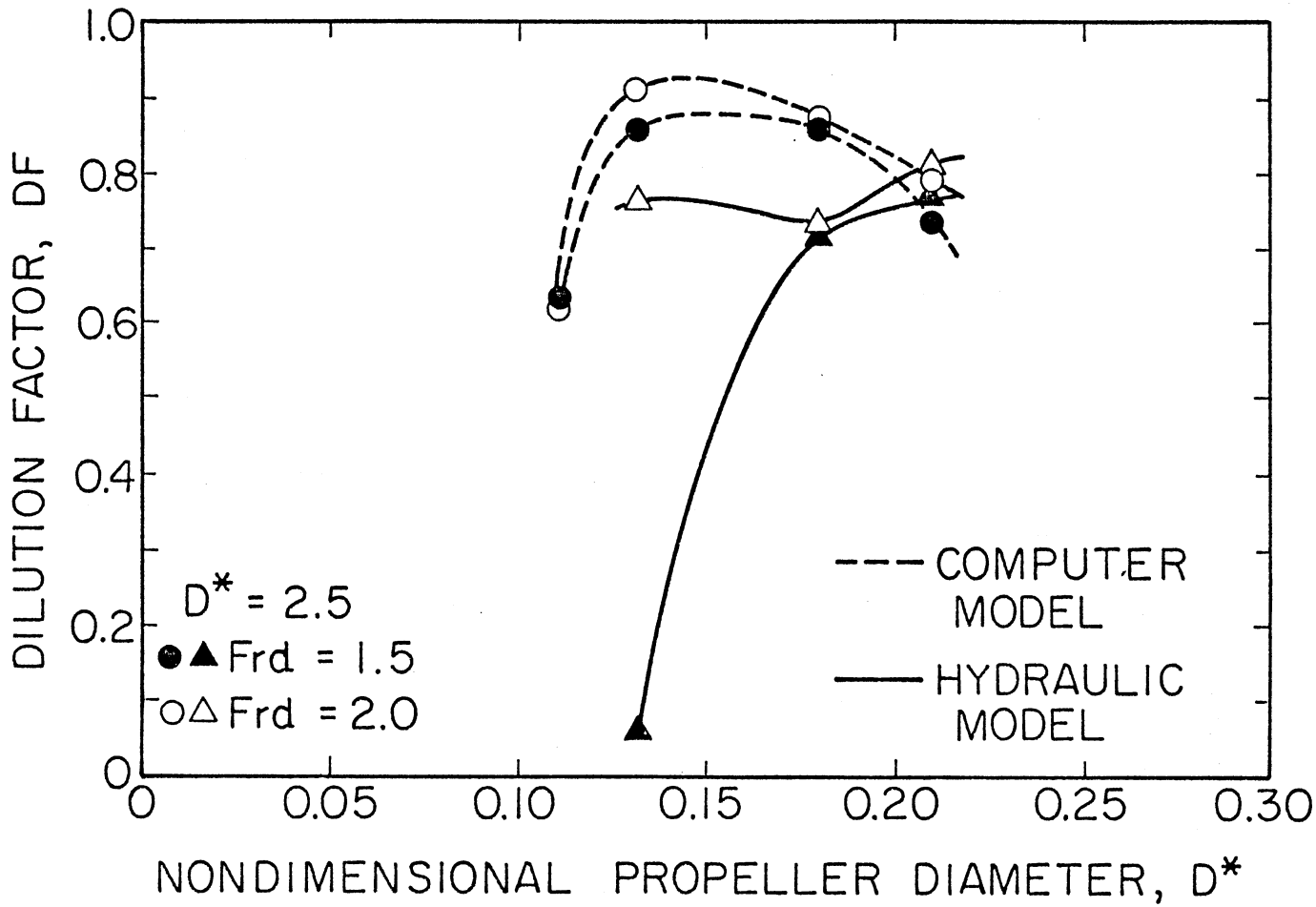

Figure 24. Dilution Factor, DF, As a Function of Nondimensional Propeller Diameter, D*, and Densimetric Froude Number, Fr_d, at Q* = 2.50

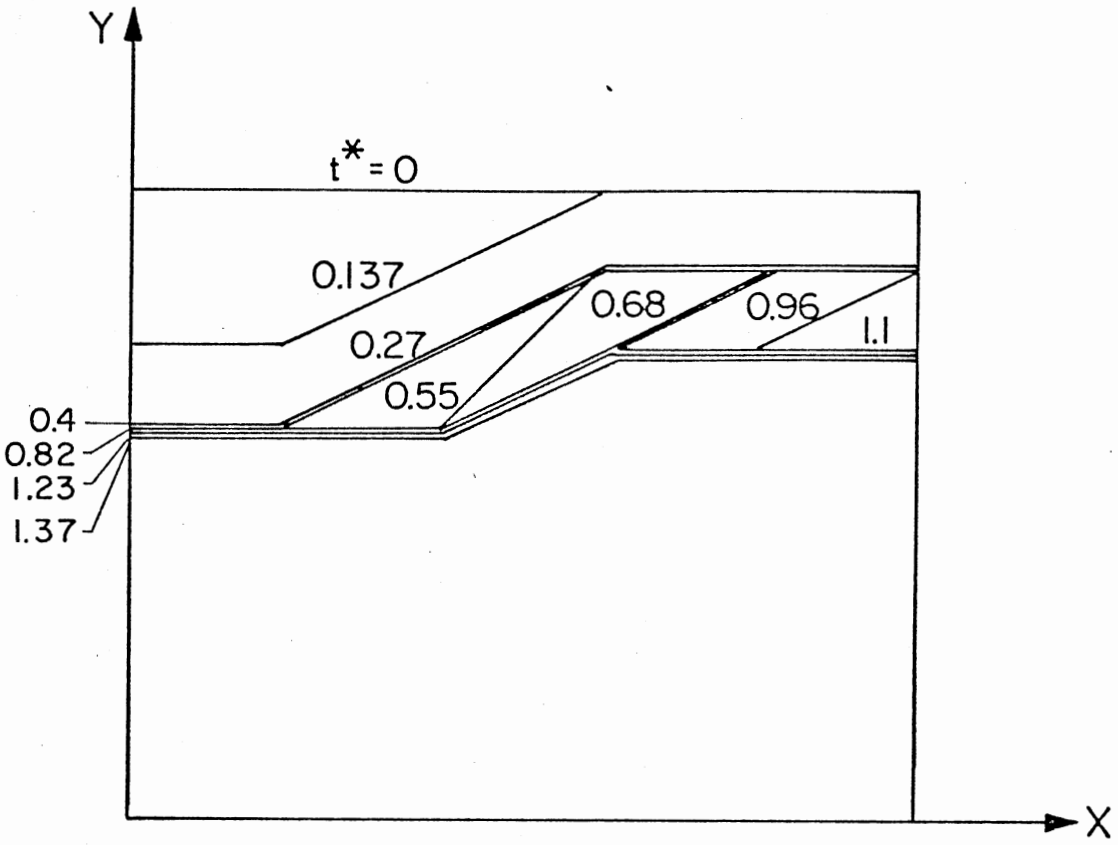

Figure 25. Location of the Interface With Nondimensional Time Increment t* for Fr_d = 0.30

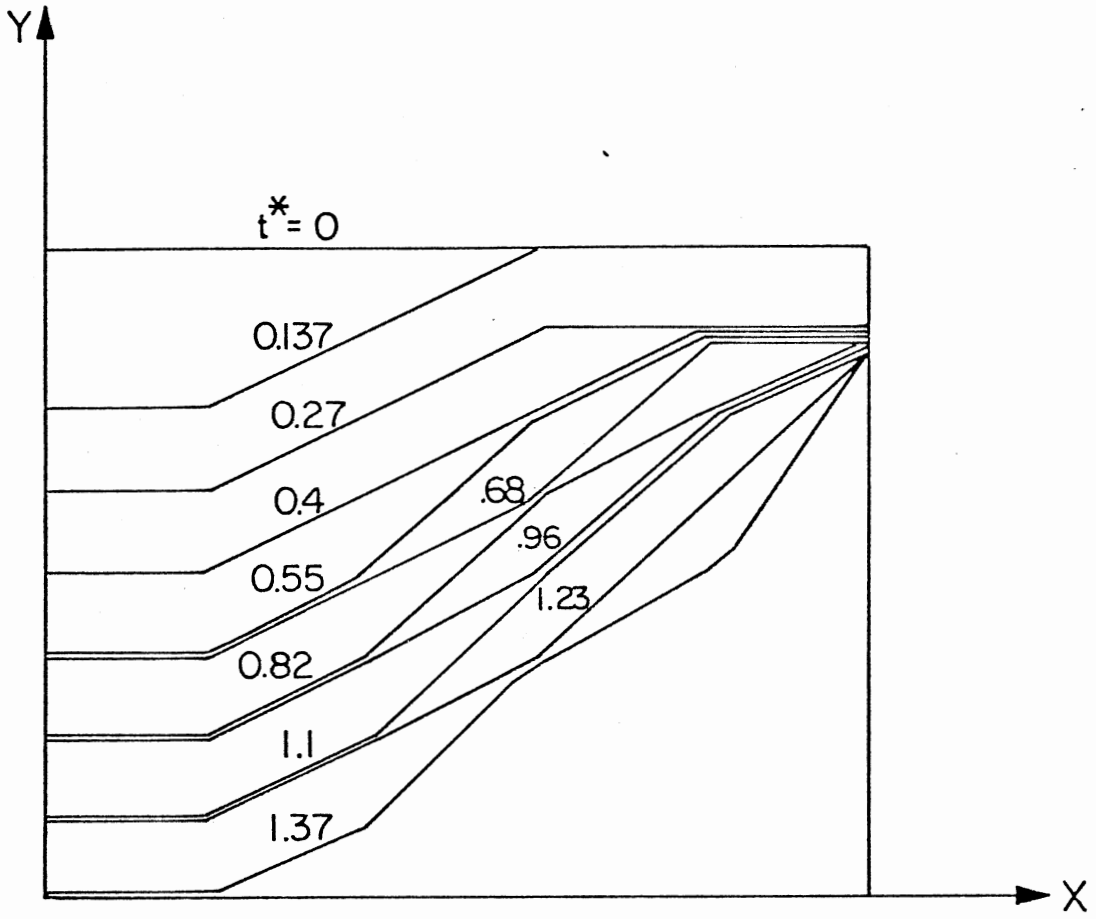

Figure 26. Location of the Interface With Nondimensional Time Increment t* for Fr_d = 1.05

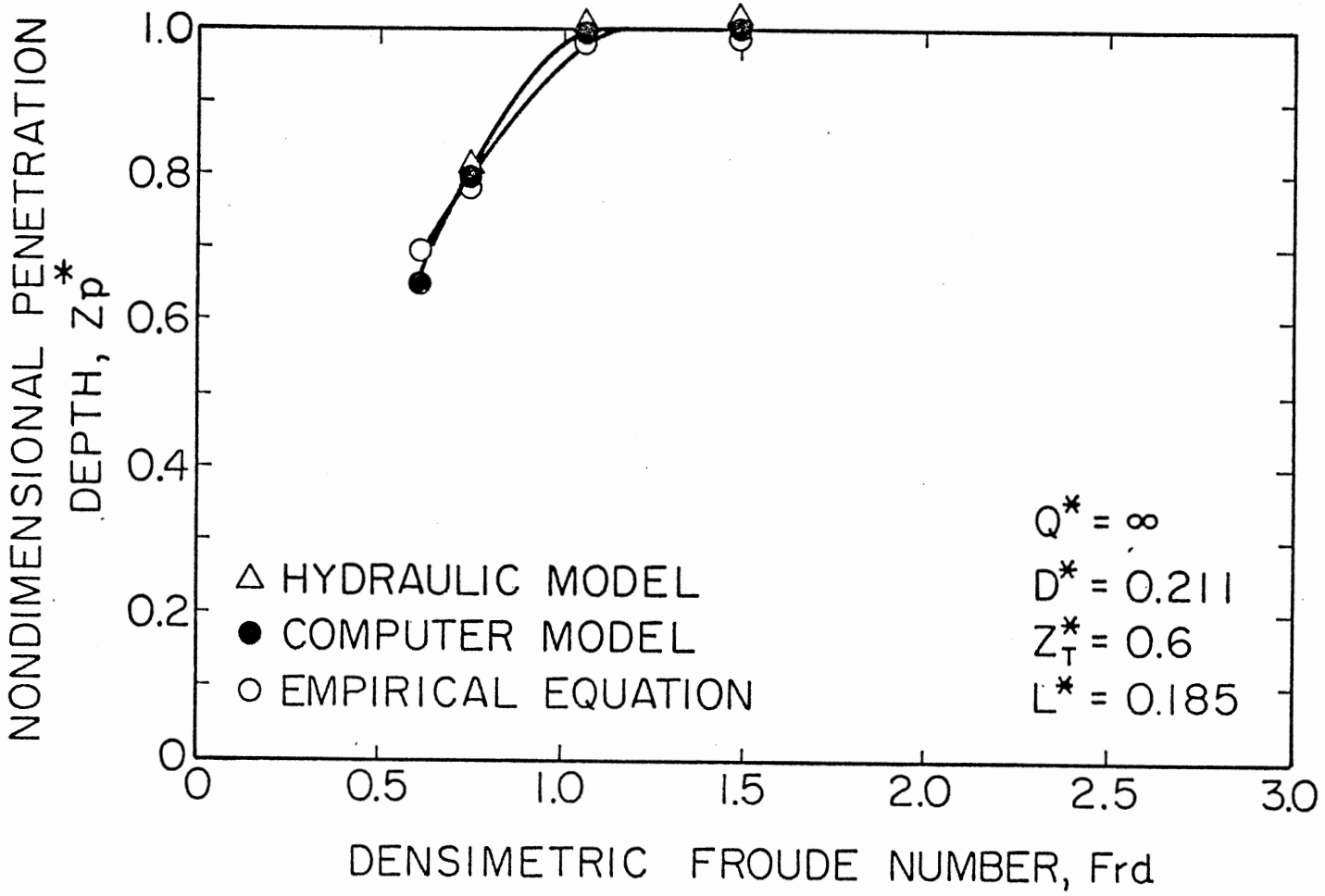

Figure 27. Nondimensional Penetration Depth, Z_p^*, As a Function of Densimetric Froude Number, Fr_d, at D* = 0.211

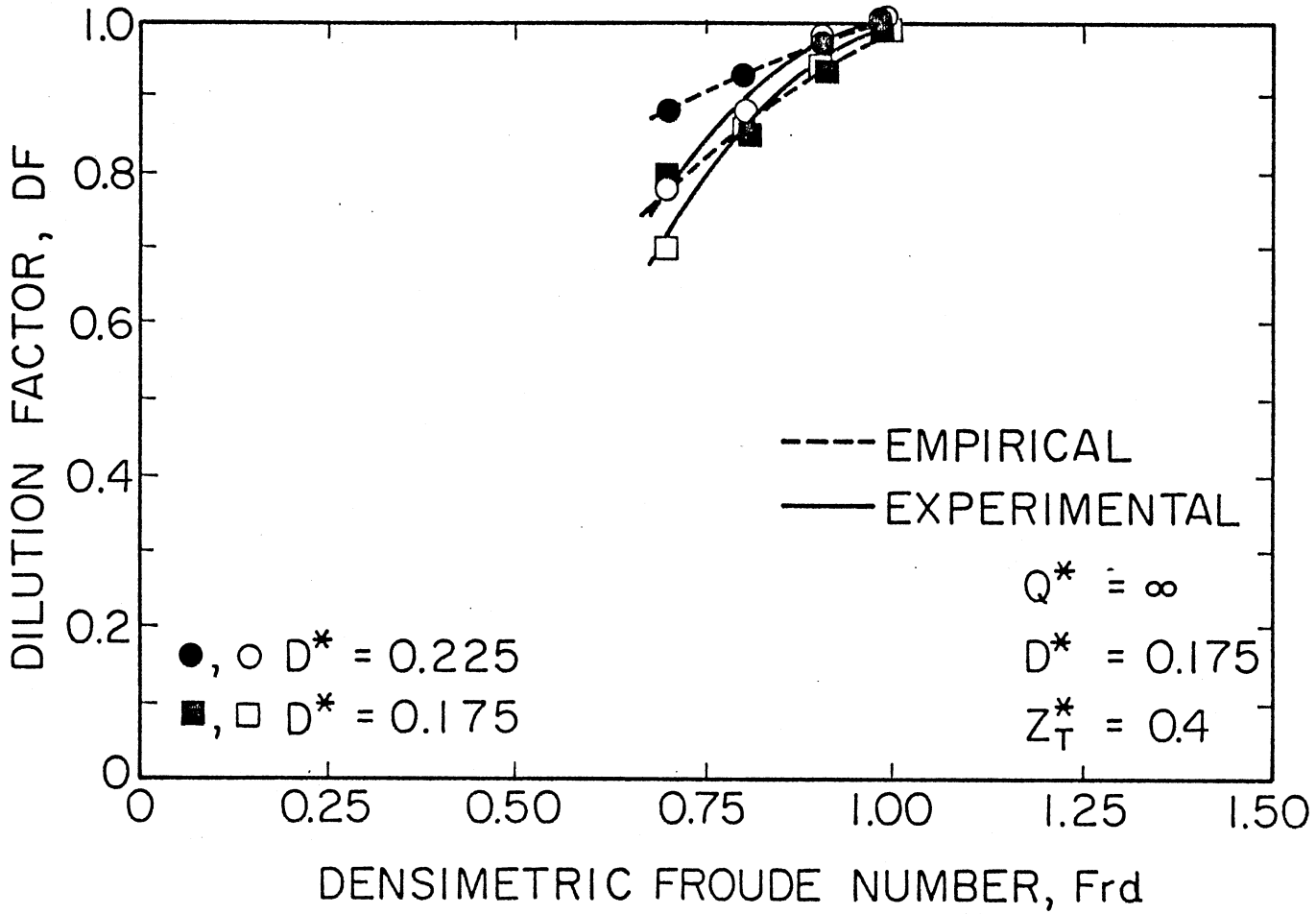

Figure 28. Nondimensional Penetration Depth, Z_p^*, As a Function of Densimetric Froude Number, Fr_d, at D* = 0.175

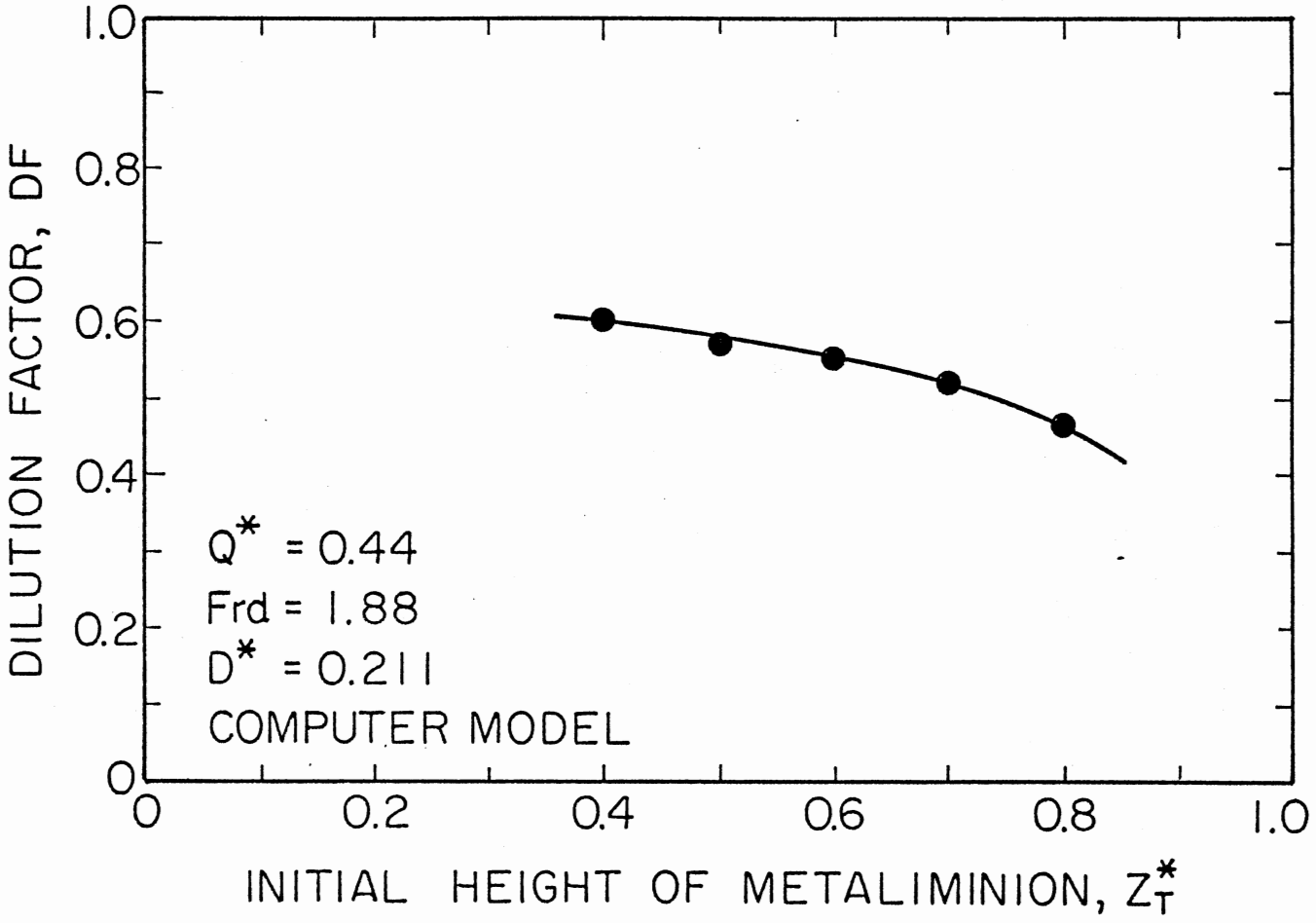

Figure 29. Dilution Factor, DF, As a Function of Initial Height of Metalimnion, Z_T^*, at D* = 0.211

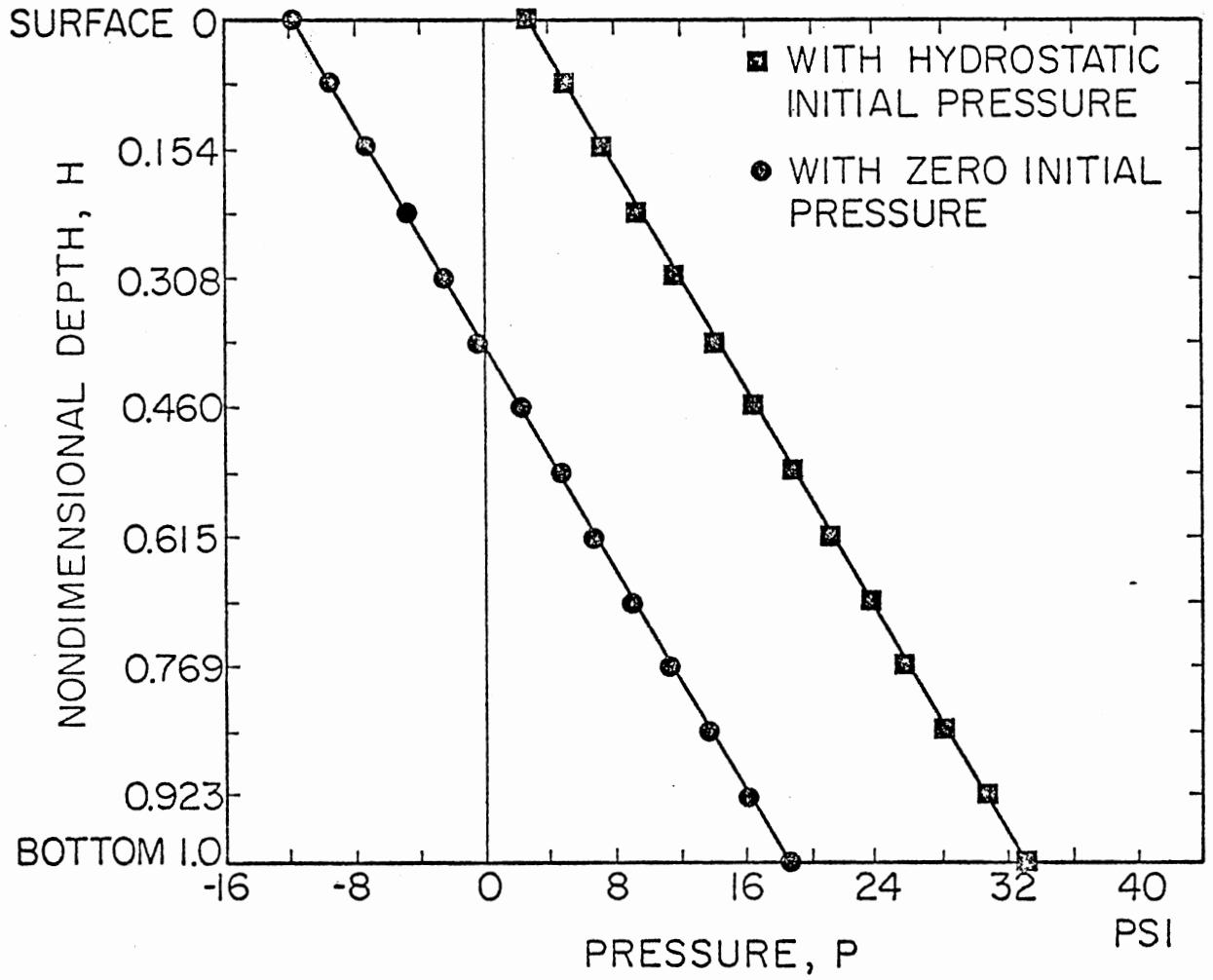

Figure 30. Hydrostatic Pressure Profile

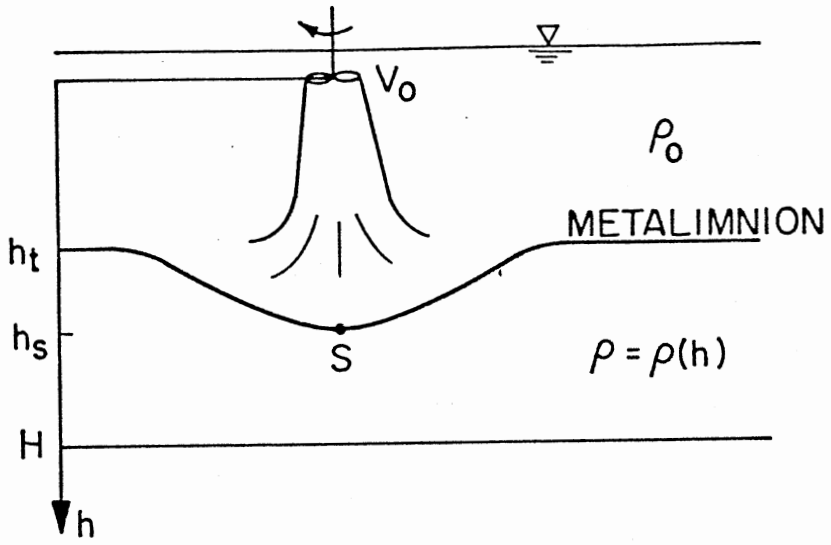

Figure 31. Jet at Stagnation Point

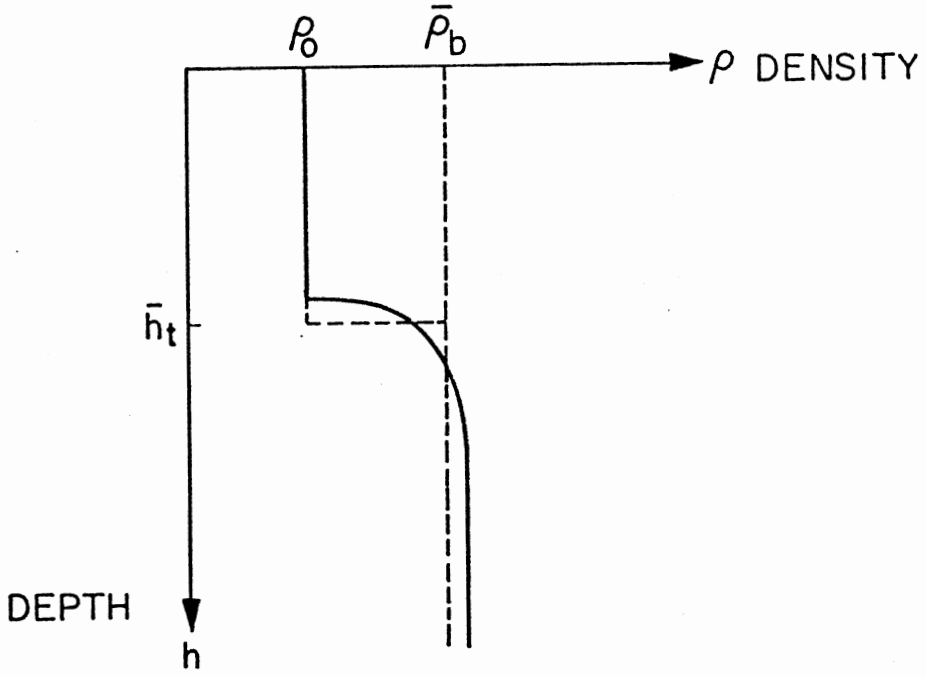

Figure 32. Density Profile

APPENDIX B

FINITE DIFFERENCE FORMULATION

The four terms on the righthand side of Equation (1) in Chapter II are defined by:

U-Equation

$$FUX = \frac{1}{4\Delta x}\left[(U_{i,j} + U_{i+1,j})^2 + \alpha|U_{i,j} + U_{i+1,j}|(U_{i,j} - U_{i+1,j})\right.$$
$$\left. - (U_{i-1,j} + U_{i,j})^2 - \alpha|U_{i-1,j} + U_{i,j}|(U_{i-1,j} - U_{i,j})\right]$$

$$FUY = \frac{1}{4\Delta y}\left[(V_{i,j} + V_{i+1,j})(U_{i,j} + U_{i,j+1})\right.$$
$$+ \alpha|V_{i,j} + V_{i+1,j}|(U_{i,j} - U_{i,j+1})$$
$$- (V_{i,j-1} + V_{i+1,j-1})(U_{i,j-1} + U_{i,j})$$
$$\left. - \alpha|V_{i,j-1} + V_{i+1,j-1}|(U_{i,j-1} - U_{i,j})\right]$$

$$FUC = \frac{1}{8\Delta x(i-1)}\left[(U_{i,j} + U_{i+1,j})^2 + (U_{i-1,j} + U_{i,j})^2\right.$$
$$+ \alpha|U_{i,j} + U_{i+1,j}|(U_{i,j} - U_{i+1,j})$$
$$\left. + \alpha|U_{i-1,j} + U_{i,j}|(U_{i-1,j} - U_{i,j})\right]$$

$$VISX = \nu\left[\frac{1}{\Delta x^2}(U_{i+1,j} - 2U_{i,j} + U_{i-1,j}) + \frac{1}{\Delta y^2}(U_{i-j+1} - 2U_{i,j}\right.$$
$$\left. + U_{i,j-1}) + \frac{1}{2\Delta x^2(i-1)}(U_{i+1,j} - U_{i-1,j}) - \frac{U_{i,j}}{\Delta x^2(i-1)}\right]$$

V-Equation

$$FVX = \frac{1}{4\Delta x}\left[(U_{i,j} + U_{i,j+1})(V_{i,j} + V_{i+1,j})\right.$$
$$+ \alpha|U_{i,j} + U_{i,j+1}|(V_{i,j} - V_{i+1,j})$$
$$- (U_{i-1,j} + U_{i-1,j+1})(V_{i-1,j} + V_{i,j})$$
$$\left. + \alpha|U_{i-1,j} + U_{i-1,j+1}|(V_{i-1,j} - V_{i,j})\right]$$

$$FVY = \frac{1}{4\Delta y}\left[(V_{i,j} + V_{i,j+1})^2 + \alpha|V_{i,j} + V_{i,j+1}|(V_{i,j} - V_{i,j+1})\right.$$

$$\left. - (V_{i,j-1} + V_{i,j})^2 - \alpha|V_{i,j-1} + V_{i,j}|(V_{i,j-1} - V_{i,j})\right]$$

$$FVC = \frac{1}{8\Delta x(i-1.5)}\left[(U_{i,j} + U_{i,j+1})(V_{i,j} + V_{i+1,j})\right.$$

$$+ (U_{i-1,j} + U_{i-1,j+1})(V_{i-1,j} + V_{i,j})$$

$$+ \alpha|U_{i,j} + U_{i,j+1}|(V_{i,j} - V_{i+1,j})$$

$$\left. + \alpha|U_{i-1,j} + U_{i-1,j+1}|(V_{i-1,j} - V_{i,j})\right]$$

$$VISY = \nu\left[\frac{1}{\Delta x^2}(V_{i+1,j} - 2V_{i,j} + V_{i-1,j})\right.$$

$$+ \frac{1}{\Delta y^2}(V_{i,j+1} - 2V_{i,j} + V_{i,j-1})$$

$$\left. + \frac{1}{2\Delta x^2(i-1.5)}(V_{i+1,j} - V_{i-1,j})\right]$$

m-Equation

$$FMX = \frac{1}{2\Delta x}\left[U_{i,j}(S_{i,j} + S_{i+1,j}) + \alpha|U_{i,j}|(S_{i,j} - S_{i+1,j})\right.$$

$$\left. - U_{i-1,j}(S_{i-1,j} + S_{i,j}) - \alpha|U_{i-1,j}|(S_{i-1,j} - S_{i,j})\right]$$

$$FMY = \frac{1}{2\Delta y}\left[V_{i,j}(S_{i,j} + S_{i,j+1}) + \alpha|V_{i,j}|(S_{i,j} - S_{i,j+1})\right.$$

$$\left. - V_{i,j-1}(S_{i,j-1} + S_{i,j}) - \alpha|V_{i,j-1}|(S_{i,j-1} - S_{i,j})\right]$$

$$FMC = \frac{1}{4\Delta x(i-1.5)}\left[U_{i,j}(S_{i,j} + S_{i+1,j})\right.$$

$$\left. + U_{i-1,j}(S_{i-1,j} + S_{i,j})\right]$$

$$VIMX = \frac{\mu}{\rho_1 \sigma_{sc}}\left[\frac{1}{\Delta x^2}(S_{i+1,j} - 2S_{i,j} + S_{i-1,j}) + \frac{1}{\Delta y^2}(S_{i,j+1}\right.$$

$$\left. - 2S_{i,j} + S_{i,j-1}) + \frac{1}{2\Delta x^2(i-1.5)}(S_{i+1,j} - S_{i-1,j})\right]$$

APPENDIX C

PENETRATION DEPTH ANALYSIS

Jet penetration can be analyzed approximately at the stagnation point considering potential flow by Bernoulli's equation. Applying Vernoulli's equation to the central stream line from the propeller plane to the stagnation point s (see Figure 31) where the axial coordinate h is considered in the downward direction.

$$P_o + \frac{\rho_o V_o^2}{2} = P_s + \frac{\rho_o V_s^2}{2} - \rho_o g h_s \tag{6}$$

Considering that the density of the jet to be ρ_o the top density (epilimnion), V_o the propeller velocity, P_o the reference pressure, P_s stagnation pressure, and V_s the velocity at stagnation point (which equals zero), and then rearranging Equation (6) gives:

$$\frac{\rho_o V_o^2}{2} = (P_s - P_o) - \rho_o g h_s \tag{7}$$

In the absence of strong currents below the stagnation point, we assume that the pressure at the point s is equal to the pressure anywhere in the lake at the level h_s where

$$P_s - P_o = g \int_o^{h_s} \rho \, dh = g\rho_o h_s + g \int_o^{h_s} (\rho - \rho_o) dh \tag{8}$$

Substituting in the Bernoulli equation,

$$\frac{\rho_o V_o^2}{2} = [g\rho_o h_s + g \int_o^{h_s} (\rho - \rho_o) dh] - \rho_o g h_s$$

$$\frac{V_o^2}{2g} = \int_o^{h_s} \frac{\rho - \rho_o}{\rho_o} dh \tag{9}$$

where

V_o = propeller-induced central velocity;

h_s = jet penetration depth;

ρ_o = epilimnion density; and

P = stratification density as a function of depth.

In a stratified lake, pressure is greater than the hydrostatic pressure with no density gradient. The difference in this case will be

$$P' = g \int_o^h (\rho - \rho_o) dh$$

and at the stagnation point,

$$P' = \frac{1}{2} \rho_o V_o$$

The density in the lake is a function of depth and this function depends on the kind of density profile which can be a profile with deep penetration, shallow penetration, or a polynomial profile, etc. We will consider here a deep penetration profile (see Figure 32). The profile is approximated by a step change in the density where it takes place at the mean thermocline depth $\overline{h_t}$, where

$$\rho = \begin{cases} \rho_o & \text{for } h < \overline{h_t} \\ \overline{\rho_b} & \text{for } h > \overline{h_t} \end{cases}$$

Then substituting in Equation (4),

$$\frac{V_o^2}{2g} = \int_o^{\overline{h_t}} \frac{\rho_o - \rho_o}{\rho_o} dh + \int_{\overline{h_t}}^{h_s} \frac{\overline{\rho_b} - \rho_o}{\rho_o} dh$$

$$= 0 + \left(\frac{\rho_b - \rho_o}{\rho_o}\right)(h_s - \overline{h_t})$$

So the penetration depth will be

$$h_s = \bar{h}_t + \left(\frac{\rho_o}{\bar{\rho}_b - \rho_o}\right) \frac{V_o^2}{2g} \tag{10}$$

or an expression for the central velocity along the central axis of the jet can be written as

$$V_y^2 = V_o^2 - 2g \int_{\bar{h}_t}^{y} \frac{\bar{\rho}_b - \rho_o}{\rho_o} dh \tag{11}$$

where $y \geq \bar{h}_t$ and $dh = dy$.

At $y = h_s$,

$$V_{h_s}^2 = V_o^2 - 2g \int_{\bar{h}_t}^{h_s} \frac{\bar{\rho}_b - \rho_o}{\rho_u} dh$$

$$= V_o^2 - V_o^2 = 0 \qquad \text{(velocity at stagnation point)}$$

The decay in the jet velocity (due to friction) is not considered in Equation (11). The centerline velocity is inversely proportional to y (21) and this can be written as

$$V_y = V_o \frac{CD}{y} \tag{12}$$

where D is the jet diameter, C is a constant, and $y \geq CD$. Then rearranging,

$$V_y^2 = V_o^2 \left(\frac{CD}{y}\right)$$

$$V_y^2 = V_o^2 - V_u^2 \left(1 - \left(\frac{CD}{y}\right)^2\right) \tag{13}$$

Equation (13) represents the jet dissipation effect (jet decay due to viscous dissipation). This effect can be added to Equation (10) which represents the stratification effect in order to consider the two effects

on the centerline jet velocity. This can be done by considering a form of an empirical equation as

$$V_y^2 = V_o^2 - 2g \int_{\bar{h}_t}^{y} \left(\frac{\bar{\rho}_b - \rho_o}{\rho_o}\right) dh - V_o^2 \left(1 - \left(\frac{CD}{y}\right)^2\right) \tag{14a}$$

$$V_y^2 = V_o^2 \left(\frac{CD}{y}\right)^2 - 2g \int_{\bar{h}_t}^{y} \left(\frac{\bar{\rho}_b - \rho_o}{\rho_o}\right) dh \tag{14b}$$

or it could be written in another form (energy) as

$$\frac{\rho_o V_y^2}{2} = \frac{\rho_o V_o^2}{2} \left(\frac{CD}{y}\right)^2 - \int_{\bar{h}_t}^{y} (\bar{\rho}_b - \rho_o)\, dh \tag{14c}$$

In Equation (14), if the considered fluid to be homogeneous, i.e., no stratification (density gradient is zero) the second term in Equation (14) will drop off (equals zero), and the equation will be reduced to Equation (13) which represents the jet dissipation effect. Also, if the flow is considered frictionless, the dissipation term can be neglected, and the equation will be reduced to Equation (11) which represents the stratification effect.

At s the stagnation point $y = h_s$

$$V_{h_s}^2 = 0 = V_o^2 \left(\frac{CD}{h_s}\right)^2 - 2g \int_{\bar{h}_t}^{h_s} \frac{\bar{\rho}_b - \rho_o}{\rho_o} dh$$

$$= V_o^2 \left(\frac{CD}{h_s}\right)^2 - 2g \left(\frac{\bar{\rho}_b - \rho_o}{\rho_o}\right)(h_s - \bar{h}_t) \tag{15}$$

This equation can now be solved for the penetration depth h_s, but the equation is cubic in h_s and in this case we will get three solutions. However, this equation (when checked) gives one real root (which is the solution) and two complex conjugates.

An application of this relation (Equation (15)) to the available experimental data shows that the value of C is 3.5. Figures 27 and 28 show the penetration depth predicted by this equation compared with the experimental data and the computed solution where it shows a fairly good agreement.

The above comparison indicates that Equation (15) can predict the penetration with an error less than 12 percent as compared with the experimental data in Figure 28; in Figure 27 the error is about 5 percent.

Now the equation is set to predict the penetration depth or velocity (if y is known), assuming that there is no release water from the flow field. In case of a release flow, an extra term is needed for the velocity expression (Equation (14)) to represent the pulling action (which increases the velocity as well as the penetration depth) on the jet.

This term will be a function of the flow rate ratio Q*, and the total depth of the flow field H, F(Q*, H). It will represent the work done on the flow by the pressure gradient induced by the release flow. The equation in its general form will be as follows:

$$V_y^2 = V_o^2 \left(\frac{CD}{y}\right)^2 - 2g \int_o^y \frac{\rho - \rho_o}{\rho_o} dh + F(Q^*, H)$$

If the value of V_y is known, one can solve for the penetration depth y. In some cases when the V_y value is high, a value of y higher than H is expected. In this case, we set y = h in the final result for convenience where H is the total depth and y equals H when the jet reaches the bottom.

APPENDIX D

HYDROSTATIC PRESSURE

The axial momentum equation used in the program without the buoyancy term in the conservative form is

$$\frac{\partial V}{\partial t} + \frac{\partial}{\partial x}(VU) + \frac{\partial}{\partial y}(V^2) + \frac{UV}{x} = g_y - \frac{1}{\rho}\frac{\partial \bar{P}}{\partial y} + \frac{\mu}{\rho}\left(\frac{\partial^2 V}{\partial x^2} + \frac{\partial^2 V}{\partial y^2} + \frac{1}{x}\frac{\partial V}{\partial x}\right)$$

where g_y, the body force, is equal to -g, the gravitational acceleration (= 32.2 ft/sec^2).

In the absence of motion,

$$\frac{\partial \bar{P}}{\partial y} = \rho g_y = -\rho g$$

Checking the pressure in the program to see if the hydrostatic pressure was calculated properly, the program was run with a zero input velocity (null case) and a zero initial pressure. In this case there is no deviation from hydrostatic pressure caused by velocity, but we do have a hydrostatic pressure case. Although the initial pressure should not be zero (where we have a hydrostatic pressure because of the difference in density in the flow field), the equations will be able to calculate the hydrostatic pressure. At the same time the pressure will be adjusted in order for the velocity to satisfy the continuity equation and since all the velocities in the field are zero, then the resulting output pressure will represent the hydrostatic pressure.

The output pressure, as shown in Figure 30, represents the hydrostatic pressure, where it shows that the pressure increases with depth. In addition, one can see that the pressure at the surface is negative. This occurred because the initial pressure was zero where it should have the initial hydrostatic pressure value. The program was run also with an initial hydrostatic pressure and zero velocity, and in this case the

pressure at the surface will represent the atmospheric pressure. The new pressure profile is shown in Figure 30 where it is shifted by a value equal to the atmospheric pressure.

Then when the buoyancy term is used in the equation as

$$\frac{\partial V}{\partial t} + \frac{\partial}{\partial x}(VU) + \frac{\partial}{\partial y}(V^2) + \frac{UV}{x} = \frac{-1}{\rho_o}\frac{\partial P}{\partial y} + g_y \frac{(\rho - \rho_o)}{\rho_o}$$

$$+ \frac{\mu}{\rho_o}\left(\frac{\partial^2 V}{\partial x^2} + \frac{\partial^2 V}{\partial y^2} + \frac{1}{x}\frac{\partial V}{\partial x}\right)$$

and as mentioned before that when V = 0 (fluid at rest), then

$$\frac{-1}{\rho_o}\frac{\partial \bar{P}}{\partial y} = \frac{\rho g}{\rho_o}$$

In this case this term (pressure gradient) will be already included in the buoyancy term; however, the pressure gradient $\frac{\partial P}{\partial y}$ will be zero because it represents the deviation from hydrostatic pressure caused by velocity.

$$\frac{\partial \bar{P}}{\partial y} = \frac{\partial}{\partial y}(P + \rho g_y h) = \frac{\partial}{\partial y} P + \frac{\partial}{\partial y} \rho g_y h = \frac{\partial}{\partial y} P + \rho g_y$$

Then adding the body force,

$$\frac{\partial \bar{P}}{\partial y} = \frac{\partial}{\partial y} P + \rho g_y - \rho_o g_y$$

Rearranging,

$$\frac{1}{\rho_o}\frac{\partial \bar{P}}{\partial y} = \frac{1}{\rho_o}\frac{\partial}{\partial y} P + g_y \frac{(\rho - \rho_o)}{\rho_o}$$

In the case of V = 0, we have P = 0; then,

$$\frac{1}{\rho_o}\frac{\bar{P}}{y} = g_y \frac{(\rho - \rho_o)}{\rho_o}$$

and when the buoyancy is used the initial pressure P value (function of velocity) will be always zero if the initial velocity field is zero.

APPENDIX E

THE DIMENSIONLESS GOVERNING EQUATIONS

The governing equations of mass, momentum, and species conservation being dimensional, can be made dimensionless by redefining the dependent and independent variables in a dimensionless form. This can be accomplished by dividing:

1. Lengths by D_p, the diameter of the propeller, or some other characteristic length.

2. Velocities by V_p, the downward velocity at the propeller.

3. Pressure by $P_{ref} = \rho_1 V_p^2$, the stagnation pressure corresponding to the reference velocity V_p.

4. Mass fraction by the initial top water mass fraction M_1 in the upper layer.

The resulting dimensionless variables will be as follows:

$$U^* = \frac{U}{V_p} \qquad V^* = \frac{V}{V_p}$$

$$y^* = \frac{y}{D_p} \qquad x^* = \frac{x}{D_p}$$

$$P^* = \frac{P}{P_{ref}} \qquad m_1^* = \frac{m_1}{M_1}$$

Inserting the dimensionless variables into the governing Equation (1) in Chapter II in the conservative form, we obtain a set of equations in the dimensionless form. The equation of continuity gives

$$\frac{\partial U^*}{\partial x^*} + \frac{\partial V^*}{\partial y^*} + \frac{U^*}{x^*} = 0$$

The steady state Navier-Stokes equations in the dimensionless form will be as follows: the x-momentum equation with $g_x = 0$,

$$\frac{\partial}{\partial x^*}(U^{*2}) + \frac{\partial}{\partial y^*}(U^* V^*) + \frac{U^{*2}}{x^*} = \frac{\partial P^*}{\partial x^*}$$

$$+ \frac{1}{Re} \left[\frac{\partial^2 U^*}{\partial x^{*2}} + \frac{\partial^2 U^*}{\partial y^{*2}} + \frac{1}{x^*} \frac{\partial U^*}{\partial x^*} - \frac{U^*}{x^{*2}}\right]$$

where $Re = V_p D_p \rho_1 / \mu$ is the Reynolds number, and the y-momentum equation,

$$\frac{\partial}{\partial x^*} (U^* V^*) + \frac{\partial}{\partial y^*} (V^{*2}) + \frac{U^* V^*}{x} = \frac{1}{Fr_d^2} - \frac{\partial P^*}{\partial y^*}$$

$$+ \frac{1}{Re} \left[\frac{\partial^2 V^*}{\partial x^{*2}} + \frac{\partial^2 V^*}{\partial y^{*2}} + \frac{1}{x^*} \frac{\partial V^*}{\partial x^*}\right]$$

where

$$Fr_d^2 = \frac{V_p}{g_y \frac{\Delta\rho}{\rho_1} H}$$

is the densimetric Froude number and $\Delta\rho = \rho - \rho_1$.

The mass diffusion equation also will be in the dimensionless form

$$\frac{\partial (U^* M_1^*)}{\partial x^*} + \frac{\partial (M_1^* V^*)}{\partial y^*} + \frac{M_1^* U^*}{x^*} = \frac{\nu}{Re\ \sigma_{sc}} \left[\frac{\partial^2 M_1^*}{\partial x^{*2}} + \frac{\partial^2 M_1^*}{\partial y^{*2}} + \frac{1}{x^*} \frac{\partial M_1^*}{\partial x^*}\right]$$

where $\frac{\nu}{Re} = \frac{\mu}{\rho} \cdot \frac{1}{\frac{\mu}{\rho D_c}}$

$$\sigma_{sc} = \frac{\mu}{\rho D_c}$$

is the Schmidt number, and D_c is the molecular diffusivity.

The dimensionless coefficients Re, Fr_d, and σ_{sc} define the governing equations and indicate the solution where, if these dimensionless coefficients are the same in the model and prototype equations, and the boundary conditions are the same, there will be a complete similitude between the model and the prototype.

The first dimensionless coefficient is the inverse of the Reynolds number, and it appears in the Navier-Stokes and mass diffusion equations. If the viscosity term is small, or if the flow is turbulent, the influence of the Reynolds number may be weak. Therefore, in many cases modeling accuracy may not be sensitive to the exact matching of the Reynolds number between the model and the prototype. The use of a too-small Reynolds number (compared to the prototype Reynolds number) in a model is investigated elsewhere (22), and from considerable experience it is known that this deviation from complete similitude produces only small errors, provided that the flow regime is turbulent for both model and prototype.

The other dimensionless and most important coefficient is the square inverse of the densimetric Froude number, Fr_d. It appears in the y-momentum equation as an independent term. The characteristic length is taken as H, the total depth. Matching the densimetric Froude number between the model and the prototype can be accomplished by increasing the density difference between the model and the prototype in order to offset a smaller depth in the model. Exact matching of the densimetric Froude number is essential (22) in the modeling process.

The third dimensionless coefficient is the Schmidt number, which appears in the mass diffusion equation. The Schmidt number should be the same between the model and the prototype, and since the flow regime is considered turbulent, the turbulent Schmidt number (with the value of unity) is used.

We can conclude that the most important dimensionless coefficient in the y-momentum equation is the square inverse of the densimetric Froude number, Fr_d. At values less than unity the dimensionless

coefficient in the y-momentum equation will be larger than unity, and will increase rapidly with decreasing Fr_d, a condition appropriate to higher buoyancy forces. For values of Fr_d greater than unity, the dimensionless coefficient decreases rapidly with increasing densimetric Froude number.

The numerical simulation of the flow field is done by matching the densimetric Froude number and Schmidt number. The Reynolds number, however, was not matched exactly, since only laminar viscosity was used. As a check, increased values of viscosity throughout the field were used to identify any sensitivity to the level of momentum exchange. That is, a large laminar viscosity roughly simulates a turbulent viscosity, the exchange coefficients in each case being similar in magnitude in these two cases. The influences on dilution factor and penetration depth were very small (5%) for the cases studied.

APPENDIX F

COMPUTER PROGRAM LISTING

```
$JOB            ,TIME=(20,00)
C
C
C
C
C    ********* NUMERICAL SIMULATION OF DESTRATIFICATION OF LAKES **********
C
C
C       THIS PROGRAM IS BASED ON LOS ALAMOS SOLA PREDICTION TECHNIQUE
C
C       IT IS EXPANDED TO INCLUDE COMPUTATIONS FOR MASS DIFFUSION AND
C
C       BOUYANCY FORCES . THE PROGRAM SOLVES NAVIER-STOKES,CONTINUITY,
C
C       AND MASS DIFFUSION EQUATIONS FOR AN AXISYMMETRIC STRATIFIED
C
C       FLOW FIELD
C
C
C
C       IBAR = NUMBER OF CELLS IN X-DIRECTION
C
C       JBAR = NUMBER OF CELLS IN Y-DIRECTION
C
C       DELT = TIME INCREMENT
C
C       NU = COEFFICIENT OF KINAMATIC VISCOSITY
C
C       MU = COEFFICIENT OF ABSOLUTE VISCOSITY
C
C       CYL = GEOMETRY INDICATOR 1.0 FOR CYLINDRICAL COORDINATES
C
C                                0.0 FOR PLANE COORDINATES
C       EPSI = PRESSURE ITERATION CONVERGENCE CRITIRION
C
C       GX = BODY ACCELERATION IN POSITIVE X-DIRECTION
C
C       GY = BODY ACCELERATION IN NEGATIVE Y-DIRECTION
C
C       OMG = OVER RELAXIATION FACTOR . A VALUE THAT IS OFTEN OPTIMUM
C
C             IS 1.8 BUT IN NO CASE SHOULD BE LARGER THAN 2.0
C
C       ALPHA = CONTROLS AMOUNT OF DONOR CELL FLUXING ,VALUES BETWEEN
C
C                 0.0 AND 1.0 ARE TO BE USED
C
C       U = RADIAL VELOCITY
C
C       V = AXIAL VELOCITY
C
C       SC = SCHMIDT NUMBER
C
C       S = MASS FRACTION M1
C
C       S2 = MASS FRACTION M2
C
C       DEN = WEIGHTED AVERAGE DENSITY
C
C       DEN1 = TOP DENSITY
```

```
C
C       DEN2 = BOTTOM DENSITY
C
C       DELX = CELL WIDTH
C
C       DELY = CELL HEIGHT
C
C       IREL = NUMBER OF CELLS OF THE RADIUS OF THE RELEASE GATE +1
C
C       JIN = NUMBER OF CELLS OF THE INTERFACE HEIGHT +1
C
C       IDISK = NUMBER OF CELLS OF THE PROPELLER RADIUS +1
C
C       JDISK = NUMBER OF CELLS OF THE PROPELLER HEIGHT +1
C
C       JNT -JNB = NUMBER OF CELLS OF THE OPENING HEIGHT FOR TOP
C
C                  WATER INLET
C
C       JNT1 -JNB1 = NUMBER OF CELLS OF THE OPENING HEIGHT FOR BOTTOM
C
C                    WATER INLET
C
C       DR = DENSITY RATIO BETWEEN THE TOP AND THE BOTTOM DENSITIES
C
C       VINITL = PROPELLER VELOCITY
C
C       QSTAR = FLOW RATE RATIO F
C       QSTAR = FLOW RATE RATIO PF PROPELLER FLOW RATE TO RELEASE
C
C                FLOW RATE
C
C       QPROP = PROPELLER FLOW RATE
C
C       QREL = RELEASE FLOW RATE
C
C       VOUT = RELEASE VELOCITY
C
C
C
C
C
C
C
C
      INTEGER CYCLE
      REAL NU,MU
      DIMENSION D(15,30),DELP(15,30),B1(15,30)
      DIMENSION U(15,30),V(15,30),P(15,30),UN(15,30),VN(15,30)
C
       DIMENSION S(15,30),S2(15,30),DEN(15,30),SN(15,30)
      IWRITE=0
      DATA U,V,P,UN,VN /2250*0.0/
C     S,SN,ETC  ARE INDICATED LATER
C
      DATA EPSI,DELX,DELY,IBAR,JBAR,GX,GY,OMG,CYL
     Y /1.E-3,0.145,0.0729,5,14,0.0,-32.2,1.7,1.0 /
C
C
      QSTAR=0.44
```

```
      C       FROUDE  NUMBER = 1.86
   10          DR=1.00247
   11          VINITL=0.7
      C
   12         CON1=0.0
   13         CON2=1.0
   14          ALPHA=0.6
   15         PI=3.14159
   16          NU=1.41E-5
   17          MU=2.73E-5
   18         SC=1.0
   19         DEN1=62.4/32.2
   20            DEN2=62.4*DR/32.2
   21         DZRO=1.0
      C
   22         IREL=3
   23          DELX=0.1875
   24          DELY=0.125
   25          IBAR=7
   26          JDISK=12
   27            JIN=9
   28          JNT=13
   29          JNB=12
   30         JNT1=7
   31         JNB1=6
   32          IDISK=2
   33         JIN1=JIN+1
   34         IMAX=IBAR+2
   35         JMAX=JBAR+2
   36         IM1=IMAX-1
   37         JM1=JMAX-1
   38         IM2=IBAR
   39         JM2=JBAR
   40         RDX=1./DELX
   41         RDY=1./DELY
      C
   42         QPROP=VINITL*PI*((IDISK-1)*DELX)**2
   43         QREL=QPROP/QSTAR
   44         VOUT=QREL/(PI*((IREL-1)*DELX)**2)
      C
      C
   45          DELT=0.02
   46         BETA=OMG/(2.0*DELT*(RDX**2+RDY**2))
      C
      C      PARAMETER CHECK                                              00013400
      C
   47          DTMAX1=0.33*DELY/VINITL
   48         DTMAX2=0.5*DELX**2*DELY**2/((DELX**2+DELY**2)*NU)            00013600
   49         ALFAMI=1.5*VINITL*DELT/DELY
   50         WRITE(6,92) DELT,DTMAX1,DTMAX2                               00013800
   51           WRITE(6,93) ALPHA,ALFAMI
      C
      C      DT REDUCTION FOR STABILITY                                   00014000
      C
   52         IF(DELT.GT.DTMAX1)DELT=DTMAX1                                   4
   53      92 FORMAT(' DELT DTMAX1 DTMAX2',3E12.4)
   54      93 FORMAT(' ALPHA ALFAMIN ',2E12.4)
      C       ----------------------------------------------------------------00014400
      C-----------INITIALIZATION                                            00014500
   55         T = 0                                                        00014600
```

```
56          ITER=0                                                          00014700
57          CYCLE=0                                                         00014800
      C           GUESS INITIAL VELOCITY FIELD                              00014900
58          DO 560 I=1,IMAX                                                 00015000
59          DO 560 J=1,JMAX                                                 00015100
60          U(I,J) = 0.                                                     00015200
61          V(I,J) = 0.                                                     00015300
62     560    CONTINUE                                                      00015500
      C
      C   ---------INITIAL  DENSITY AND MASS FRACTION FIELD
      C
63          DO 555 I=1,IMAX
64          DO 555 J=1,JIN
65          S(I,J)=0.0
66          S2(I,J)=1.0
67          SN(I,J)=0.0
68          DEN(I,J)=DEN2
69     555  CONTINUE
      C
70          DO 556 I=1,IMAX
71          DO 556 J=JIN1,JMAX
72          S(I,J)=1.0
73          S2(I,J)=0.0
74           SN(I,J)=1.0
75          DEN(I,J)=DEN1
76     556  CONTINUE
      C      ------------------------------------------------------------------00015600
      C
77           ASSIGN  5000 TO KRET                                           00015800
78          GO TO 2000                                                      00015900
79     1000 CONTINUE                                                        00016000
80           ITER=0                                                         00016100
81           FLG=1.0                                                        00016200
82           ASSIGN  3000 TO KRET                                           00016300
      C
      C      ------------------------------------------------------------------00016500
      C----------APPLY MOMENTA EQUS FOR TIME ADVANCED U, V, W                00016600
      C
83          DO 1100 I = 2,IM1                                               00016800
84          DO 1100 J = 2,JM1                                               00016900
85           FUX=((UN(I,J)+UN(I+1,J))*(UN(I,J)+UN(I+1,J))+ALPHA*ABS(UN(I,J)+UN(00017000
            1I+1,J))*(UN(I,J)-UN(I+1,J))-(UN(I-1,J)+UN(I,J))*(UN(I-1,J)+UN(I,J)00017100
            2)-ALPHA*ABS(UN(I-1,J) + UN(I,J)) *(UN(I-1,J)-UN(I,J)))/(4*DELX)   00017200
86           FUY=((VN(I,J)+VN(I+1,J))*(UN(I,J) + UN(I,J+1))                    00017300
            1 + ALPHA *     ABS(VN(I,J)+VN(I+1,J)) * (UN(I,J)-UN(I,J+1))      00017400
            2-(VN(I,J-1)+VN(I+1,J-1)) * (UN(I,J-1) + UN(I,J)))                00017500
            3-ALPHA*ABS(VN(I,J-1)+VN(I+1,J-1))*(UN(I,J-1) - UN(I,J)))/(4.*DELY)00017600
87           FUC=CYL*((UN(I,J)+UN(I+1,J))*(UN(I,J)+UN(I+1,J))+(UN(I-1,J)+UN(I,J00017700
            1))*(UN(I-1,J)+UN(I,J))                                           00017800
            2+ALPHA * ABS(UN(I,J) + UN(I+1,J)) * (UN(I,J)-UN(I+1,J))          00017900
            3+ALPHA * ABS(UN(I-1,J)+UN(I,J)) * (UN(I-1,J)-UN(I,J)))           00018000
            4 /(8.*DELX*FLOAT(I-1))                                           00018100
88           FVX=((UN(I,J)+UN                                                 00018200
            C               (I,J+1))*(VN(I,J)+VN(I+1,J))+ALPHA*ABS(UN(I,J)+UN( 00018300
            1I,J+1))*(VN(I,J)-VN(I+1,J))-(UN(I-1,J)+UN(I-1,J+1))*(VN(I-1,J)+VN(00018400
            2I,J))-ALPHA*ABS(UN(I-1,J)+UN(I-1,J+1))*(VN(I-1,J)-VN(I,J)))/(4.*DE00018500
            3LX)                                                              00018600
89           FVY=((VN(I,J)+VN(I,J+1))*(VN(I,J)+VN(I,J+1))+ALPHA*ABS(VN(I,J)+VN 00018700
            1(I,J+1))*(VN(I,J)-VN(I,J+1))-(VN(I,J-1)+VN(I,J))*(VN(I,J-1)+VN(I,J00018800
            2))-ALPHA*ABS(VN(I,J-1)+VN(I,J))*(VN(I,J-1)-VN(I,J)))/(4.*DELY)    00018900
```

```
90          FVC=CYL*((UN(I,J)+UN(I,J+1))*(VN(I,J)+VN(I+1,J))+(UN(I-1,J)+UN(I-100019000
           1,J+1))*(VN(I-1,J)+VN(I,J)))+ALPHA*ABS(UN(I,J)+UN(I,J+1))*(VN(I,J)-V00019100
           2N(I+1,J))+ALPHA*ABS(UN(I-1,J)+UN(I-1,J+1))*(VN(I-1,J)-VN(I,J)))   00019200
           3/(8.*DELX*(FLOAT(I-1)-.5))                                        00019300
91          VISX= MU * ((UN(I+1,J)-2.*UN(I,J) + UN(I-1,J))/DELX**2+           00019400
           1            (UN(I,J+1)-2.*UN(I,J) + UN(I,J-1))/DELY**2            00019500
           2 +CYL * ((UN(I+1,J)-UN(I-1,J))/(2.*DELX*DELX*FLOAT(I-1))          00019600
           3  -UN(I,J)/(DELX*FLOAT(I-1))**2))/DEN1
92.         VISY= MU* ((VN(I+1,J)-2.*VN(I,J) + VN(I-1,J))/DELX**2+            00019800
           1           (VN(I,J+1)-2.*VN(I,J) + VN(I,J-1))/DELY**2             00019900
           2 +CYL *  (VN(I+1,J)-VN(I-1,J))/(2.*DELX*DELX*(FLOAT(I)-1.5)))/DEN1
93          FMX=(UN(I,J)*(SN(I,J)+SN(I+1,J))+ALPHA*(ABS(UN(I,J)))*(SN(I,J)-SN(00020100
           ,      I+1,J))-UN(I-1,J)*(SN(I-1,J)+SN(I,J))-ALPHA*(ABS(UN(I-1,J)))*00020200
           ,      (SN(I-1,J)-SN(I,J)))/(2*DELX)                              00020300
94          FMY=(VN(I,J)*(SN(I,J)+SN(I,J+1))+ALPHA*(ABS(VN(I,J)))*(SN(I,J)-SN(00020400
           ,      I,J+1))-VN(I,J-1)*(SN(I,J-1)+SN(I,J))-ALPHA*(ABS(VN(I,J-1)))*00020500
           ,      (SN(I,J-1)-SN(I,J)))/(2*DELY)                              00020600
95          FMC=(UN(I,J)*(SN(I,J)+SN(I+1,J)*CON2)+UN(I-1,J)*(SN(I-1,J)+SN(I,J
           .))*CON2+ALPHA*(ABS(UN(I,J)))*(SN(I,J)-SN(I+1,J))*CON1+ALPHA*(ABS(
           .UN(I-1,J)))*(SN(I-1,J)-SN(I,J))*CON1)/(4*DELX*(I-1.5))*CYL
96          VIMX=((SN(I+1,J)-2*SN(I,J)+SN(I-1,J))/(DELX**2)+(SN(I,J+1)-2*SN(I,00021000
           ,      J)+SN(I,J-1))/(DELY**2)+(SN(I+1,J)-SN(I-1,J))/(2*(DELX**2)*(00021100
           ,      I-1.5))*CYL)*(MU/(SC*DEN1))
97          U(I,J)=UN(I,J)+DELT*((P(I,J)-P(I+1,J))*RDX/DEN1+GX-FUX-FUY-FUC+
           .VISX)
98          V(I,J)=VN(I,J)+DELT*((P(I,J)-P(I,J+1))*RDY/DEN1+GY*(DEN(I,J)-DEN1)
           . /DEN1-FVX-FVY-FVC+VISY)
99          S(I,J)=SN(I,J)+DELT*(-FMX-FMY-FMC+VIMX)
100         IF(CYCLE.EQ.1) S(I,J)=SN(I,J)
101           S2(I,J)=1.0-S(I,J)
102         DEN(I,J)=S(I,J)*DEN1+S2(I,J)*DEN2
103         B1(I,J)=GY*(DEN(I,J)-DEN1)/DEN1
104       1100 CONTINUE                                                        00021800
          C     ------------------------------------------------------------00021900
          C
105       2000 CONTINUE                                                      00022100
          C
          C     ------------------------------------------------------------00022300
          C
106         QS=0.0
107         A=0.0
108         DO 551  I=2,IREL
109           QS=QS+S(I,2)*(PI*((I-1)*DELX)**2-A)*VOUT
110           A=PI*((I-1)*DELX)**2
111       551  CONTINUE
          C
112         QS2=0.0
113         A=0.0
114         DO 552  I=2,IREL
115           QS2=QS2+S2(I,2)*(PI*((I-1)*DELX)**2-A)*VOUT
116           A=PI*((I-1)*DELX)**2
117       552  CONTINUE
118         UT=QS/(2*PI*IBAR*(JNT-JNB+1)*DELY*DELX)
119         UB=QS2/(2*PI*IBAR*(JNT1-JNB1+1)*DELY*DELX)
120         DENAC=(QS*DEN1+QS2*DEN2)/(PI*((IREL-1)*DELX)**2*VOUT)
121          DF=(DENAC-DEN2)/(DEN1-DEN2)
          C
          C-----------GENERAL BOUNDARY CONDITIONS                            00022500
          C
122         DO 2200 J=1,JMAX
```

```
      C     -------------BOUNDARY CONDITIONS ON LEFT--FREE SLIP
      C
  123           U(1,J)=0.0
  124           V(1,J)=V(2,J)
  125           S(1,J)=S(2,J)
      C
      C     -----------BOUNDARY CONDITIONS ON RIGHT--NO SLIP
      C
  126           U(IM1,J)=0.0
  127           V(IMAX,J)=-V(IM1,J)
  128           S(IMAX,J)=S(IM1,J)
  129     2200  CONTINUE
  130           DO 2500 I=1,IMAX
      C
      C    ------------BOUNDARY CONDITIONS ON TOP--FREE SLIP
      C
  131           V(I,JM1)=0.0
  132           U(I,JMAX)=U(I,JM1)
  133           S(I,JMAX)=S(I,JM1)
      C
      C    ------------BOUNDARY CONDITIONS ON BOTTOM-NO SLIP
      C
  134           V(I,1)=0.0
  135           U(I,1)=-U(I,2)
  136           S(I,1)=S(I,2)
  137      2500 CONTINUE
      C
  138           JDISK1=JDISK-1
      C
      C     ---------------INLET FLOW
      C
  139           DO 2811 I=2,IDISK
  140             V(I,JDISK)=-VINITL
  141           V(I,JDISK1)=V(I,JDISK)
  142             U(I,JDISK)=0.0
  143      2811 CONTINUE
      C
  144           DO 558  J=JNB,JNT
  145             V(IMAX,J)=0.0
  146             U(IMAX,J)=-UT
  147             U(IM1,J)=-UT
  148             S(IMAX,J)=S(IM1,J)
  149      558  CONTINUE
      C
  150           DO 559  J=JNB1,JNT1
  151             V(IMAX,J)=0.0
  152             U(IMAX,J)=-UB
  153             U(IM1,J)=-UB
  154             S(IMAX,J)=S(IM1,J)
  155      559  CONTINUE
      C  ------------  OUTLET FLOW
      C
  156           DO 557  I=2,IREL
  157             U(I,1)=0.0
  158             V(I,1)=-VOUT
  159             V(I,2)=-VOUT
  160             S(I,1)=S(I,2)
  161      557  CONTINUE
      C
  162      2801 CONTINUE
```

```
163           GO TO KRET,(3000,5000)
164   3000     CONTINUE                                                    00041900
      C
      C ------------CHECK IF CONVERGENCE HAS BEEN REACHED
      C
165           IF (FLG.EQ.0) GOTO4000                                      00042000
166           ITER=ITER+1                                                 00042100
167           IF(ITER.LT.50) GO TO 3050
168           IF(CYCLE.LT.20)GOTO 4000                                    00042400
      C      TERMINATION CONDITION                                       00042500
169           T=1E+10                                                     00042600
170           GOTO5000                                                    00042700
171   3050     FLG=0.0                                                   00042800
      C
      C  ----------PRESSURE ITERATION AND P, U, V UPDATE
      C
172           DO 3500 J=2,JM1                                             00043100
173           DO 3500 I=2,IM1                                             00043200
174           D(I,J)=RDX*(U(I,J)-U(I-1,J))+RDY*(V(I,J)-V(I,J-1))+CYL*(U(I,J)
             *  +U(I-1,J))/(2.*DELX*(FLOAT(I)-1.5))
175           IF(ABS(D(I,J)/DZRO).GE.EPSI) FLG=1.0
176           DELP(I,J)= -BETA*D(I,J)
177           P(I,J)=P(I,J)+DELP(I,J)
178           U(I,J)=U(I,J)+DELT*RDX*DELP(I,J)
179           U(I-1,J) = U(I-1,J) - DELT*RDX*DELP(I,J)
180           V(I,J)=V(I,J)+DELT*RDY*DELP(I,J)
181           V(I,J-1) = V(I,J-1)-DELT*RDY*DELP(I,J)
      C
182    3500 CONTINUE                                                      00044300
      C-----------CHECKPRINTS DURING PRESSURE CYCLE                      00044500
183           IWRITE=0                                                    00044600
184           IF(ITER.LE.2)IWRITE=1                                       00044700
185            IF(CYCLE.GT.2.AND.CYCLE.LT.500)  IWRITE=0
186           IF(IWRITE.EQ.1)GO TO 5152                                   00044900
      C      RETURN FROM PRINTING SECTION                                00045000
187    3501 CONTINUE                                                      00045100
188           IWRITE=0                                                    00045200
      C
189           GO TO 2000                                                  00045400
190   4000    CONTINUE                                                    00045500
191   5000    CONTINUE                                                    00045600
      C-------------------------------------------------------------------00045700
      C-----------INTERMEDIATE PRINTING                                   00045800
      C        IF(CYCLE.EQ.500)CALL PLOT(U,V,IMAX,JMAX,DELX,DELY)
192           IF(CYCLE.EQ.10) GO TO 5152
193           IF(CYCLE.EQ.20) GO TO 5152
194           IF(CYCLE.EQ.30) GO TO 5152
195           IF(CYCLE.EQ.40) GO TO 5152
196           IF(CYCLE.EQ.50) GO TO 5152
197          IF(CYCLE.EQ.60) GO TO 5152
198          IF(CYCLE.EQ.70) GO TO 5152
199          IF(CYCLE.EQ.80) GO TO 5152
200          IF(CYCLE.EQ.90) GO TO 5152
201          IF(CYCLE.EQ.100) GO TO 5152
202          IF(CYCLE.EQ.110) GO TO 5152
203          IF(CYCLE.EQ.120) GO TO 5152
204          IF(CYCLE.EQ.130) GO TO 5152
205          IF(CYCLE.EQ.140) GO TO 5152
206          IF(CYCLE.EQ.150) GO TO 5152
207          IF(CYCLE.EQ.160) GO TO 5152
```

```
      IF(CYCLE.EQ.170) GO TO 5152
      IF(CYCLE.EQ.180) GO TO 5152
      IF(CYCLE.EQ.190) GO TO 5152
      IF(CYCLE.EQ.200) GO TO 5152
      IF(CYCLE.EQ.210) GO TO 5152
      IF(CYCLE.EQ.220) GO TO 5152
      IF(CYCLE.EQ.230) GO TO 5152
      IF(CYCLE.EQ.240) GO TO 5152
      IF(CYCLE.EQ.250) GO TO 5152
      IF(CYCLE.EQ.260) GO TO 5152
      IF(CYCLE.EQ.270) GO TO 5152
      IF(CYCLE.EQ.280) GO TO 5152
      IF(CYCLE.EQ.286) GO TO 5152
      IF(CYCLE.EQ.287) GO TO 5152
      IF(CYCLE.EQ.288) GO TO 5152
      IF(CYCLE.EQ.289) GO TO 5152
      IF(CYCLE.EQ.290) GO TO 5152
       IF(CYCLE.EQ.293) GO TO 5152
       IF(CYCLE.EQ.295) GO TO 5152
       IF(CYCLE.EQ.297) GO TO 5152
       IF(CYCLE.EQ.299) GO TO 5152
       IF(CYCLE.EQ.300) GO TO 5152
       IF(CYCLE.EQ.310) GO TO 5152
       IF(CYCLE.EQ.320) GO TO 5152
       IF(CYCLE.EQ.330) GO TO 5152
       IF(CYCLE.EQ.340) GO TO 5152
       IF(CYCLE.EQ.350) GO TO 5152
       IF(CYCLE.EQ.360) GO TO 5152
       IF(CYCLE.EQ.370) GO TO 5152
      IF(CYCLE.EQ.380) GO TO 5152
      IF(CYCLE.EQ.390) GO TO 5152
      IF(CYCLE.EQ.395) GO TO 5152
      IF(CYCLE.EQ.397) GO TO 5152
      IF(CYCLE.EQ.399) GO TO 5152
      IF(CYCLE.EQ.400) GO TO 5152
       IF(CYCLE.EQ.2) GO TO 5152
      IF(CYCLE.EQ.1) GO TO 5152
      IF(CYCLE.EQ.0) GO TO 5152
       GO TO 5251
5152   CONTINUE                                                  00046700
       PRINT 53,ITER,T ,CYCLE                                    00046800
      PRINT 54,DF
       WRITE(6,48)                                               00046900
C
C  ----------  LIST U, V, P, S, DEN, D, B1
C
      DO 7001 J=1,JMAX                                           00047000
      JMMJ=JMAX-J+1                                              00047100
       WRITE(6,47) (U(I,JMMJ),I=1,IMAX)                          00047200
7001   CONTINUE                                                  00047300
       WRITE(6,49)                                               00047400
       DO 7002 J=1,JMAX                                          00047500
      JMMJ=JMAX-J+1                                              00047600
       WRITE(6,47) (V(I,JMMJ),I=1,IMAX)                          00047700
7002   CONTINUE                                                  00047800
7014      CONTINUE                                               00046500
       WRITE(6,51)                                               00048600
       DO 7004 J=1,JMAX                                          00048700
      JMMJ=JMAX-J+1                                              00048800
       WRITE(6,47) (P(I,JMMJ),I=1,IMAX)                          00048900
```

```
 7004   CONTINUE                                                        00049000
        WRITE(6,62)
        DO 7005 J=1,JMAX
        JMMJ=JMAX-J+1
        WRITE(6,47) (S(I,JMMJ),I=1,IMAX)
 7005 CONTINUE
        WRITE(6,63)
        DO 7006 J=1,JMAX
        JMMJ=JMAX-J+1
        WRITE(6,47) (DEN(I,JMMJ),I=1,IMAX)
 7006 CONTINUE
        WRITE(6,64)
        DO 7007 J=1,JMAX
        JMMJ=JMAX-J+1
        WRITE(6,47) (D(I,JMMJ),I=1,IMAX)
 7007 CONTINUE
        WRITE(6,65)
        DO 7008 J=1,JMAX
        JMMJ=JMAX-J+1
        WRITE(6,47) (B1(I,JMMJ),I=1,IMAX)
 7008 CONTINUE
 5251     CONTINUE                                                      00050200
C
C       RETURN TO PRESSURE ITERATION CYCLE IF THESE WERE ONLY CHECKPRINTS 00050400
        IF(IWRITE.EQ.1)GO TO 3501                                       00050500
C---------------------------------------------------------------------00050600
C-----------REPACKAGING                                               00050700
         DO 6101 I=1,IMAX                                               00050800
         DO 6101 J=1,JMAX                                               00050900
         UN(I,J)=U(I,J)                                                 00051000
         VN(I,J)=V(I,J)                                                 00051100
        SN(I,J)=S(I,J)
 6101 CONTINUE                                                          00051300
C---------------------------------------------------------------------00052300
C        ADVANCE TIME AND CYCLE.                                        00052400
         T=T+DELT                                                       00052500
         IF(CYCLE.EQ.300) GO TO 6500
         CYCLE=CYCLE+1                                                  00052700
         GOTO 1000                                                      00052800
 6500 CONTINUE                                                          00052900
        STOP                                                            00053000
   47   FORMAT(1X,12(E11.4))
48       FORMAT(///,2X,8H U-FIELD,/)                                    00053200
49       FORMAT(///,2X,8H V-FIELD,/)                                    00053300
51       FORMAT(///,2X,8H P-FIELD,/)                                    00053400
   53   FORMAT(///,6X,5HITER=,I5,9X,5HTIME=,1PE12.5,10X,6HCYCLE=,I4)
   54   FORMAT(//,5X,'DILUTION FACTOR=',1E12.4)
   62   FORMAT(//,2X,8H S-FIELD,/)
   63   FORMAT(//,2X,10H DEN-FIELD,/)
   64   FORMAT(//,2X,8H D-FIELD,/)
   65   FORMAT(//,2X,9H B1-FIELD,/)
        END                                                             00054000
C
C
C
C
C
C
C
C
```

ITER= 1 TIME= 5.99988E 00 CYCLE= 300

DILUTION FACTOR= 0.5299E 00

U-FIELD

0.0000E 00-0.5304E-01-0.1518E-01-0.2202E-01-0.1915E-01-0.1479E-01-0.8311E-02 0.0000E 00 0.0000E 00
0.0000E 00-0.5304E-01-0.1518E-01-0.2202E-01-0.1915E-01-0.1479E-01-0.8311E-02 0.0000E 00 0.0000E 00
0.0000E 00-0.7458E-01-0.9340E-02-0.2688E-01-0.2078E-01-0.1654E-01-0.1088E-01 0.0000E 00 0.0000E 00
0.0000E 00-0.3974E 00-0.5263E-01-0.4082E-01-0.2287E-01-0.2131E-01-0.2932E-01-0.4513E-01-0.4513E-01
0.0000E 00 0.0000E 00-0.1075E 00-0.2596E-01-0.2191E-01-0.2010E-01-0.2916E-01-0.4513E-01-0.4513E-01
0.0000E 00 0.2706E-02-0.2680E-01-0.2228E-01-0.1676E-01-0.1249E-01-0.7991E-02 0.0000E 00 0.0000E 00
0.0000E 00 0.7062E-02-0.2292E-02-0.1025E-01-0.1424E-01-0.1223E-01-0.5229E-02 0.0000E 00 0.0000E 00
0.0000E 00 0.8228E-02-0.2222E-01-0.1473E-01-0.1352E-01-0.6831E-02-0.2439E-03 0.0000E 00 0.0000E 00
0.0000E 00 0.8744E-02-0.2068E-01-0.1789E-01-0.1501E-01-0.1144E-01-0.5804E-02 0.0000E 00 0.0000E 00
0.0000E 00 0.9398E-02-0.2013E-01-0.2201E-01-0.2493E-01-0.3272E-01-0.4158E-01-0.4009E-01-0.4009E-01
0.0000E 00 0.8252E-02-0.2353E-01-0.2479E-01-0.2755E-01-0.3528E-01-0.4393E-01-0.4009E-01-0.4009E-01
0.0000E 00 0.1702E-01-0.3765E-01-0.2508E-01-0.2223E-01-0.1673E-01-0.1081E-01 0.0000E 00 0.0000E 00
0.0000E 00 0.5433E-02-0.5564E-01-0.2678E-01-0.2244E-01-0.1114E-01-0.3083E-03 0.0000E 00 0.0000E 00
0.0000E 00 0.1590E 00-0.2030E 00-0.3247E-01-0.2900E-01-0.1190E-01-0.1753E-02 0.0000E 00 0.0000E 00
0.0000E 00-0.1070E-04-0.1557E-04-0.8578E-01-0.2631E-01-0.1313E-01-0.3467E-02 0.0000E 00 0.0000E 00
-0.0000E 00 0.0000E 00 0.0000E 00 0.8578E-01 0.2631E-01 0.1313E-01 0.3467E-02-0.0000E 00-0.0000E 00

V-FIELD

0.0000E 00 0.0000E 00 0.0000E 00 0.0000E 00 0.0000E 00 0.0000E 00 0.0000E 00 0.0000E 00-0.0000E 00
0.0000E 00 0.0000E 00 0.0000E 00 0.0000E 00 0.0000E 00 0.0000E 00 0.0000E 00 0.0000E 00 0.0000E 00
-0.7072E-01-0.7072E-01 0.1008E-01-0.9516E-02-0.2009E-02 0.3916E-03 0.2922E-02 0.5115E-02-0.5115E-02
-0.1702E 00-0.1702E 00 0.3452E-01-0.2604E-01-0.2479E-02 0.4526E-03 0.5035E-02 0.1181E-01 0.0000E 00
-0.7000E 00-0.7000E 00 0.1648E 00-0.3063E-01 0.3426E-02-0.1784E-02-0.3369E-02-0.2551E-02 0.0000E 00
-0.7000E 00-0.7000E 00 0.6922E-01 0.5920E-02 0.1506E-02-0.3687E-02-0.1240E-01-0.1701E-01 0.1701E-01
-0.6963E 00-0.6963E 00 0.4417E-01 0.2393E-02 0.1526E-02-0.3004E-02-0.1063E-01-0.1210E-01 0.1210E-01
-0.6869E 00-0.6869E 00 0.3901E-01-0.4585E-02-0.3462E-02-0.3620E-02-0.7028E-02-0.8876E-02 0.8876E-02
-0.6759E 00-0.6759E 00 0.1559E-01-0.4518E-02-0.5337E-02-0.2155E-02-0.1853E-02-0.8724E-02 0.8724E-02

-0.6643E 00-0.6643E 00-0.6677E-02-0.7795E-02-0.7164E-02-0.1260E-02 0.8586E-03-0.5154E-02 0.0000E 00
-0.6518E 00-0.6518E 00-0.2871E-01-0.1467E-01-0.1358E-01-0.1073E-01-0.9553E-02-0.8348E-02 0.0000E 00
-0.6408E 00-0.6408E 00-0.5330E-01-0.2197E-01-0.2040E-01-0.2054E-01-0.2012E-01-0.1010E-01 0.1010E-01
-0.6170E 00-0.6170E 00-0.9472E-01-0.2196E-01-0.2302E-01-0.1975E-01-0.1783E-01-0.3452E-02 0.3452E-02
-0.6098E 00-0.6098E 00-0.1466E 00-0.1368E-01-0.2482E-01-0.1469E-01-0.1138E-01-0.3213E-02 0.3213E-02
-0.3977E 00-0.3977E 00-0.3977E 00 0.6862E-01-0.2897E-01-0.5860E-02-0.5448E-02-0.2131E-02 0.2131E-02
0.0000E 00-0.3977E 00-0.3977E 00 0.0000E 00 0.0000E 00 0.0000E 00 0.0000E 00 0.0000E 00 0.0000E 00

P-FIELD

```
0.0000E 00 0.0000E 00 0.0000E 00 0.0000E 00 0.0000E 00 0.0000E 00 0.0000E 00 0.0000E 00 0.0000E 00
0.0000E 00-0.4326E-01-0.4026E-01-0.4220E-01-0.4255E-01-0.4254E-01-0.4257E-01-0.4285E-01 0.0000E 00
0.0000E 00-0.6169E-01-0.4067E-01-0.4308E-01-0.4273E-01-0.4256E-01-0.4254E-01-0.4309E-01 0.0000E 00
0.0000E 00-0.2680E 00-0.6432E-01-0.4549E-01-0.4306E-01-0.4262E-01-0.4251E-01-0.4300E-01 0.0000E 00
0.0000E 00-0.2287E-01-0.5629E-01-0.4436E-01-0.4295E-01-0.4262E-01-0.4248E-01-0.4290E-01 0.0000E 00
0.0000E 00-0.3909E-01-0.4283E-01-0.4156E-01-0.4201E-01-0.4213E-01-0.4217E-01-0.4284E-01 0.0000E 00
0.0000E 00-0.3066E-01-0.3406E-01-0.3580E-01-0.3704E-01-0.3748E-01-0.3766E-01-0.3795E-01 0.0000E 00
0.0000E 00-0.1486E-01-0.1622E-01-0.1676E-01-0.1749E-01-0.1801E-01-0.1874E-01-0.1951E-01 0.0000E 00
0.0000E 00 0.2910E-02 0.1983E-02 0.1629E-02 0.1334E-02 0.9657E-03 0.3963E-03 0.1493E-03 0.0000E 00
0.0000E 00 0.2111E-01 0.2010E-01 0.2005E-01 0.2010E-01 0.2000E-01 0.1958E-01 0.1968E-01 0.0000E 00
0.0000E 00 0.3928E-01 0.3724E-01 0.3832E-01 0.3877E-01 0.3889E-01 0.3856E-01 0.3855E-01 0.0000E 00
0.0000E 00 0.5990E-01 0.5350E-01 0.5669E-01 0.5741E-01 0.5769E-01 0.5740E-01 0.5707E-01 0.0000E 00
0.0000E 00 0.8895E-01 0.8210E-01 0.7497E-01 0.7597E-01 0.7664E-01 0.7665E-01 0.7648E-01 0.0000E 00
0.0000E 00 0.1554E 00 0.4280E-01 0.8875E-01 0.9434E-01 0.9579E-01 0.9601E-01 0.9586E-01 0.0000E 00
0.0000E 00 0.4616E-01 0.1933E 00 0.1086E 00 0.1137E 00 0.1151E 00 0.1153E 00 0.1152E 00 0.0000E 00
0.0000E 00 0.0000E 00 0.0000E 00 0.0000E 00 0.0000E 00 0.0000E 00 0.0000E 00 0.0000E 00 0.0000E 00
```

S-FIELD

```
0.9998E 00 0.9998E 00 0.9998E 00 0.1000E 01 0.9999E 00 0.9999E 00 0.9999E 00 0.9999E 00 0.9999E 00
0.9998E 00 0.9998E 00 0.9998E 00 0.1000E 01 0.9999E 00 0.9999E 00 0.9999E 00 0.9999E 00 0.9999E 00
0.1001E 01 0.1001E 01 0.9968E 00 0.9999E 00 0.9999E 00 0.9999E 00 0.9999E 00 0.9999E 00 0.9999E 00
0.9891E 00 0.9891E 00 0.9830E 00 0.1001E 01 0.9997E 00 0.9999E 00 0.9999E 00 0.9999E 00 0.9999E 00
0.9899E 00 0.9899E 00 0.9734E 00 0.9867E 00 0.9966E 00 0.9981E 00 0.9991E 00 0.9999E 00 0.9999E 00
0.9908E 00 0.9908E 00 0.9438E 00 0.8987E 00 0.9557E 00 0.9695E 00 0.9792E 00 0.9882E 00 0.9882E 00
0.9915E 00 0.9915E 00 0.8885E 00 0.6489E 00 0.7347E 00 0.7479E 00 0.7638E 00 0.7985E 00 0.7985E 00
0.9947E 00 0.9947E 00 0.5244E 00-0.3409E-01-0.3657E-01-0.2666E-01 0.1455E-01 0.8759E-01 0.8759E-01
0.9980E 00 0.9980E 00 0.4890E 00 0.1455E-01-0.1589E-02 0.1370E-02 0.2384E-02 0.5637E-02 0.5637E-02
0.1003E 01 0.1003E 01 0.4492E 00 0.1298E-01-0.1010E-02-0.2668E-04-0.1311E-03 0.5913E-04 0.5913E-04
0.1003E 01 0.1003E 01 0.4169E 00 0.7549E-02-0.7220E-03 0.1526E-04-0.1960E-04-0.9469E-05-0.9469E-05
0.1020E 01 0.1020E 01 0.3778E 00-0.9250E-02-0.1426E-04 0.3725E-05-0.3005E-05-0.9012E-06-0.9012E-06
0.9943E 00 0.9943E 00 0.2807E 00-0.1573E-01 0.2704E-03-0.3086E-05-0.2576E-06-0.1556E-07-0.1556E-07
0.1115E 01 0.1115E 01 0.3254E 00-0.5182E-01 0.1620E-02-0.3566E-04 0.2426E-06-0.2721E-09-0.2721E-09
0.1115E 01 0.1115E 01 0.3345E 00 0.8197E-02-0.2098E-03 0.2824E-05-0.1636E-07 0.2753E-10 0.2753E-10
0.1115E 01 0.1115E 01 0.3345E 00 0.8197E-02-0.2098E-03 0.2824E-05-0.1636E-07 0.2753E-10 0.2753E-10
```

DEN-FIELD

```
0.1938E 01 0.1938E 01 0.1938E 01 0.1938E 01 0.1938E 01 0.1938E 01 0.1938E 01 0.1938E 01 0.1938E 01
0.1938E 01 0.1938E 01 0.1938E 01 0.1938E 01 0.1938E 01 0.1938E 01 0.1938E 01 0.1938E 01 0.1938E 01
0.1938E 01 0.1938E 01 0.1938E 01 0.1938E 01 0.1938E 01 0.1938E 01 0.1938E 01 0.1938E 01 0.1938E 01
0.1938E 01 0.1938E 01 0.1938E 01 0.1938E 01 0.1938E 01 0.1938E 01 0.1938E 01 0.1938E 01 0.1938E 01
0.1938E 01 0.1938E 01 0.1938E 01 0.1938E 01 0.1938E 01 0.1938E 01 0.1938E 01 0.1938E 01 0.1938E 01
0.1938E 01 0.1938E 01 0.1938E 01 0.1938E 01 0.1938E 01 0.1938E 01 0.1938E 01 0.1938E 01 0.1938E 01
0.1938E 01 0.1938E 01 0.1938E 01 0.1940E 01 0.1939E 01 0.1939E 01 0.1939E 01 0.1939E 01 0.1938E 01
0.1943E 01 0.1938E 01 0.1940E 01 0.1943E 01 0.1943E 01 0.1943E 01 0.1943E 01 0.1942E 01 0.1943E 01

0.1943E 01 0.1938E 01 0.1940E 01 0.1943E 01 0.1943E 01 0.1943E 01 0.1943E 01 0.1943E 01 0.1943E 01
0.1943E 01 0.1938E 01 0.1941E 01 0.1943E 01 0.1943E 01 0.1943E 01 0.1943E 01 0.1943E 01 0.1943E 01
0.1943E 01 0.1938E 01 0.1941E 01 0.1943E 01 0.1943E 01 0.1943E 01 0.1943E 01 0.1943E 01 0.1943E 01
0.1943E 01 0.1938E 01 0.1941E 01 0.1943E 01 0.1943E 01 0.1943E 01 0.1943E 01 0.1943E 01 0.1943E 01
0.1943E 01 0.1938E 01 0.1941E 01 0.1943E 01 0.1943E 01 0.1943E 01 0.1943E 01 0.1943E 01 0.1943E 01
0.1943E 01 0.1937E 01 0.1941E 01 0.1943E 01 0.1943E 01 0.1943E 01 0.1943E 01 0.1943E 01 0.1943E 01
0.1943E 01 0.1937E 01 0.1941E 01 0.1943E 01 0.1943E 01 0.1943E 01 0.1943E 01 0.1943E 01 0.1943E 01
0.1943E 01 0.1943E 01 0.1943E 01 0.1943E 01 0.1943E 01 0.1943E 01 0.1943E 01 0.1943E 01 0.1943E 01
```

VITA[2]

Ahmed Ali Busnaina

Candidate for the Degree of

Master of Science

Thesis: NUMERICAL SIMULATION OF LOCAL DESTRATIFICATION OF LAKES

Major Field: Mechanical Engineering

Biographical:

Personal Data: Born in Benghazi, Libya, September 2, 1953, the son of Mr. and Mrs. Ali Busnaina.

Education: Graduated from Benghazi Secondary School, Benghazi, Libya, in May, 1971; received the Bachelor of Science degree in Mechanical Engineering from University of Al-Fateh in July, 1976; completed requirements for the Master of Science degree at Oklahoma State University in December, 1979.

Professional Experience: Maintenance engineer, General Wires and Electrical Products Company, Benghazi, Libya, 1976; maintenance engineer, Esso Oil Company, Briga, Libya, February, 1977, to August, 1977; teaching assistant, University of Garyounis, Benghazi, Libya, August to December, 1977; graduate research assistant, Oklahoma State University, 1978-1979.

Professional Societies: American Institute of Aeronautics and Astronautics; American Society of Mechanical Engineers.